Dissection of the microRNA transcriptomes of CD4$^+$ T cell subsets in autoimmune inflammation identifies novel regulators of disease pathogenesis

Carolina Cunha[1], Paula Vargas Romero[1], Daniel Inácio[1], Ana Teresa Pais[1], Catarina Pelicano[1], Marina Costa[1], Sofia Mensurado[1], Natacha Gonçalves-Sousa[1], Pedro H. Papotto[1], Daniel Neves[2], Daniel Sobral[3], Francisco Enguita[1], Bruno Silva-Santos[1,4¶*] and Anita Q. Gomes[1,5¶*]

[1] Gulbenkian Institute for Molecular Medicine, Lisbon, Portugal

[2]SGS Global Biosciences Center, Lisbon, Portugal

[3]Instituto Nacional de Saúde Dr. Ricardo Jorge, Lisboa, Lisbon, Portugal.

[4]Faculdade de Medicina, Universidade de Lisboa, Lisbon, Portugal

[5]H&TRC Health & Technology Research Center, ESTeSL - Escola Superior de Tecnologia da Saúde, Instituto Politécnico de Lisboa, Lisbon, Portugal.

* Corresponding authors

E-mail: anita.gomes@gimm.pt (A.Q.G.) or bssantos@medicina.ulisboa.pt (B.S.-S.)

¶These authors contributed equally to this work.

Abstract

MicroRNAs (miRNAs) are key regulators of CD4$^+$ T cell differentiation, but how they contribute to the course of an autoimmune disease *in vivo* remains poorly studied. Given the known roles in autoimmunity of pro-inflammatory T helper 1 (Th)1 and Th17 cells, and anti-inflammatory Foxp3$^+$ regulatory cells, we established a triple reporter mouse for *Ifng*, *Il17* and *Foxp3,* and subjected it to experimental autoimmune encephalomyelitis (EAE) to characterize the miRNomes of the corresponding CD4$^+$ T cell subsets. We identified 110 miRNAs differentially expressed between the pro-inflammatory (Th1 and Th17 cells) and the Treg cell subsets. Among these, we found novel functions for miR-122-5p and miR-1247 as regulators of Th17 cell proliferation and Th1 cell differentiation, thus impacting the course or severity of EAE, respectively. Importantly, their expression patterns suggest miR-122-5p and miR-1247 act as peripheral brakes to CD4$^+$ T cell pathogenicity that are subverted in the inflamed central nervous system.

Introduction

CD4$^+$ T cells can differentiate into multiple functional subsets through networks of cytokines and transcription factors (TFs) that dictate lineage specific transcriptional programs. Interferon-γ (IFN-γ)-producing Thelper 1 (Th1) and interleukin (IL)-17A-producing Th17 cells are two of the key effector CD4$^+$ T cell populations that orchestrate complementary immune responses to major pathogens, such as viruses and intracellular bacteria (Th1), or fungi and extracellular bacteria (Th17). Critically, these effector CD4$^+$ T cells are also involved in the development of chronic inflammatory and autoimmune diseases such as type I diabetes, rheumatoid arthritis, psoriasis, colitis or multiple sclerosis (MS) (1, 2). On the other hand, CD4$^+$ T cells can also differentiate, either in the thymus or in the periphery, into anti-inflammatory regulatory T cells (Treg) that are able to curtail the function of effector cells (Teff) (2, 3),

and whose relevance is highlighted by the very severe autoimmune manifestations of Treg-defective IPEX patients and *Foxp3* mutant mice (4).

More specifically in MS, effector Th1 and Th17 $CD4^+$ T cells contribute to disease pathogenesis after differentiation in the periphery and infiltration into the central nervous system (CNS), causing local inflammation and demyelination (5, 6). With regard to Th1 cells, genetic polymorphisms of IFN-γ have been associated with susceptibility to MS, and increased T cell-derived IFN-γ levels preceded disease exacerbation and correlated with active lesions *in vivo*, and killed oligodentrocytes *in vitro* (reviewed in 7). Th17 cells, on the other hand, activate microglia and recruit neutrophils, macrophages, and lymphocytes (8) through synergy of IL-17A with other proinflammatory cytokines such as IL-6, IL-23, IL-1β and GM-CSF (9,10). Critically, myelin oligodendrocyte glycoprotein (MOG)-specific Th1 and Th17 cells were shown to induce experimental autoimmune encephalomyelitis (EAE), the well-established mouse model of MS, upon adoptive transfer (6, 11, 12).

Immunosuppressive Tregs also play a role in MS by reducing the function of effector cells, often prevailing in remitting phases of the disease (13). In fact, when Treg cells were administered therapeutically in the EAE model, there was a reduction in disease severity, which coincided with limited immune cell infiltration, principally Th17 cells, into the CNS (14). These results reinforce the concept that the balance between Teff and Treg subsets is a major determinant of the outcome of the local inflammatory/ autoimmune response (2, 3). As such, it is important to identify molecular mechanisms that control Teff or Treg cells across their transition from the periphery to the target CNS.

MicroRNAs (miRNAs) have emerged as key players in the fine-tuning of gene expression at the post-transcriptional level. They are highly conserved small (~22 nucleotide-long) non-coding RNAs that bind to the 3′UTR, and less frequently to the coding sequence (CDS), of target mRNAs to induce either degradation or translation repression (15, 16). miRNAs are known to regulate $CD4^+$ T cell differentiation; most strikingly, the ablation of (all) miRNAs in T cells caused impaired T cell proliferation and survival, reduced Treg numbers, and increased production of IFN-γ and IL-17A by $CD4^+$ T cells, leading to

spontaneous lethal inflammatory disease (17, 18, 19, 20). However, only a few specific miRNAs have been identified as underlying such overt phenotypes. For example, miR-29 (21) and the miR-106-363 cluster (22) were shown to inhibit Th1 and Th17 differentiation, respectively, whereas miR-125a promoted Treg activity (23). In the EAE/ MS setting, miR-326 associated with Th17 cells and disease severity, and *in vivo* miR-326 silencing reduced Th17 numbers and EAE pathogenesis (24). Moreover, MS-enriched miR-92 limited Treg induction while supporting Th17 responses, and its inhibition ameliorated EAE (25).

Building on these foundations, we set out to characterize the global miRNomes of Th1, Th17 and Treg cells in EAE, with the ultimate goal of identifying novel miRNA regulators of $CD4^+$ T cell functions *in vivo*. In order to gain resolution compared to previous studies, where candidates were selected based on the analysis of total $CD4^+$ T cells of EAE mice or MS patients (compared to controls), we established a triple reporter mouse for IFN-γ (YFP^+), IL-17A (GFP^+) and Foxp3 ($hCD2^+$) to isolate the corresponding $CD4^+$ T cell subsets upon EAE induction. This allowed us to dissect their distinct miRNomes, and to identify new miRNAs, miR-122-5p and miR-1247-5p, that respectively regulate Th17 and Th1 cells, and thus impact EAE disease onset or severity *in vivo*.

Results

Identification of the miRNomes of *in vivo*-generated Th1, Th17 and Treg cells

In order to identify miRNA repertoires of $CD4^+$ T cell subsets under inflammatory conditions *in vivo*, we established a triple reporter mouse for IFN-γ (YFP^+), IL-17A (GFP^+) and Foxp3 ($hCD2^+$) (triple *Foxp3*^{hCD2}.*Ifng*^{YFP}.*Il17a*^{GFP} reporter mice **Fig. 1a**), by crossing previously described single reporter lines (26, 27, 28). As the response is triggered in peripheral lymphoid organs, we isolated these populations by FACS from the spleen and lymph nodes of EAE-induced triple *Foxp3*^{hCD2}.*Ifng*^{YFP}.*Il17a*^{GFP} reporter mice at the peak-plateau phase of the disease, and extracted RNA to perform both small RNA- and messenger-

RNA sequencing (small RNA-seq and mRNA-seq, respectively) (**Fig. 1b, Fig. S1a**). Both datasets showed that the isolated YFP^+, GFP^+ and $hCD2^+$ $CD4^+$ T cell populations segregated unambiguously on a principal component analysis (**Fig. S1b and c, respectively**), and importantly, differentially expressed the signature genes of each corresponding $CD4^+$ T cell subset (**Fig. S1d**), thus attesting the reliability and reproducibility of our experimental system. The small RNA-seq data revealed clearly distinct miRNomes, with 110 miRNAs differentially expressed between Teff and Treg cell populations *in vivo* (**Fig. 1c and d, Table S1**). These data are a valuable resource for the community, from which we decided to zoom in on miRNAs specifically enriched or depleted in one of the $CD4^+$ T cell subsets. Interestingly, within this candidate list of differentially expressed miRNAs, only nine were specifically up- or down-regulated in one subset (i.e. Th1, Th17 or Treg) compared with the other two subsets (**Fig. 1e**): miR-1247-5p was up-regulated in Th1 cells; miR-126a-5p, miR-5108 and miR-122-5p were up-regulated in Th17 cells, miR-211-5p, miR-15b-5p, miR-151-3p and miR-467a-5p were up-regulated in Treg cells; and miR-125a-5p was down-regulated in Th17 cells. We performed validation studies by RT-qPCR analysis of independent Th1, Th17 and Treg samples isolated by FACS from the spleen/lymph nodes of triple reporter mice with EAE. These confirmed the expression profiles of six of the candidate miRNAs (**Fig. 1f**), with the exceptions of miR-151-3p, miR-5108 and miR-467a-5p. Notably, two of the validated miRNAs, miR-15b-5p and miR-125a-5p, have already been thoroughly studied and, consistent with our expression data, shown to be involved in Treg or Th17 differentiation and/or function (29, 30, 23, 30, 31). Thus, for subsequent "proof-of-concept" functional assays, and since the effector cell populations are the major drivers of EAE, we focused on the candidates displaying higher fold change expression levels in either Th1 or Th17 cells, miR-1247-5p and miR-122-5p, respectively (**Fig. 1e and f**).

Overexpression of miR-122-5p or miR-1247 directly impacts Th17 and Th1 cells *in vitro*

We inquired whether these miRNAs might have a cell-intrinsic role in Th17 (miR-122-5p) or Th1 (miR-1247) cells by performing overexpression experiments in *in vitro*-differentiated cells (from isolated

naïve $CD4^+$ T cells – **Fig. S2**). Upon transduction with retroviral GFP reporter vectors (RVs) encoding the native stem loop of miR-122 (RV-122) (**Fig. 2a**), we observed an upregulation of miR-122-5p levels in *in vitro*-differentiated Th17 cells (**Fig. S3a**). While no differences were observed in the frequency of IL-$17A^+$ (**Fig. 2 b and c**), Th17 cells overexpressing miR-122 had a significantly lower proliferation rate when compared with control cells (RV-empty), as observed by the frequency of proliferating GFP^+ T cells upon CTV labeling as well as their division index (**Fig. 2d-f**). Notably, miR-122 overexpression did not impact Th1 or Treg cell differentiation *in vitro* (**Fig. S3b and c**). These results suggest that miR-122-5p negatively regulates Th17 cell function by limiting their proliferative capacity.

In what refers to miR-1247-5p, its overexpression with retroviral vectors in differentiating Th1 cells (**Fig. 2g, Fig. S3d**) led to a decreased frequency of IFN-γ^+ $CD4^+$ T cells (**Fig. 2h and i**), but did not affect cell proliferation (**Fig. 2 j-l**), nor Treg or Th17 *in vitro*-polarization (**Fig. S3c and e**). These results indicate that miR-1247-5p selectively down-regulates IFN-γ production in Th1 cells.

miR-122-5p is a peripheral brake to Th17 pathogenicity that is overruled in the CNS

We next aimed at dissecting the molecular cues that regulate miR-122-5p and miR-1247-5p expression. For this, we sorted naïve $CD4^+$ T cells from the spleen and lymph nodes of WT mice and cultured them in the presence of different cytokines involved in Th17 or Th1 cell differentiation, respectively. Starting with the Th17-biased miR-122-5p, its expression reached maximal levels in the presence of IL-6 and TGF-β, but decreased when stimulated with IL-1β and especially with IL-23 (**Fig. 3a**). IL-6 and TGF-β are the key cytokines involved in the polarization of naïve $CD4^+$ T cells into the Th17 subset, while IL-1β and IL-23 are critical for lineage maintenance and the acquisition of a pathogenic phenotype (27). Thus, our data suggests that miR-122 might limit the pathogenicity of Th17 cells but is downregulated in a strong (IL-23/ IL-1β-rich) inflammatory environment. To build on this premise *in vivo*, we characterized miR-122-5p expression levels in $CD4^+$ T cell subsets isolated from the CNS of triple *Foxp3*^{hCD2}.*Ifng*^{YFP}.*Il17a*^{GFP} reporter mice challenged with EAE. Interestingly, our data

showed that miR-122-5p was markedly downregulated in cells isolated from the CNS compared with peripheral Th17 cells (**Fig. 3b**). To further provide biological context to these observations, we performed mRNA-seq in Th17 cells isolated from both sites, i.e. spleen/lymph nodes *vs* CNS. This showed that genes associated with a pathogenic phenotype – such as those encoding key cytokines as IFN-γ and GM-CSF (*Ifng* and *Csf2*), chemokines (*Ccl4* and *Cxcl3*) and TFs (*Tbx21* and *Runx1*) - were all increased in CNS-derived Th17 cells when compared to peripheral Th17 cells (**Fig. 3c**) (27). These results link miR-122 expression dynamics with the pathophysiology of EAE, with its downregulation in the CNS associating with enhanced pathogenicity of Th17 cells.

miR-1247 limits Th1 pathogenicity in the periphery but is subverted in the CNS

We performed similar studies for miR-1247, the Th1-biased miRNA that downregulated IFN-γ production *in vitro* (**Fig. 2g**). Although miR-1247-5p was upregulated on *in vivo*-generated Th1 cells (**Fig. 1e and f**), its expression levels were low in Th1 cells differentiated *in vitro* in the presence of IL-12 and anti-IL-4 antibody (**Fig. 3d**). We also tested IL-18, IL-15 and IFN-γ, since IL-18 and IL-15 can promote IFN-γ production in the presence of IL-12 (32); and IFN-γ regulates its own production in an autocrine loop (33). However, none of these cytokines was able to induce miR-1247-5p expression in Th1 cells (**Fig. 3d**). We then reasoned that, as miR-1247-5p limits IFN-γ production by Th1 cells, its expression might be controlled by anti-inflammatory cytokines. Indeed**,** we found that TGF-β and IL-10 were the key inducers of miR-1247-5p expression *in vitro*, even in the presence of IL-12 (**Fig. 3d**). Moreover, when we challenged our triple reporter mice with EAE, we observed that, similarly to miR-122-5p (**Fig. 3b**), the expression levels of miR-1247-5p collapsed in Th1 cells isolated from the CNS when compared to peripheral Th1 cells (**Fig. 3e**). Furthermore, upon mRNA-seq analysis of Th1 cells isolated from both sites (spleen/lymph nodes *vs* CNS), we established a CNS-specific pro-inflammatory signature, including the signature Th1 cytokine (*Ifng*) and TF (*Tbx21*), as well as chemokines (*Ccl3* and *Ccl4*) and receptors (*Il12rb2*, *Il18r1*, *Il18rap*), which contrasted with a set of "self-regulatory genes", including *Il10*, that were

upregulated in Th1 cells from the secondary lymphoid organs (**Fig. 3f**). These data suggest that miR-1247 is part of an anti-inflammatory (TGF-β/ IL-10-mediated) regulatory loop that is subverted once Th1 cells invade the CNS and shut down its expression.

Identification of putative mRNA targets of miR-122-5p in Th17 cells

Given that miRNAs exert their functions by suppressing mRNAs, and each miRNA can impact the expression of many mRNAs (34), we next aimed at identifying the repertoires of mRNAs directly regulated by miR-122-5p and miR-1247-5p. We devised a strategy based on differential Ago2-immunoprecipitation followed by RNA-seq (Ago2 RIP-seq) in lineage-specific cells overexpressing each candidate miRNA (upon retroviral transduction) versus control cells (mock-transduced) (**Fig. S4a**). Briefly, naïve $CD4^+$ T cells were sorted and activated under polarizing conditions (Th1 or Th17 as appropriate), transduced at day 1 with pre-miR RV particles (as used above for the overexpression experiments) and further incubated for 36h, when GFP^+ T cells were sorted and subjected to UV-cross linking and Ago2 immunoprecipitation with high affinity antibody (**Fig. S4a**).

Starting with miR-122-5p, RT-qPCR analysis after the Ago-IP confirmed its enrichment in the Argonaute complex of retrovirally miR-122 transduced Th17 cells (RV-122) relative to the empty vector control (RV-empty), whereas other miRNAs, such as miR-126a-5p or miR15b-5p, showed similar levels between RV-122 and RV-empty treated cells (**Fig. S4b**). The results of the differential Ago2 RIP-seq in Th17 cells identified 587 mRNAs overexpressed in miR-122-5p-transduced Th17 cells, of which 339 (57,8%) had predicted miR-122-5p binding sites (**Fig. S4c**). From these, as proof-of-concept, we inspected our mRNA-seq data for those upregulated in the CNS compared to peripheral Th17 cells, based on the previous observation that miR-122-5p had the opposite expression pattern (**Fig. 3b**). This retrieved 27 mRNAs (FC>1,5, p<0,05) (**Fig. 4a**), including 16 whose function was of relevance for Th17 cell biology and/or proliferation (**Table S2**). Based on literature curation, we further analyzed the expression levels of 5 genes (*Pttglip*, *Nudt4*, *Il18rap*, *Spred2* and *Sap130*) in retrovirally transduced Th17 cells with the native

stem loop of miR-122 (RV-122), and observed that *Nudt4*, *Il18rap* and *Sap130* were specifically downregulated in miR-122 overexpressing (versus control) cells, further reinforcing their potential to be functional targets of miR-122 in the context of Th17 cells in EAE (**Fig. 4b**). Finally, to biochemically validate these 3 mRNAs as direct miR-122-5p targets, we performed luciferase assays. The three putative targets have predicted miR-122-5p binding sites in the 3'UTR of *Nudt4* and *Il18rap* and the CDS of *Sap130* (**Fig. 4c**). To determine whether miR-122-5p was directly targeting these mRNAs, we designed reporter constructs in a pmirGLO Dual-luciferase miRNA target expression vector for the 3′UTRs of *Nudt4* and *Il18rap* and the CDS of *Sap130*. We additionally included a negative control vector containing a 3′UTR without miR-122-5p binding sites and a positive control containing the 3′UTR of *Cpeb1*, a previously validated miR-122-5p target (35). We transiently transfected these constructs into human embryonic kidney (HEK) 293 T cells together with an expression plasmid for either miR-122-5p or an unrelated miRNA. Co-transfection of miR-122-5p (but not an unrelated miRNA) showed a significant repression of luciferase activity compared with control for the three mRNA targets (**Fig. 4c**). Mutations in the miR-122-5p binding sites of *Nudt4*, *Il18rap* and *Sap130* led to significant recoveries of luciferase levels, attesting specificity (**Fig. 4c**). Together, these data suggest that miR-122-5p targets *Nudt4*, *Il18rap* and *Sap130* in Th17 cells. Furthermore, it provides a much larger Ago2 RIP-seq data set that constitutes a resource for those interested in assessing miR-122-5p in future studies on T cell differentiation.

Identification of putative mRNA targets of miR-1247-5p in Th1 cells

We employed the same experimental approach to identify miR-1247-5p targets in the context of Th1 cell differentiation. The differential Ago2 RIP-seq (**Fig. S4a**) showed that the RNA-induced silencing complex (RISC) of miR-1247-overexpressing Th1 cells (as confirmed by RT-qPCR, **Fig. S4b**) was enriched (compared to mock-transduced Th1 cells) in 644 mRNAs, of which 423 (65,7%) had predicted binding sites for miR-1247-5p (**Fig. S4c**). Upon examination of our mRNA-seq data for Th1 cells, we found 41 mRNAs upregulated (FC>1,5 and p>0,05) in the CNS (**Fig. 4d**), of which 18 had relevant

functions for Th1 cell biology (**Table S2**). Based on literature curation, we selected 5 genes - *Gng2*, *Arfip2*, *C2h2c3*, *Rasal3* and *Wipf1*- to further test *in vitro*, i.e. upon retroviral transduction of the native stem loop of miR-1247 in Th1 cells (Fig. 4e). Of these, *Gng2* and *Rasal3* were validated as miR-1247-5p targets both *in vitro*, as showed by their downregulation upon miR-1247-5p overexpression (**Fig. 4e**), and in luciferase assays demonstrating direct binding of *Gng2* and *Rasal3* using the same strategy as described above for miR-122-5p target genes (**Fig. 4f**). More specifically, the 3'UTR regions of both wild-type and mutant *Gng2* and *Rasal3* (**Fig. 4f**) were introduced into a pmirGLO Dual-luciferase miRNA target expression vector and co-expressed with either miR-1247-5p or a control unrelated miRNA. These assays showed a decrease in luminescence in the presence of the miRNA that was abolished when the 3'UTR target regions were mutated (**Fig. 4f**). Thus, our results indicate that miR-1247-5p targets *Gng2* and *Rasal3*. Moreover, they provide the community with a comprehensive Ago2 RIP-seq data set for additional studies on miR-1247-5p in the context of effector T cell differentiation.

miR-122-5p inhibition increases the frequency of IL-17A$^+$ cells and anticipates EAE onset

Next, to assess if the candidate miRNAs play a role in EAE pathophysiology, we treated mice challenged with EAE with synthetic antagomiRs and evaluated their impact on disease course and on the frequency of Teff and Treg subsets in the lymph nodes of antagomiR-treated mice at the end of the experiment. As depicted in **Fig. 5a**, we injected the antagomiRs of the candidate miRNAs at days 7, 9 and 11 after immunization, which corresponds to a preclinical stage (onset of symptoms usually occurs around day 10). Focusing first on miR-122-5p antagomiR treatment - which efficiently reduced miR-122-5p expression levels (**Fig. S5a**) - we observed an anticipation of EAE disease onset as mice started to develop symptoms and lose weight earlier than those treated with the control antagomiR (**Fig. 5b**). Importantly**,** all mice that were subjected to miR-122-5p antagomiR injections were symptomatic already at day 12 post immunization (p.i.), whereas the control group needed an additional 5 days (day 17 p.i.) to present symptoms, thus entering the peak plateau stage later on (**Fig. S5b**).

Analysis of cervical and lumbar LNs (cLNs) showed no differences in the total $CD4^+$ T cell frequency **Fig. S5c**), but an increased percentage of IL-$17A^+$ $CD4^+$ T cells in mice subjected to miR-122-5p antagomir treatment when compared with controls (**Fig. 5c and d**), consistent with the early onset of the disease. We found no differences in the frequency and total cell numbers of Th1 (IFN-γ^+) and Treg ($Foxp3^+$) cell populations in this case (**Fig. 5d**, **Fig. S5d and e**). Moreover, no differences were observed in the frequency of other immune cells between mice treated with miR-122-5p or control antagomiRs (**Fig. S5f**) based on the gating strategy highlighted in **Fig. S6a** (T cell populations) and **Fig. S6b** (other immune cell populations).

To assess the selectivity of these phenotypes, we studied the impact of an anti-miR-126a antagomiR. While this resulted in the downregulation of miR-126a (**Fig. S7a**), it had no impact neither on clinical scores nor on weight loss, since the specific antagomir-treated mice followed a similar disease course as the control group (**Fig. S7b**), and no differences were found on the frequency of IFN-γ^+ and IL-$17A^+$ nor Treg (Foxp3+) cell populations (**Fig. S7c**). These data highlight our finding that miR-122-5p inhibition selectively increases the frequency of Th17 cells and anticipates EAE onset.

Upregulation of miR-1247 limits IFN-γ production by Th1 cells and reduces EAE severity

We next analysed the *in vivo* effects of miR-1247 manipulation. Unlike the previous antagomiRs (**Fig. S5a**), the miR-1247-5p construct led to increased levels of miR-1247-5p in various tissues (**Fig. S8a**), thus constituting an overexpression strategy. Consistent with this, we found decreased levels of previously validated miR-1247 targets, namely *Trappc9* and *Synj2bp*, in matching organs (**Fig. S8b).** While the progression of symptoms followed a similar course (**Fig. S9a**), we observed decreased EAE severity, as well as reduced weight loss, in mice overexpressing miR-1247-5p compared with the control group (**Fig. 6a**). Furthermore, this phenotype associated with a selective decrease in the numbers of IFN-γ^+ $CD4^+$ T cells (**Fig. 6b and c**), without affecting the total $CD4^+$ T cell frequency (**Fig. S9b**), in the draining lymph nodes of miR-1247-5p-treated group. Of note, the frequency of other immune cells also

did not change upon miR-1247-5p overexpression (**Fig. S9c**). Thus, the upregulation of miR-1247 expression restricts IFN-γ production by Th1 cells and reduces EAE severity.

Collectively, our *in vivo* experiments have identified two novel miRNAs, miR-1247-5p and miR-122, that control Th1 and Th17 cell pathogenicity and thus impact the disease course of EAE.

Discussion

This study aimed to provide novel insights on how miRNAs regulate $CD4^+$ T cell subsets during an autoimmune response *in vivo*. Previous studies on the topic had focused on a limited set of miRNAs, such as miR-29[21] and the miR-106-363 cluster (22) which were shown to inhibit Th1 and Th17 differentiation, respectively, by directly targeting either T-bet (and Eomes) or RORγt, TFs that directly regulate the production of IFN-γ or IL-17. Furthermore, several miRNAs had been shown to be either up-regulated – e.g. let-7e, miR-155, miR-223 and miR-326 – or down-regulated – e.g. miR-20b, miR-26a and miR-30a - in $CD4^+$ Th cell subsets of MS patients or EAE-challenged mice, with some being functionally implicated in MS or EAE – for example, miR-326 upregulation stimulated the production of IL-17 in Th17 cells and enhanced pathogenesis (24) while miR-92 restricted Treg induction and supported Th17 responses, consistent with its elevated levels in $CD4^+$ T cells of MS patients (25). Notably, two of our validated miRNAs, miR-15b-5p and miR-125a-5p, have already been shown to control Treg/Th17 cell function in EAE. Thus, miR-15b-5p, which was downregulated in EAE and MS, suppressed Th17 cells while increasing peripheral Treg differentiation (29, 30); and miR-125a-5p stabilized the immunoregulatory capacity of Treg cells, thereby impacting EAE severity (23, 31).

We now provide a global resource on miRNAs, as well as mRNAs, expressed on Th1, Th17 and Treg cell subsets from the peripheral lymphoid organs and the CNS (for mRNA-seq) of EAE-challenged mice, which can be exploited in further studies. The functional analyses of miR-122-5p and miR-1247 as "proof-of-concept" for our resource provided a key conceptual insight: they constitute molecular brakes to pro-inflammatory Th1 and Th17 cells that are subverted in the CNS. Thus, miR-122-5p and miR-1247

were strikingly downregulated in respectively Th17 and Th1 cells from the CNS compared with their lymphoid organ counterparts, and this was accompanied by an upregulation of pro-inflammatory/ pathogenic signatures (like *Ifng*, *Tbx21* or *Csf2*, the later encoding GM-CSF) at the mRNA level. We further identified the molecular cues that regulate the dynamic expression of these two miRNAs. For Th17-biased miR-122, we found it to be induced by IL-6 and TGF-β, but downregulated by IL-1β and especially IL-23. This is particularly interesting because while IL-6 and TGF-β are the key cytokines promoting Th17 cell polarization from naïve $CD4^+$ T cells, IL-1β and IL-23 are critical for Th17 cell maintenance, expansion and, most importantly, the acquisition of a pathogenic phenotype in the target organ (27). As for the Th1-biased miR-1247-5p, we identified TGF-β and IL-10 as the key inducers of its expression, even in the presence of IL-12. Given that TGF-β induces the expression of IL-10 in Th1 cells to reduce their encephalogenicity (36, 37), we conceptualize miR-1247 as part of this self-regulatory mechanism to control excessive IFN-γ levels in Th1 cells.

To gain molecular insight on miR-122-5p and miR-1247 functions, we aimed to characterize direct mRNA targets relevant to Th17 or Th1 cell biology, respectively. In fact, mRNA target identification arguably remains the greatest challenge in miRNA biology, as it is now clear that each miRNA can fine-tune the expression of hundreds of mRNAs in any given cell type (34). To tackle this problem, and in line with the resource nature of our study, we used differential Ago2 RIP-seq on *in vitro*-polarized $CD4^+$ T cells: by overexpressing the candidate miRNA, we promoted its binding to target mRNAs, thus enriching them in Ago2 complexes that are UV-cross linked and immunoprecipitated, followed by RNA-seq. This resulted in large Ago2 RIP-seq datasets that can be used by the community for other studies on these miRNAs in effector $CD4^+$ T cells. Here we zoomed in on candidate mRNAs targets using the following criteria: 1) having predicted binding sites for the candidate miRNA; 2) being upregulated in the CNS compared to secondary lymphoid organs, thus inversely correlating with the miRNA expression; 3) being downregulated upon retroviral overexpression of the miRNA *in vitro*; 4) directly binding to the mRNA sequence as indicated by luciferase assays.

Using this pipeline, we identified *Nudt4*, *Il18rap* and *Sap130* as putative validated targets of miR-122-5p in Th17 cells. Nudt4 is a hydrolase that catalyses the m^7G tRNA modification that promotes the translation of cell cycle mRNAs (38), consistent with the Th17 cell proliferation phenotypes upon miR-122-5p modulation. On the other hand, polymorphisms in the IL18R1-IL18RAP locus, an IL-18 receptor-associated and responsive protein, have been associated with autoimmune disease susceptibility and IL18RAP was shown to be associated with pathogenic Th17 signatures (39, 40, 41). Moreover, IL-18 has been reported to play a similar role to IL-1β in the promotion of IL-17 production and autoimmunity (41). Finally, Sap130 function remains more enigmatic, but it is known to associate with Sin3A (42), which is essential for IL-17 production (43). Collectively, the identification of these 3 direct targets provide new biological context to miR-122-5p-mediated regulation of Th17 cells.

With regard to miR-1247, our analysis pinpointed *Gng2* and *Rasal3* as direct targets in Th1 cells. Gng2, G-protein gamma subunit 2, acts as a tumor suppressor gene by inhibiting Akt and Erk activity (44). In turn, Erk1-deficient mice exhibit increased Th1 cell differentiation and earlier EAE onset than wild-type controls (45). As for Rasal3, Ras GTPase activating protein-like 3, it is a member of the GTPase-activating proteins family required for survival of naïve and activated T cells (46). Importantly, both Rasal3 and its partner GTPase, Rac2 (47) have been shown to promote T-cell production of IFN-γ (48, 49). This previous knowledge on Gng2 and Rasal3 nicely fits our proposed model where miR-1247-mediated targeting impacts Th1 responses in EAE. Overall, by meeting the criteria stated above, these validated mRNA targets offer mechanistic insight into the functions of miR-122-5p and miR-1247 in regulating the pathogenicity of T helper cell subsets in EAE.

Notably, our functional analyses demonstrated the pathophysiological impact of miR-122 and miR-1247 on EAE onset and severity, which associated with intrinsic effects on Th17 cell proliferation and Th1 cell differentiation, respectively. As both miRNAs suppress these pro-inflammatory responses, our findings highlight the potential of modulating specific miRNAs to control the pathogenic immune populations implicated in autoimmune diseases like MS.

A limitation of our current study is that it does not address the role of miRNAs in $CD4^+$ T cell plasticity during EAE (50). Th17 cells, in particular, are known to transdifferentiate into Th1 cells under the IL-23-rich inflammatory environment of EAE (51), but we opted for a snapshot of the effector $CD4^+$ T cell subsets at the peak of EAE using dynamic reporter mice, rather than fate mapping (50). We also did not address the impact of our miRNA candidates on the production of GM-CSF, which has been shown by Becher and colleagues to initiate autoimmune neuroinflammation (52), particularly with its secretion by Th1 and Th17 cells being sufficient to induce EAE (5, 53). Conversely, the key contributions of this study are the global resource on miRNAs expressed in Th1, Th17 and Treg cells at the peak of EAE disease severity; the identification of two new miRNA determinants of Th1/ Th17 cell function, their repertoires of putative mRNA targets in those cells, the intricate regulation by a network of cytokines and their expression dynamics *in vivo* across lymphoid organs and the CNS, which open new avenues to explore in both mice and humans, with the ultimate goal of devising miRNA-based immunotherapies for MS.

Resource availability

Lead contact: Anita Quintal Gomes, anita.gomes@gimm.pt

Materials availability: All unique/stable reagents generated in this study are available from the lead contact without restriction.

Data and code availability: $CD4^+$ T cell RNA-seq data are available from the Sequence Read Archive (SRA) under the accession code PRJNA1067547 (https://www.ncbi.nlm.nih.gov/bioproject/PRJNA1067547). All other data that support the findings of this study are available in the article and Supplementary Information.

Author contributions

C.C., A.Q.G., and B.S.-S. designed the research and wrote the paper; C.C., P.V.R., D.I., A.T.P., C.P., D.S., M.C., S.M., N.G.-S., P.H.P., F.E. and A.Q.G. performed experiments and analyzed the data; B.S.-S. and A.Q.G. supervised the research.

Declaration of interests

The authors declared no competing interests.

Material and Methods

Mice

All mice used were females 6 to 12 weeks of age. C57Bl/6J (B6) WT mice were purchased from Charles River Laboratories. Triple *Foxp3-hCD2.Ifng-YFP.Il17a-GFP* reporter mice were generated and bred in house by crossing the following single reporter strains: B6.Foxp3hCD2 (http://www.informatics.jax.org/allele/MGI:4950682) (54), Great (Ifng-YFP) (http://www.informatics.jax.org/allele/MGI:5317415) (26), and IL17-GFP (http://www.informatics.jax.org/allele/MGI:5426354) (27). B6.Foxp3hCD2 and Great mice were obtained from the Jackson Laboratory and Il17a-GFP mice were from Biocytogen, LLC. Mice were bred and maintained in the specific pathogen–free animal facilities of Gulbenkian Institute for Molecular Medicine (Lisbon, Portugal). All experiments involving animals were approved by the Ethics Animal Welfare Body of Gulbenkian Institute for Molecular Medicine (ORBEA-GIMM), set up in accordance with Portuguese law (article 34 of Decreto-Lei 113/2013, transposed from the European Directive 2010/63/EU), and submitted to the local competent authority Direcção-Geral de Alimentação e Veterinária (DGAV) for authorization. Euthanasia was performed by CO2 inhalation and anesthesia was performed by isofluorane inhalation.

395

396 **EAE induction and scoring**

397 Triple *Foxp3-hCD2.Ifng-YFP.Il17a-GFP* reporter mice were immunized s.c. in both flanks with 100 µg of
398 myelin oligodendrocyte glycoprotein (MOG) 35–55 peptide (MEVGWYRSPFSRVVHLYRNGK)
399 (Eurogentec S.A.) emulsified in CFA solution (4 mg/ml of heat-inactivated M. tuberculosis in IFA) (Difco
400 Laboratories). On the day of immunization and 2 days after, mice received 200 ng pertussis toxin (PTx)
401 (List Biological Laboratories) in 100 µl PBS i.v.. Mice were weighed daily and scored for EAE clinical
402 signs. In brief, the score system ranged from 0 to 5, with 0.5 increments, being score 0 attributed to
403 animals with no clinical signs of EAE and five representative of death. Score 1 consisted in limp tail;
404 score 2 consisted in limp tail together with hind legs weakness; score 3 consisted in complete limb
405 paralysis; and finally, score 4 consisted in complete hind leg paralysis and partial front paralysis. Mice
406 were euthanized if they lose 20% of body weight or if they scored 4 for 2 consecutive days.

407

408 **AntagomiR treatment**

409 AntagomiRs were custom synthesized according to (55) (Merck). Antagomir sequences are as follows:
410 antagomiR-1247-5p - 5'-U*C*CGGGGACGAACGGGACG*G*G*U*-chol; antagomiR-122-5p - 5'-
411 C*A*AACACCAUUGUCACACU*C*C*A*-chol; antagomiR-126a-5p - 5'-
412 C*G*CGUACCAAAAGUAAUA*A*U*G*-chol; AntagomiR for cel-miR-67-3p was used as negative
413 control: antagomiR-ctl - 5'-U*C*UACUCUUUCUAGGAGGUUG*U*G*A*-chol. All ribonucleotides
414 were 2′-O-methyl modified and (*) represents a phosphorothioate modification of the backbone. A
415 cholesterol molecule was added at the 3′-end of the oligonucleotides. Lyophilized antagomiRs were
416 resuspended in RNase-free water at the desired concentration at room temperature for 30 min with slight
417 shaking. *Foxp3-hCD2.Ifng-YFP.Il17a-GFP* reporter mice with EAE were treated with 5 µg/kg specific
418 antagomiRs at days 7, 9 and 11 after immunization, which corresponds to a preclinical stage (onset of
419 symptoms occurs around day 10) through i.v. injection in the eye. Treatments were randomized per cage
420 and EAE scoring was performed by a researcher blinded to each animal's treatment group.

421

422 **Monoclonal antibodies**

423 The following anti-mouse fluorescently labeled monoclonal antibodies (mAbs) were used (antigens and
424 clones): CD3 (145.2C11), CD4 (GK1.5 and RM4-5), CD25 (PC61), CD44 (IM7), CD62L (DREG.55),
425 IFN-γ (XMG1.2), IL-17A (eBio17B7), Foxp3 (FJK-16s), CD8 (53–6.7), TCRδ (GL3), F4/80 (BM8),
426 NK1.1 (PK136), CD19 (6D5), Ly6G (1A8), Ly6C (HK1.4), CD11B (M1/70), CD11C (N418) and CD45
427 (30-F11). The anti-human CD2 (RPA-2.10) antibody was also used. Antibodies were purchased from BD
428 Biosciences, eBiosciences, or BioLegend.

429

430 **Cell preparation, cell sorting, and flow cytometry and analysis**

431 Cell suspensions were obtained from spleens, lymph nodes (cervical, axillary, brachial, inguinal and
432 lumbar), and the central nervous system (brain and spinal cord). For the preparation of lymph nodes and
433 spleen, tissues were filtered through a 70-µm cell strainer and erythrocytes from the spleen were
434 osmotically lysed in red blood cell lysis buffer (BioLegend). For the preparation of brain and spinal cord,
435 mice were perfused through the left cardiac ventricle with cold PBS. Brain and spinal cord were dissected
436 and cut into pieces, and further digested with collagenase type IV (1.5 mg/ml; Roche) and DNase I (0.10
437 mg/ml) (Sigma-Aldrich) in RPMI 1640 containing 5% fetal bovine serum (FBS) for 30 min, at 37°C.
438 Mononuclear cells were isolated by passing the tissue through a 100-µm cell strainer, followed by a 40-
439 70% Percoll (Sigma-Aldrich) gradient and 30-min centrifugation at 2400 rpm. Mononuclear cells were
440 recovered from the interphase, resuspended, and used for further analysis.

441 For cell surface staining, single-cell suspensions were incubated in the presence of anti-CD16/CD32
442 (eBioscience) with saturating concentrations of combinations of the antibodies listed above for 15 min.
443 For viability assessment, cells were stained in the presence of LIVE/DEAD Fixable Near-IR (Thermo
444 Fisher Scientific) or Zombie Aqua (BioLegend), according with manufacturer's instructions.

445 For intracellular cytokine staining or reporter analysis, cells were stimulated with PMA (phorbol 12-
446 myristate 13-acetate) (50 ng/ml) and ionomycin (1 µg/ml), in the presence of Brefeldin A (10 µg/ml) (all

from Sigma) for 3-3,5h at 37°C. Cells were stained for the identified above cell surface markers, fixed for 30 min at 4°C with the Foxp3/Transcription Factor Staining Buffer set (eBioscience), and finally incubated for 45-60 min at 4°C with identified above intracellular antibodies in permeabilization buffer. Cells were analyzed using FACSFortessa (BD Biosciences) and FlowJo software (Tree Star).

For cell sorting, single cell suspensions were stained for cell surface markers as mentioned above and then electronically sorted on a FACSAria (BD Biosciences). Cell sorting based on reporter genes, included stimulation with PMA/ionomycin/Brefeldin A before the staining.

RNA isolation, complementary DNA synthesis, and RT-qPCR

RNA was isolated from fluorescence-activated cell sorting (FACS)–sorted cell populations using an miRNeasy Mini kit (Qiagen). For total RNA, reverse transcription was performed with random oligonucleotides (Invitrogen) using Moloney murine leukemia virus reverse transcriptase (Promega). For miRNA, reverse transcription was performed with a Universal cDNA Synthesis kit II (Exiqon). For total RNA samples, relative quantification of specific complementary DNA (cDNA) species to endogenous references HPRT, β-2-microglobulin or β-actin was carried out using SYBR on a ViiA7 cycler (Applied Biosystems). Primers were either designed manually or by the Universal ProbeLibrary Assay Design Center (Roche), and their sequences are indicated in the **Table S3**. For miRNA samples, relative quantification of specific cDNA species to reference miR-423-3p was carried out using SYBR on a ViiA7 cycler (Applied Biosystems). The respective miRNA LNA primers were used (Exiqon). In both cases, relative quantification was performed using ddCT method as indicated in each section.

RNA- and small-RNA-sequencing

Deep sequencing (small non-coding RNA and RNA-seq) was performed at the GeneCore facility of EMBL (http://www.genecore.embl.de/). For RNA-seq samples were processed with NEBNext Ultra II RNA Library kit for Illumina. Specifically, the protocol used was that for purified mRNA or rRNA depleted RNA, with an optimization of the following steps to accommodate the low input: Fragmentation

time (4.1.3) 10 minutes, First strand synthesis step 2 (4.2.3) was increased to 50 minutes for a longer insert, Adaptor was diluted to 1:30 (4.5.4) and final PCR (4.8.3) was increased to 18 cycles. For small RNA-seq samples were processed with the NEBNext Small RNA Library Prep Set for Illumina.

miRNA-Seq data analysis

Sequenced reads were processed using the CAP-miRSeq pipeline (56). Namely, reads were quality filtered and adaptors removed using cutadapt. Filtered reads were aligned to the mouse genome (GRCm38) using bowtie (57). miRNA prediction and quantification was performed using miRDeep2 (58), where known miRNAs were obtained from mirbase (version 21) (59). Differential expression analysis was performed using the edgeR R package (60). Namely, count data was normalized using the TMM normalization (61), and moderated bayesian statistics (62) was applied to obtain differentially expressed genes (FDR < 0.05 and [Log2FC] > 1) between conditions. Comparisons were performed between Treg and Th (i.e. combining Th17 and Th1), Treg and Th1, and Treg and Th17.

RNA-Seq data analysis

Sequenced reads were quality filtered and adaptors removed using cutadapt. Filtered reads were aligned to the mouse genome (GRCm38) using Hisat2 (63). Gene count tables were obtained using featureCounts (64) against the mouse gene models (gencode M16).

***In vitro* CD4$^+$ T cell subset polarization**

Naive CD4$^+$ T cells (CD3$^+$ CD4$^+$ CD25$^-$ CD62L$^+$CD44^{low}) were FACS-sorted from the LNs and spleen of B6 WT mice and differentiated under polarizing conditions for 4 days. For Th1 cell culture conditions, naive CD4$^+$ T cells were incubated with plate-bound anti-CD3ε (145.2C11) and soluble anti-CD28 (37.51) antibodies (both at 2 μg/ml) in the presence of IL-12 (10 ng/ml) and neutralizing anti–IL-4 antibody (11B11) (5 μg/ml). For Treg cells, naive CD4$^+$ T cells were incubated with plate-bound anti-CD3ε and soluble anti-CD28 (both at 2 μg/ml) in the presence of IL-2 (10 ng/ml) and TGF-β (2 ng/ml). For Th17

cell polarization, naive $CD4^+$ T cells were incubated with plate-bound anti-CD3ε (1 μg/ml) and anti-CD28 (10 μg/ml) in the presence of IL-1β (10 ng/ml), IL-6 (20 ng/ml), IL-23 (20 ng/ml), TGF-β (2 ng/ml) and neutralizing anti–IFN-γ antibody (R4-6A2) (10 μg/ml). All cytokines were from PeproTech, except TGF-β and IL-23, which were from R&D systems.

Retroviral overexpression of miR-122 and miR-1247

The retroviral constructs encoding either mmu-miR-122 and mmu-miR-1247 were generated by inserting the respective native pre-miRNA sequences flanked by about 200 bp into a modified pMig.IRES-GFP retroviral vector (Addgene #9044), as previously reported (65). For retroviral transduction, $CD4^+$ T cells were sorted from LNs and spleen of C57BL/6J mice and polarized towards Th17, Th1 or Treg cells as mentioned above. At polarization day 1, cells were transduced with retrovirus encoding the precursor forms of miR-122 (RV-122), miR-1247 (RV-1247) or the control vector (RV-empty), in the presence with polybrene (8 μg/ml; Sigma-Aldrich). At day 4, differentiation was analysed by flow cytometry cells and gene expression by qPCR.

Proliferation assay

For analysis of proliferation, naïve $CD4^+$ T cells were stained with 1 mM of CellTrace Violet (Thermo Fisher Scientific) in PBS for 20 minutes at room temperature. Reactions were quenched by washing with ice-cold RPMI medium supplemented with 10% (v/v) FBS. CTV-labeled cells were then polarized towards Th1 or Th17 cells and, on the next day, retrovirally transduced with retrovirus encoding the precursor forms of miR-122 (RV-122), miR-1247 (RV-1247), respectively, or the control vector (RV-empty), as previously described. After 4 days, proliferation was assessed by flow cytometry.

Differential argonaute 2 RNA immunoprecipitation followed by deep sequencing

Th17 and Th1 were retrovirally transduced with RV-control vector and RV-miR-122 or RV-miR-1247 vector, respectively. Seventy-two hours after transduction, GFP^+ live cells were FACS-sorted and UV-

525 cross-linked in Stratalinker 2400 (400 mJ cm−2). Cell lysates were pulled from independent experiments
526 (~1 million Th17 and ~400 000 Th1 cells per replicate) and lysed on ice for 15 min before
527 immunoprecipitation. Argonaute (Ago) protein immunoprecipitation was performed using Protein G
528 Dynabeads (Invitrogen) and the 2A8 anti-Ago antibody (Millipore). Briefly, Dynabeads were coated with
529 AffiniPure rabbit anti-mouse IgG antibody (Jackson ImmunoResearch) for 50 min at room temperature,
530 and incubated for additional 4h at 4ºC with the 2A8 anti-Ago antibody (both with spinning). After
531 incubation, cell lysates were added to antibody-coated beads and incubated overnight at 4°C while
532 spinning. Ago2-bound RNA was then partially digested using RNase T1 (ThermoFisher Scientific) and,
533 after proteinase K treatment, RNA was isolated using phenol chloroform isoamyl (Fisher Scientific)
534 extraction. Deep sequencing was performed as above mentioned.
535
536 **Ago2 RIP-seq data analysis**
537 Raw Illumina sequence reads obtained by the pair-end sequencing strategy were quality-checked with the
538 FastQC tool (66) (version 0.11.9; Babraham Bioinformatics, UK) and were filtered and trimmed, with
539 Trimmomatic software (67). Filtered and trimmed sequence reads were aligned with the mouse genome
540 (genome build GRCm38, release 102) using the STAR aligner (68) (version 2.7.10b). Differential gene
541 expression among sample groups was analysed by the DESeq2 algorithm, implemented in the
542 Nasqar platform for high-throughput sequencing data analysis and visualization. Predicted miRNA targets
543 for mmu-miR-1247-5p and mmu-mir-122 were determined by the miRWalk2 platform.
544
545 **Dual luciferase reporter assay**
546 Plasmid vectors pMig-miR-122-5p and pMig-miR-1247-5p that allow for the overexpression of miR-122-
547 5p or mir-1247-5p, respectively, were generated as described above. The binding regions of miR-122-5p
548 targets – Nudt4, Il18rap and Sap130 and of miR-1247-5p targets Gng2 and Rasal13 and respective regions
549 with mutations in the predicted target sequences were directly synthesised into pmiRGLO vector
550 (GeneCust Europe). Each luciferase reporter vector carrying one of the sequences described above was co-

551 transfected with either the pMig-miR-122-5p or pMig-miR-1247-5p expression vectors or a control empty
552 pMig vector into HEK293 T cells (ATCC CRL-3216) using X-tremeGENE HP DNA Transfection
553 Reagent (Roche). After 48 h, firefly and Renilla luciferase activity were measured by using the Dual-Glo
554 Luciferase Assay System (Promega). Renilla luciferase activity served as the internal control, and relative
555 luciferase activity was normalized to empty pMirGlo and to empty pMig-IRES-GFP.
556
557 **Statistical analysis**
558 The statistical significance of differences between two groups was assessed using non-parametric two-
559 tailed Mann-Whitney test or, if both groups followed a normal distribution (tested by Shapiro-
560 Wilk normality test), using two-tailed unpaired Student's t-test. Wilcoxon-matched-pairs or paired t-test
561 were used for paired samples, following normality testing as above. When more than two groups were
562 compared, two-way ANOVA followed by Sidak's post hoc test was performed. Unless otherwise
563 indicated, individual values and mean are plotted, or mean ± SD. $p < 0.05$ was considered significant and
564 is indicated on the figures.
565
566 **Acknowledgements**
567 We thank Vladimir Benes and his team at European Molecular Biology Laboratory GeneCore facility for
568 assistance with library preparation for both the RNA and small-RNA-sequencing; and the staff of the Flow
569 Cytometry and Rodent facilities of GIMM for valuable technical assistance. This work was funded by the
570 European Research Council (CoG_646701 to B.S.-S.); and by Fundação para a Ciência e Tecnologia
571 (SFRH/BD/145352/2019 PhD grant to D. I.).
572

References

1. Korn T, Bettelli E, Oukka M, Kuchroo VK. IL-17 and Th17 Cells. Annual Review of Immunology. 2009 Apr;27(1):485–517.
2. Jäger A, Kuchroo VK. Effector and Regulatory T-cell Subsets in Autoimmunity and Tissue Inflammation. Scandinavian Journal of Immunology. 2010 Jun 14;72(3):173–84.
3. Sakaguchi S, Miyara M, Costantino CM, Hafler DA. FOXP3+ regulatory T cells in the human immune system. Nature Reviews Immunology. 2010 Jun 18;10(7):490–500.
4. Bennett CL, Ochs HD. IPEX is a unique X-linked syndrome characterized by immune dysfunction, polyendocrinopathy, enteropathy, and a variety of autoimmune phenomena. Current Opinion in Pediatrics. 2001 Dec;13(6):533–8.
5. Codarri L, Gyülvészi G, Tosevski V, Hesske L, Fontana A, Magnenat L, et al. RORγt drives production of the cytokine GM-CSF in helper T cells, which is essential for the effector phase of autoimmune neuroinflammation. Nature Immunology. 2011 Apr 24;12(6):560–7.
6. Jäger A, Dardalhon V, Sobel RA, Bettelli E, Kuchroo VK. Th1, Th17, and Th9 Effector Cells Induce Experimental Autoimmune Encephalomyelitis with Different Pathological Phenotypes. The Journal of Immunology. 2009 Nov 4;183(11):7169–77.
7. Baecher-Allan C, Kaskow BJ, Weiner HL. Multiple Sclerosis: Mechanisms and Immunotherapy. Neuron 2018 Feb;97(4):742–68.
8. Steinman L. A brief history of TH17, the first major revision in the TH1/TH2 hypothesis of T cell–mediated tissue damage. Nature Medicine. 2007 Feb;13(2):139–45.
9. McGeachy MJ, Chen Y, Tato CM, Laurence A, Joyce-Shaikh B, Blumenschein WM, et al. The interleukin 23 receptor is essential for the terminal differentiation of interleukin 17-producing effector T helper cells in vivo. Nature immunology. 2009 [cited 2019 Apr 11];10(3):314–24.
10. Onishi RM, Gaffen SL. Interleukin-17 and its target genes: mechanisms of interleukin-17 function in disease. Immunology. 2010 Mar;129(3):311–21.
11. O'Connor RA, Prendergast CT, Sabatos CA, Lau CWZ, Leech MD, Wraith DC, et al. Cutting Edge: Th1 Cells Facilitate the Entry of Th17 Cells to the Central Nervous System during Experimental Autoimmune Encephalomyelitis. The Journal of Immunology. 2008 Sep 3;181(6):3750–4.
12. Loos J, Schmaul S, Theresa Marie Noll, Paterka M, Schillner M, Löffel JT, et al. Functional characteristics of Th1, Th17, and ex-Th17 cells in EAE revealed by intravital two-photon microscopy. Journal of Neuroinflammation. 2020 Nov 26;17(1).
13. McGeachy MJ, Stephens LA, Anderton SM. Natural Recovery and Protection from Autoimmune Encephalomyelitis: Contribution of CD4+CD25+ Regulatory Cells within the Central Nervous System. The Journal of Immunology. 2005 Aug 22;175(5):3025–32.
14. Stephens GL, Swerdlow B, Benjamin E, Coyle AJ, Humbles A, Kolbeck R, et al. IL-9 is a Th17-derived cytokine that limits pathogenic activity in organ-specific autoimmune disease. European Journal of Immunology. 2011 Feb 24;41(4):952–62.
15. Friedman RC, Farh KKH ., Burge CB, Bartel DP. Most mammalian mRNAs are conserved targets of microRNAs. Genome Research. 2008 Oct 29;19(1):92–105.
16. Ha M, Kim VN. Regulation of microRNA biogenesis. Nature Reviews Molecular Cell Biology. 2014 Jul 16;15(8):509–24.

17. Muljo SA, Ansel KM, Kanellopoulou C, Livingston DM, Rao A, Rajewsky K. Aberrant T cell differentiation in the absence of Dicer. Journal of Experimental Medicine. 2005 Jul 11;202(2):261–9.
18. Cobb BS, Hertweck A, Smith J, O'Connor E, Graf D, Cook T, et al. A role for Dicer in immune regulation. Journal of Experimental Medicine. 2006 Oct 23;203(11):2519–27.
19. Chong MMW, Rasmussen JP, Rudensky AY, Littman DR. The RNAseIII enzyme Drosha is critical in T cells for preventing lethal inflammatory disease. Journal of Experimental Medicine. 2008 Aug 25;205(9):2005–17.
20. Zhou X, Jeker LT, Fife BT, Zhu S, Anderson MS, McManus MT, et al. Selective miRNA disruption in T reg cells leads to uncontrolled autoimmunity. Journal of Experimental Medicine. 2008 Aug 25;205(9):1983–91.
21. Steiner David F, Thomas Molly F, Hu Joyce K, Yang Z, Babiarz Joshua E, Allen Christopher DC, et al. MicroRNA-29 Regulates T-Box Transcription Factors and Interferon-γ Production in Helper T Cells. Immunity. 2011 Aug;35(2):169–81.
22. Kästle M, Bartel S, Geillinger-Kästle K, Irmler M, Beckers J, Bernhard Ryffel, et al. microRNA cluster 106a~363 is involved in T helper 17 cell differentiation. Immunology. 2017 Jun 15;152(3):402–13.
23. Pan W, Zhu S, Dai D, Liu Z, Li D, Li B, et al. MiR-125a targets effector programs to stabilize Treg-mediated immune homeostasis. Nature Communications. 2015 May 12;6(1). 1.
24. Du C, Liu C, Kang J, Zhao G, Ye Z, Huang S, et al. MicroRNA miR-326 regulates TH-17 differentiation and is associated with the pathogenesis of multiple sclerosis. Nature Immunology. 2009 Oct 18;10(12):1252–9.
25. Fujiwara M, Raheja R, Garo LP, Ajay AK, Ryoko Kadowaki-Saga, Karandikar SH, et al. microRNA-92a promotes CNS autoimmunity by modulating the regulatory and inflammatory T cell balance. Journal of Clinical Investigation. 2022 May 16;132(10).
26. Reinhardt RL, Liang HE, Locksley RM. Cytokine-secreting follicular T cells shape the antibody repertoire. Nature Immunology. 2009 Mar 1;10(4):385–93.
27. Lee Y, Awasthi A, Yosef N, Quintana FJ, Xiao S, Peters A, et al. Induction and molecular signature of pathogenic TH17 cells. Nature Immunology. 2012 Sep 9;13(10):991–9.
28. Kendal AR, Chen Y, Regateiro FS, Ma J, Adams E, Cobbold SP, et al. Sustained suppression by Foxp3+ regulatory T cells is vital for infectious transplantation tolerance. Journal of Experimental Medicine. 2011 Aug 29;208(10):2043–53.
29. Singh Y, Garden OA, Lang F, Cobb BS. MicroRNA-15b/16 Enhances the Induction of Regulatory T Cells by Regulating the Expression of Rictor and mTOR. The Journal of Immunology. 2015 Dec 15;195(12):5667–77.
30. Liu R, Ma X, Chen L, Yang Y, Zeng Y, Gao J, et al. MicroRNA-15b Suppresses Th17 Differentiation and Is Associated with Pathogenesis of Multiple Sclerosis by Targeting *O*-GlcNAc Transferase. The Journal of Immunology. 2017 Apr 1;198(7):2626–39.
31. Li D, Kong C, Tsun A, Chen C, Song H, Shi G, et al. MiR-125a-5p Decreases the Sensitivity of Treg cells Toward IL-6-Mediated Conversion by Inhibiting IL-6R and STAT3 Expression. Scientific reports. 2015 Oct 1;5(1).
32. Nakanishi K. Unique Action of Interleukin-18 on T Cells and Other Immune Cells. Frontiers in Immunology. 2018 Apr 20;9.
33. Bhat P, Leggatt G, Waterhouse N, Frazer IH. Interferon-γ derived from cytotoxic lymphocytes directly enhances their motility and cytotoxicity. Cell Death and Disease. 2017 Jun 1;8(6):e2836.
34. Wilczynska A, Bushell M. The complexity of miRNA-mediated repression. Cell Death & Differentiation. 2014 Sep 5;22(1):22–33.

35. Wang T, Li F, Geng W, Ruan Q, Shi W. MicroRNA-122 ameliorates corneal allograft rejection through the downregulation of its target CPEB1. Cell Death Discovery. 2017 May 15;3(1).
36. Huss DJ, Winger RC, Peng H, Yang Y, Racke MK, Lovett-Racke AE. TGF-β Enhances Effector Th1 Cell Activation but Promotes Self-Regulation via IL-10. The Journal of Immunology. 2010 May 15;184(10):5628–36.
37. Huss DJ, Winger RC, Cox GM, Mireia Guerau‐de‐Arellano, Yang Y, Racke MK, et al. TGF‐β signaling via Smad4 drives IL‐10 production in effector Th1 cells and reduces T‐cell trafficking in EAE. European Journal of Immunology. 2011 Jul 4;41(10):2987–96.
38. Liu Y, Jiang B, Lin C, Zhu W, Chen D, Sheng Y, et al. m7G-related gene NUDT4 as a novel biomarker promoting cancer cell proliferation in lung adenocarcinoma. Frontiers in Oncology. 2023 Jan 24;12.
39. Barrett JC, Hansoul S, Nicolae DL, Cho JH, Duerr RH, Rioux JD, et al. Genome-wide association defines more than thirty distinct susceptibility loci for Crohn's disease. Nature genetics. 2008 Aug 1;40(8):955–62.
40. Imielinski M, Baldassano RN, Griffiths A, Russell RK, Annese V, Dubinsky M, et al. Common variants at five new loci associated with early-onset inflammatory bowel disease. Nature Genetics. 2009 Nov 15;41(12):1335–40.
41. Lalor SJ, Dungan LS, Sutton CE, Basdeo SA, Fletcher JM, Mills KHG. Caspase-1–Processed Cytokines IL-1β and IL-18 Promote IL-17 Production by γδ and CD4 T Cells That Mediate Autoimmunity. The Journal of Immunology. 2011 Apr 6;186(10):5738–48.
42. Fleischer TC, Yun UJ, Ayer DE. Identification and Characterization of Three New Components of the mSin3A Corepressor Complex. Molecular and Cellular Biology. 2003 May 15;23(10):3456–67.
43. Perucho L, Icardi L, Simone ED, Basso V, Agresti A, Amaia Vilas Zornoza, et al. The transcriptional regulator Sin3A balances IL‐17A and Foxp3 expression in primary CD4 T cells. EMBO Reports. 2023 Mar 16;24(5).
44. Zhao A, Li D, Mao X, Yang M, Deng W, Hu W, et al. GNG2 acts as a tumor suppressor in breast cancer through stimulating MRAS signaling. Cell Death & Disease. 2022 Mar;13(3).
45. Agrawal A, Dillon S, Denning TL, Pulendran B. ERK1−/− Mice Exhibit Th1 Cell Polarization and Increased Susceptibility to Experimental Autoimmune Encephalomyelitis. The Journal of Immunology. 2006 May 2;176(10):5788–96.
46. Muro R, Nitta T, Okada T, Ideta H, Tsubata T, Suzuki H. The Ras GTPase-Activating Protein Rasal3 Supports Survival of Naive T Cells. Akiyama T, editor. PLOS ONE. 2015 Mar 20;10(3):e0119898.
47. Shin Y, Kim Y, Kim H, Shin N, Kim T, Kwon T, et al. RASAL3 preferentially stimulates GTP hydrolysis of the Rho family small GTPase Rac2. Biomedical Reports. 2018 Jul 2;
48. Saito S, Kawamura T, Higuchi M, Kobayashi T, Manami Yoshita‐Takahashi, Yamazaki M, et al. RASAL3, a novel hematopoietic RasGAP protein, regulates the number and functions of NKT cells. European Journal of Immunology. 2015 Feb 4;45(5):1512–23.
49. Li B. Role of the Guanosine Triphosphatase Rac2 in T Helper 1 Cell Differentiation. Science. 2000 Jun 23;288(5474):2219–22.
50. Hirota K, Duarte JH, Veldhoen M, Hornsby E, Li Y, Cua DJ, et al. Fate mapping of interleukin 17-producing T cells in inflammatory responses. Nature immunology. 2011 Mar 1 [cited 2021 Jan 29];12(3):255–63.
51. Muranski P, Restifo NP. Essentials of Th17 cell commitment and plasticity. Blood. 2013 Mar 28 [cited 2021 May 9];121(13):2402–14.

52. Becher B, Segal BM. TH17 cytokines in autoimmune neuro-inflammation. Current Opinion in Immunology. 2011 Dec;23(6):707–12.
53. El-Behi M, Ciric B, Dai H, Yan Y, Cullimore M, Safavi F, et al. The encephalitogenicity of TH17 cells is dependent on IL-1- and IL-23-induced production of the cytokine GM-CSF. Nature Immunology. 2011 Jun 1;12(6):568–75.
54. Komatsu N, Mariotti-Ferrandiz ME, Wang Y, Malissen B, Waldmann H, Hori S. Heterogeneity of natural Foxp3+ T cells: A committed regulatory T-cell lineage and an uncommitted minor population retaining plasticity. Proceedings of the National Academy of Sciences of the United States of America. 2009 Feb 10 [cited 2021 Aug 20];106(6):1903–8.
55. Krützfeldt J, Rajewsky N, Braich R, Rajeev KG, Tuschl T, Manoharan M, et al. Silencing of microRNAs in vivo with "antagomirs." Nature. 2005 Oct 30;438(7068):685–9.
56. Sun Z, Evans J, Bhagwate A, Middha S, Bockol M, Yan H, et al. CAP-miRSeq: a comprehensive analysis pipeline for microRNA sequencing data. BMC Genomics. 2014;15(1):423.
57. Langmead B, Trapnell C, Pop M, Salzberg SL. Ultrafast and memory-efficient alignment of short DNA sequences to the human genome. Genome Biology. 2009;10(3):R25.
58. Friedländer MR, Mackowiak SD, Li N, Chen W, Rajewsky N. miRDeep2 accurately identifies known and hundreds of novel microRNA genes in seven animal clades. Nucleic Acids Research. 2011 Sep 10;40(1):37–52.
59. Griffiths-Jones S, Saini HK, van Dongen S, Enright AJ. miRBase: tools for microRNA genomics. Nucleic Acids Research. 2007 Dec 23;36(Database):D154–8.
60. Robinson MD, McCarthy DJ, Smyth GK. edgeR: a Bioconductor package for differential expression analysis of digital gene expression data. Bioinformatics. 2009 Nov 11;26(1):139–40.
61. Robinson MD, Oshlack A. A scaling normalization method for differential expression analysis of RNA-seq data. Genome Biology. 2010;11(3):R25.
62. Robinson MD, Smyth GK. Moderated statistical tests for assessing differences in tag abundance. Bioinformatics. 2007 Sep 19;23(21):2881–7.
63. Kim D, Paggi JM, Park C, Bennett C, Salzberg SL. Graph-based genome alignment and genotyping with HISAT2 and HISAT-genotype. Nature Biotechnology. 2019 Aug;37(8):907–15.
64. Liao Y, Smyth GK, Shi W. featureCounts: an efficient general purpose program for assigning sequence reads to genomic features. Bioinformatics. 2013 Nov 13;30(7):923–30.
65. Schmolka N, Papotto PH, Romero PV, Amado T, Enguita FJ, Amorim A, et al. MicroRNA-146a controls functional plasticity in γδ T cells by targeting NOD1. Science Immunology. 2018 May 4;3(23).
66. Andrews, S. (2010). FastQC: A Quality Control Tool for High Throughput Sequence Data http://www.bioinformatics.babraham.ac.uk/projects/fastqc/.
67. Bolger AM, Lohse M, Usadel B. Trimmomatic: a flexible trimmer for Illumina sequence data. Bioinformatics. 2014 Apr 1;30(15):2114–20.
68. Dobin A, Davis CA, Schlesinger F, Drenkow J, Zaleski C, Jha S, et al. STAR: ultrafast universal RNA-seq aligner. Bioinformatics. 2012 Oct 25;29(1):15–21.

Figure legends

Fig. 1. Identification of the miRNomes of Th1, Th17 and Treg cells from EAE-challenged *Foxp3*^{hCD2}*.Ifng*^{YFP}*.IL17a*^{GFP} reporter mice. (a) Schematic representation of the genomic alterations introduced in the triple *Foxp3-hCD2.Ifng-YFP.Il17a-GFP* reporter mouse strain with the respective CD4$^+$ T cell subset. In the loci of each reporter gene, a sequence for an independently translated reporter protein was inserted downstream of the gene endogenous translational stop codon. (b) Experimental setup: triple *Foxp3-hCD2.Ifng-YFP.Il17a-GFP* reporter mice were subjected to EAE and at the peak plateau stage Treg, Th1 and Th17 cells were isolated from the spleen and lymph nodes by FACS, according with each reporter gene. After RNA isolation samples were subjected to both mRNA-seq and small RNA-seq. (c, d) Heatmaps depicting differentially expressed miRNAs between Treg and effector Th (up in Treg vs Th1 or Treg vs Th17 (c); versus up in Th1 vs Treg or Th17 vs Treg (d)). Colors indicate the direction and magnitude of calculated z-scores, with red representing higher expression of a miRNA in a given cell subset and blue, the opposite. (e) Volcano plots depicting differentially expressed miRNAs between Th1, Th17 and Treg subsets. miRNAs names are indicated when differentially expressed (log2FC > 1; FDR < 0.05) in two comparisons. (f) RT-qPCR analysis of the 9 candidate miRNAs' expression in Treg, Th1 and Th17 cells isolated and pooled from the lymph nodes and spleen of triple Foxp3-hCD2.Ifng-YFP.Il17a-GFP reporter mice at EAE peak plateau. Box-and-whiskers indicate median, 25 and 75% percentiles, minimum and maximum expression levels of candidate miRNAs. Results are presented relative to miR-423-3p expression from 7 independent experiments. *p<0.05 (Wilcoxon test).

Fig. 2. miR-122-5p and miR-1247 intrinsically impact Th17 cell proliferation and Th1 cell function. (a) Experimental setup: naive CD4$^+$ T cells were sorted from WT mice and differentiated *in vitro* towards Th17 cells for 4 days. At day 1, cells were transduced with retroviral vectors encoding the precursor forms of miR-122 and differentiation was analysed by flow cytometry. Empty vector was used as control. (b) Representative flow cytometry plots of IL-17A$^+$ cells in retrovirally transduced Th17 cells expressing a

783 control vector (RV-empty) or miR-122 (RV-122) and frequency of IL-17A$^+$ cells in retrovirally
784 transduced Th17 cells expressing a control vector (RV-empty) or miR-122 (RV-122) from 5 independent
785 experiments (c). Dotted lines link cells from the same mouse. (d) Representative histogram of
786 proliferating CTV$^+$ cells in retrovirally transduced Th17 cells expressing a control vector (RV-empty) or
787 miR-122 (RV-122). (e) Frequency of proliferating CTV$^+$ cells in retrovirally transduced Th17 cells
788 expressing a control vector (RV-empty) or miR-122 (RV-122). Results are mean ± SD from 2 independent
789 experiments (n = 4). *p<0.05 and **p<0.01 (two-way ANOVA followed by Sidak's multiple comparisons
790 test). (f) Division index of retrovirally transduced Th17 cells expressing a control vector (RV-empty) or
791 miR-122 (RV-122). Dotted lines link cells from the same mouse. *p<0.05 (Paired t-test). (g) Experimental
792 setup: naive CD4$^+$ T cells were sorted from WT mice and differentiated in vitro towards Th1 cells for 4
793 days. At day 1, cells were transduced with retroviral vectors encoding the precursor forms of miR-1247
794 and differentiation was analysed by flow cytometry. Empty vector was used as control. (h) Representative
795 flow cytometry plots of IFN-γ^+ cells in retrovirally transduced Th1 cells expressing a control vector (RV-
796 empty) or miR-1247 (RV-1247) and frequency of IFN-γ^+ cells in retrovirally transduced Th1 cells
797 expressing a control vector (RV-empty) or miR-122 (RV-122) from 5 independent experiments (i). Dotted
798 lines link cells from the same mouse. *p<0.05 (Paired t-test). (j) Representative histogram of proliferating
799 CTV$^+$ cells in retrovirally transduced Th1 cells expressing a control vector (RV-empty) or miR-1247 (RV-
800 1247). (k) Frequency of proliferating CTV$^+$ cells in retrovirally transduced Th1 cells expressing a control
801 vector (RV-empty) or miR-1247 (RV-1247). Results are mean ± SD from 3 independent experiments (n =
802 5). (l) Division index of retrovirally transduced Th1 cells expressing a control vector (RV-empty) or miR-
803 1247 (RV-1247). Dotted lines link cells from the same mouse.
804
805 **Fig. 3. miR-122 and miR-1247 act as brakes on pro-inflammatory Th17/Th1 phenotypes that are**
806 **subverted in the CNS. (a)** RT-qPCR analysis of miR-122 expression in CD4$^+$ T cells cultured *in vitro* for
807 4 days in the presence of indicated cytokines and antibodies. Results are presented relative to miR-423-3p

808 expression and represent mean ± SD (n=6-7) . *p<0.05 and **p<0.01 (non parametric Mann-Whitney
809 test). **(b)** RT-qPCR analysis of miR-122 expression in Treg, Th1 and Th17 cells isolated and pooled from
810 the periphery (lymph nodes and spleen) and the CNS of triple Foxp3-hCD2.Ifng-YFP.Il17a-GFP reporter
811 mice at EAE peak plateau stage. Results are presented as fold vs. Treg in each specific tissue (ddct) and
812 represent mean ± SD (n=7). miR-423-3p was used as reference gene. *p<0.05 (Wilcoxon test). **(c)** Gene
813 expression determined by RNA-seq of pathogenic vs non pathogenic signature genes in Th17 cells
814 isolated and pooled from the periphery (lymph nodes and spleen) and the CNS of triple Foxp3-hCD2.Ifng-
815 YFP.Il17a-GFP reporter mice at EAE peak plateau stage. Results are represented as mean of log fold
816 change (logFC) between periphery and CNS Th17 cells. **(d)** RT-qPCR analysis of miR-1247 expression in
817 $CD4^+$ T cells cultured *in vitro* for 4 days in the presence of indicated cytokines and antibodies. Results are
818 presented relative to miR-423-3p expression and represent mean ± SD (n=2-12). *p<0.05 and p<0.01 (non
819 parametric Mann-Whitney test). **(e)** RT-qPCR analysis of miR-1247 expression in Treg, Th1 and Th17
820 cells isolated and pooled from the periphery (lymph nodes and spleen) and the CNS of triple Foxp3-
821 hCD2.Ifng-YFP.Il17a-GFP reporter mice at EAE peak plateau stage. Results are presented as fold vs.
822 Treg in each specific tissue (ddct) and represent mean ± SD (n=7). miR-423-3p was used as reference
823 gene. *p<0.05 (Wilcoxon test). **(f)** Gene expression determined by RNA-seq of self-regulation vs
824 proinflammatory genes in Th1 cells isolated and pooled from the periphery (lymph nodes and spleen) and
825 the CNS of triple Foxp3-hCD2.Ifng-YFP.Il17a-GFP reporter mice at EAE peak plateau stage. Results are
826 represented as mean of log fold change (logFC) between periphery and CNS Th1 cells.
827
828 **Fig. 4. Identification of putative mRNA targets of miR-122-5p and miR-1247-5p in Th17 and Th1**
829 **cells.** (a) Gene expression determined by RNA-seq of candidate miR-122-5p mRNA targets that are
830 upregulated in Th17 cells isolated from the CNS of triple Foxp3-hCD2.Ifng-YFP.Il17a-GFP reporter mice
831 at EAE peak plateau stage when compared to Th17 isolated from the periphery (lymph nodes and spleen)
832 of the same mice (FC>1,5; p<0.05). Results are represented as mean of log fold change (logFC) between

833 periphery- and CNS-derived Th17 cells. (b) RT-qPCR analysis of candidate miR-122-5p mRNA targets in
834 retrovirally transduced Th17 cells expressing a control vector (RV-empty) or miR-122 (RV-122). Results
835 are presented as fold vs. RV-empty (n=4). Grey dashed lines link cells from the same mouse. Black
836 dashed line represents the baseline expression level of controls. *p<0.05 (paired students t-test). (c)
837 Luciferase activity in HEK293T cells co-transfected with a pmirGLO Dual-Luciferase miRNA target
838 expression vector containing either the WT or mutated miR-122-5p-binding sites of Sap130, Il18rap and
839 Nudt4 mRNAs plus a vector containing miR-122-5p or an unrelated miRNA. An unrelated construct
840 (without miR-122-5p binding sites) and a positive construct (Cpeb1) were included. Schematic
841 representation of miR-122-5p putative binding sites of in the miR response elements of Sap130, Il18rap
842 and Nudt4 mRNAs are included. Results are presented as fold vs. unrelated miRNA and represent mean +
843 SD (n=5). *p<0.05 and **p<0.01 (paired students t-test). (d) Gene expression determined by RNA-seq of
844 candidate miR-1247-5p mRNA targets that are upregulated in Th1 cells isolated from the CNS of triple
845 Foxp3-hCD2.Ifng-YFP.Il17a-GFP reporter mice at EAE peak plateau stage when compared to Th1
846 isolated from the periphery (lymph nodes and spleen) of the same mice (FC>1,5; p<0.05). Results are
847 represented as mean of log fold change (logFC) between periphery- and CNS-derived Th1 cells. (e) RT-
848 qPCR analysis of candidate miR-1247-5p mRNA targets in retrovirally transduced Th1 cells expressing a
849 control vector (RV-empty) or miR-1247 (RV-1247). Results are presented as fold vs. RV-empty (n=3).
850 Grey dashed lines link cells from the same mouse. Black dashed line represents the baseline expression
851 level of controls. *p<0.05 (paired students t-test). (f) Luciferase activity in HEK293T cells co-transfected
852 with a pmirGLO Dual-Luciferase miRNA target expression vector containing either the WT or mutated
853 miR-1247-5p-binding sites of Rasal3 and Gng2 mRNAs plus a vector containing miR-1247-5p or an
854 unrelated miRNA. An unrelated construct (without miR-1247-5p binding sites) and a positive construct
855 (Trappc9) were included. Schematic representation of miR-1247-5p putative binding sites of in the miR
856 response elements of Rasal3 and Gng2 mRNAs are included. Results are presented as fold vs. unrelated
857 miRNA and represent mean + SD (n=5). *p<0.05 and **p<0.01 (paired students t-test).

858

859 **Fig. 5. miR-122-5p inhibition antecipates EAE onset.**

860 **(a)** Experimental setup: triple *Foxp3-hCD2.Ifng-YFP.Il17a-GFP* reporter mice were immunized s.c. in
861 both flanks with 100 µg of myelin oligodendrocyte glicoprotein $(MOG)^{35-55}$ peptide emulsified in CFA
862 solution (day 0). On the day of immunization and 2 days later, mice received a retro orbital injection of
863 200 ng of pertussis toxin. At days 7, 9 and 11, mice received 5 µmol/kg of specific antagomiRs (retro
864 orbital injection). AntagomiR for cel-miR-67-3p was used as control. **(b)** Mice treated with control and
865 miR-122-5p antagomiRs were scored for EAE clinical signs and weighed daily for 28 days. Results are
866 mean ± SD from 3 independent experiments (n = 9-11). *p<0.05 and **p<0.01 (two-way ANOVA
867 followed by Sidak's multiple comparisons test). **(c)** Representative flow cytometry plots of IFN-γ^+ and IL-
868 $17A^+$ $CD4^+$ T cells in the cervical and lumbar lymph nodes of triple *Foxp3-hCD2.Ifng-YFP.Il17a-GFP*
869 reporter mice with EAE and treated with control and miR-122-5p antagomiRs. **(d)** Frequency and absolute
870 numbers of IL-$17A^+$ $CD4^+$ T cells in the cervical and lumbar lymph nodes of triple *Foxp3-hCD2.Ifng-*
871 *YFP.Il17a-GFP* reporter mice with EAE and treated with control and miR-122-5p antagomiRs. Results
872 are mean + SD from 3 independent experiments (n = 9-11). Each dot represents an individual mouse.
873 *p<0.05 (non-parametric Mann-Whitney test).

874

875

876

877 **Fig. 6. miR-1247-5p upregulation limits EAE severity.**

878 **(a)** Mice treated with control and miR-1247-5p antagomiRs were scored for EAE clinical signs and
879 weighed daily for 28 days. Results are mean ± SD from 3 independent experiments (n = 10-11). *p<0.05
880 and **p<0.01 (two-way ANOVA followed by Sidak's multiple comparisons test). **(b)** Representative flow
881 cytometry plots of IFN-γ^+ and IL-$17A^+$ $CD4^+$ T cells in the draining lymph nodes (inguinal, axillary and
882 brachial) of triple Foxp3-hCD2.Ifng-YFP.Il17a-GFP reporter mice with EAE and treated with control and

miR-1247-5p antagomiRs. **(c)** Frequency and absolute numbers of IFN-γ^+ $CD4^+$ T cells in the draining lymph nodes (inguinal, axillary and brachial) of triple Foxp3-hCD2.Ifng-YFP.Il17a-GFP reporter mice with EAE and treated with control and miR-1247-5p antagomiRs. Results are mean + SD from 3 independent experiments (n = 10-11). Each dot represents an individual mouse. *p<0.05 (non parametric Mann-Whitney test).

Supporting information

Fig S1. *In vivo* isolation of Th1, Th17 and Treg cell populations and their global characterization

(a) FACS gating strategy to isolate pure Th1, Th17 and Treg cells from EAE mice. Lymphocytes were selected based on a forward scatter (FSC)/side scatter (SSC) plot. After selection of live singlets, lymphocytes were gated on a CD4/CD3 plot to select $CD4^+$ T cells. $CD4^+$ lymphocytes were then gated on a GFP/YFP plot to sort Th1 cells (GFP^-YFP^+) and Th17 cells (GFP^+YFP^-). Finally, Treg cells were defined as $GFP^-YFP^-hCD2^+$. (b-c) Principal component analysis (PCA) of the *in vivo*-generated Treg, Th1 and Th17 subsets subjected to RNA-seq. (c) and to small RNA-seq. (d) Heatmap depicting Treg, Th1 and Th17 signature genes that are enriched within, YFP^+, GFP^+ and $hCD2^+$sorted populations, respectively. Colors indicate the direction and magnitude of calculated z-scores.

Fig. S2. FACS gating strategy for naïve $CD4^+$ T cells.

Lymphocytes were selected based on a FSC/SSC plot. After selection of live singlets, lymphocytes were gated on a CD4/CD3 plot to select $CD4^+$ T cells. $CD4^+$ lymphocytes were then gated on a CD4/CD25 plot to exclude $CD25^+$ Treg cells. Finally, $CD4^+CD25^-$ cells were gated on a CD44/CD62L to sort naïve $CD4^+$ T cells.

Fig. S3. miR-122-5p and miR-1247-5p overexpression does not impact Teff and Treg differentiation *in vitro* (a) RT-qPCR analysis of miR-122-5p expression in retrovirally transduced Th17 cells expressing a control vector (RV-empty) or miR-122 (RV-122). Results are mean from 2 independent experiments. Each dot represents cells from an individual mouse. (b) Frequency of IFN-γ^+ $CD4^+$ T cells in retrovirally transduced Th1 cells expressing a control vector (RV-empty) or miR-122 (RV-122). Results are mean ± SD from 5 independent experiments (n= 8-9). Each dot represents cells from an individual mouse. (c) Frequency of $Foxp3^+$ $CD4^+$ T cells in retrovirally transduced Treg cells expressing a control vector (RV-empty), miR-122 (RV-122) or miR-1247 (RV-1247). Results are mean ± SD from 3 independent experiments (n= 4-6). Each dot represents cells from an individual mouse. (d) RT-qPCR analysis of miR-1247-5p expression in retrovirally transduced Th1 cells expressing a control vector (RV-empty) or miR-1247 (RV-1247). Results are mean from 2 independent experiments. Each dot represents cells from an individual mouse. (e) Frequency of IL-$17A^+$ $CD4^+$ T cells in retrovirally transduced Th17 cells expressing a control vector (RV-empty) or miR-1247 (RV-1247). Results are mean ± SD from 3 independent experiments (n=5). Each dot represents cells from an individual mouse.

Fig. S4. Identification of miR-122-5p and miR-1247-5p targets using differential Ago-RIPseq (a) Experimental setup: naive $CD4^+$ T cells were sorted from WT mice and differentiated *in vitro* towards Th17 or Th1 cells for 4 days. At day 1, cells were transduced with retroviral vectors encoding the precursor forms of miR-122 (for Th17) or miR-1247 (Th1) and at day 4 GFP^+ cell were sorted. Empty vector was used as control. GFP^+ cells were UV-crosslinked and subjected to Ago2-RNA immuniprecipitation followed by RNA sequencing to identify targets mRNA that were enriched in the samples overexpressing candidate miRNAs – miR-122 for Th17 cells and miR-1247 for Th1 cells. (b) RT-qPCR analysis of miR-122-5p, miR-126a-5p and miR-15b-5p expression after differential Ago2-immunoprecipitation of retrovirally transduced Th17 cells expressing a control vector (RV-empty) or

miR-122 (RV-122) (*left panel*). RT-qPCR analysis of miR-1247-5p, miR-15b-5p and miR-16-5p expression after differential Ago2-immunoprecipitation of retrovirally transduced Th1 cells expressing a control vector (RV-empty) or miR-1247 (RV-1247) (*right panel*). Results are presented relative to miR-423-3p expression and represent mean (n=3). Each dot represents one biological replicate. (c) Following differential expression analysis, we identified 587 mRNAs overexpressed in RV-122 samples of which 57,8% (339 mRNAs) had predicted miR-122-5p binding sites (*left panels*); and 644 mRNAs overexpressed in RV-1247 samples of which 65,7% (423 mRNAs) had predicted miR-1247-5p binding sites (*right panels*).

Fig. S5. Lack of effect of miR-122-5p antagomiR in non-CD4$^+$ T-cell immune cell populations. (a) RT-qPCR analysis of miR-122-5p expression in spleen (SPL), liver (LV) and heart (HT) harvested from antagomiR-treated mice at day 13 post immunization. (b) Pie charts depicting the relative number of mice treated with control and miR-122-5p antagomiRs reaching the onset of clinical symptoms or the peak plateau stage (defined as 3 days with the same score ± 0,5) in a certain day. (c) Frequency of CD4$^+$ T cells in cervical and lumbar lymph nodes (cLNs) of triple Foxp3-hCD2.Ifng-YFP.Il17a-GFP reporter mice with EAE and treated with control and miR-122-5p antagomiRs. Results are mean ± SD from 3 independent experiments (n = 9-10). Each dot represents an individual mouse. (d) Representative flow cytometry plots of Foxp3$^+$ CD4$^+$ T cells in the cervical and lumbar lymph nodes of triple *Foxp3-hCD2.Ifng-YFP.Il17a-GFP* reporter mice with EAE and treated with control and miR-122-5p antagomiRs. (e) Frequency and absolute numbers of Foxp3$^+$ CD4$^+$ T cells in the cervical and lumbar lymph nodes of triple *Foxp3-hCD2.Ifng-YFP.Il17a-GFP* reporter mice with EAE and treated with control and miR-122-5p antagomiRs. Results are mean + SD from 3 independent experiments (n = 9-11). Each dot represents an individual mouse. (f) Frequency of CD8$^+$ and γδ$^+$ T cells, B cells, monocytes, macrophages, neutrophils and dendritic cells in cervical and lumbar LNs (cLNs) of triple Foxp3-hCD2.Ifng-YFP.Il17a-GFP reporter mice with

EAE and treated with control and miR-122-5p antagomiRs. Results are mean ± SD from 3 independent experiments (n = 9-10). Each dot represents an individual mouse.

Fig. S6. Gating strategies for immune cells populations. (a) Gating strategy for T cells: cells were selected based on a FSC/SSC plot. After selection of live singlets, lymphocytes were gated on a FSC-A/CD45 plot to select $CD45^+$ immune cells. After this, lymphocyte populations were defined as following: γδ T cells - $CD3^+TCR\delta^+$, $CD4^+$ T cells - $CD3^+$ $TCR\delta^-CD4^+CD8^-$, and $CD8^+$ T cells - $CD3^+$ $TCR\delta^-CD4^-CD8^+$. (b) Gating strategy for myeloid and B cells: cells were selected based on a FSC/SSC plot. After selection of live singlets, lymphocytes were gated on a FSC-A/CD45 plot to select $CD45^+$ immune cells. After this, immune cell populations were defined as: B cells - $CD19^+CD3^-$, monocytes: $CD11B^+LY6G^-LY6C^+$, macrophages - $CD11B^+LY6G^-LY6C^-F4/80^+$, Neutrophils - $CD11B^+LY6C^-LY6G^+$, and dendritic cells - $CD45^+CD11C^+$.

Fig. S7. AntagomiR treatment for miR-126a does not impact EAE progression (a) RT-qPCR analysis of miR-126a-5p expression in spleen (SPL), liver (LV) and heart (HT) harvested from antagomiR-treated mice at day 13 post immunization. (b) EAE clinical signs and weight daily for mice treated with miR-126a-5p or control antagomiRs. Results are mean ± SD from 1 or 2 independent experiments (n = 3-7). Control mice are from the same experiment as shown in Figures 5 and 6. (c) Frequency of $FoxP3^+$, IFN-γ^+ and IL-$17A^+$ $CD4^+$ T cells in draining lymph nodes (dLNs - inguinal, axillary and brachial) and cervical and lumbar LNs (cLNs) of triple Foxp3-hCD2.Ifng-YFP.Il17a-GFP reporter mice with EAE and treated with control and miR-126a-5p antagomiRs. Results are mean ± SD from 1 or 2 independent experiments (n = 3-7). Each dot represents an individual mouse. Control mice are the same as in figure 5 and 6.

Fig. S8. Treatment with miR-1247-5p antagomiR induces an unantecipated upregulation of miR-1247-5p levels. (a) RT-qPCR analysis of miR-1247-5p expression in spleen (SPL), liver (LV) and heart

(HT) harvested from antagomiR-treated mice at day 13 post immunization. (b) RT-qPCR analysis of Trapc9 and Synj2bp expression in spleen (SPL), liver (LV) and heart (HT) harvested from antagomiR-treated mice at day 13 post immunization.

Fig. S9. Lack of effect of miR-1247 antagomiR in non-CD4$^+$ T-cell immune cell populations. (a) Pie charts depicting the relative number of mice treated with control and miR-122-5p antagomiRs reaching the onset of clinical symptoms or the peak plateau stage (defined as 3 days with the same score ± 0,5) in a certain day.(b) Frequency of CD4$^+$ T cells in cervical and lumbar lymph nodes (cLNs) of triple Foxp3-hCD2.Ifng-YFP.Il17a-GFP reporter mice with EAE and treated with control and miR-122-5p antagomiRs. Results are mean ± SD from 3 independent experiments (n = 9-10). Each dot represents an individual mouse. (c) Representative flow cytometry plots of Foxp3$^+$ CD4$^+$ T cells in the draining lymph nodes (inguinal, axillary and brachial) of triple Foxp3-hCD2.Ifng-YFP.Il17a-GFP reporter mice with EAE and treated with control and miR-1247-5p antagomiRs. (d) Frequency and absolute numbers of Foxp3$^+$ CD4$^+$ T cells in the draining lymph nodes (inguinal, axillary and brachial) of triple Foxp3-hCD2.Ifng-YFP.Il17a-GFP reporter mice with EAE and treated with control and miR-1247-5p antagomiRs. Results are mean + SD from 3 independent experiments (n = 10-11). Each dot represents an individual mouse. (e) Frequency of CD8$^+$ and γδ$^+$ T cells, B cells, monocytes, macrophages, neutrophils and dendritic cells in cervical and lumbar LNs (cLNs) of triple Foxp3-hCD2.Ifng-YFP.Il17a-GFP reporter mice with EAE and treated with control and miR-122-5p antagomiRs. Results are mean ± SD from 3 independent experiments (n = 9-10). Each dot represents an individual mouse.

Table S1. Genes differentially expressed between Teff and Treg cells

Table S2. Candidate mRNA targets identified by differential Ago2-RIPseq

Table S3. Primers used for qPCR analysis

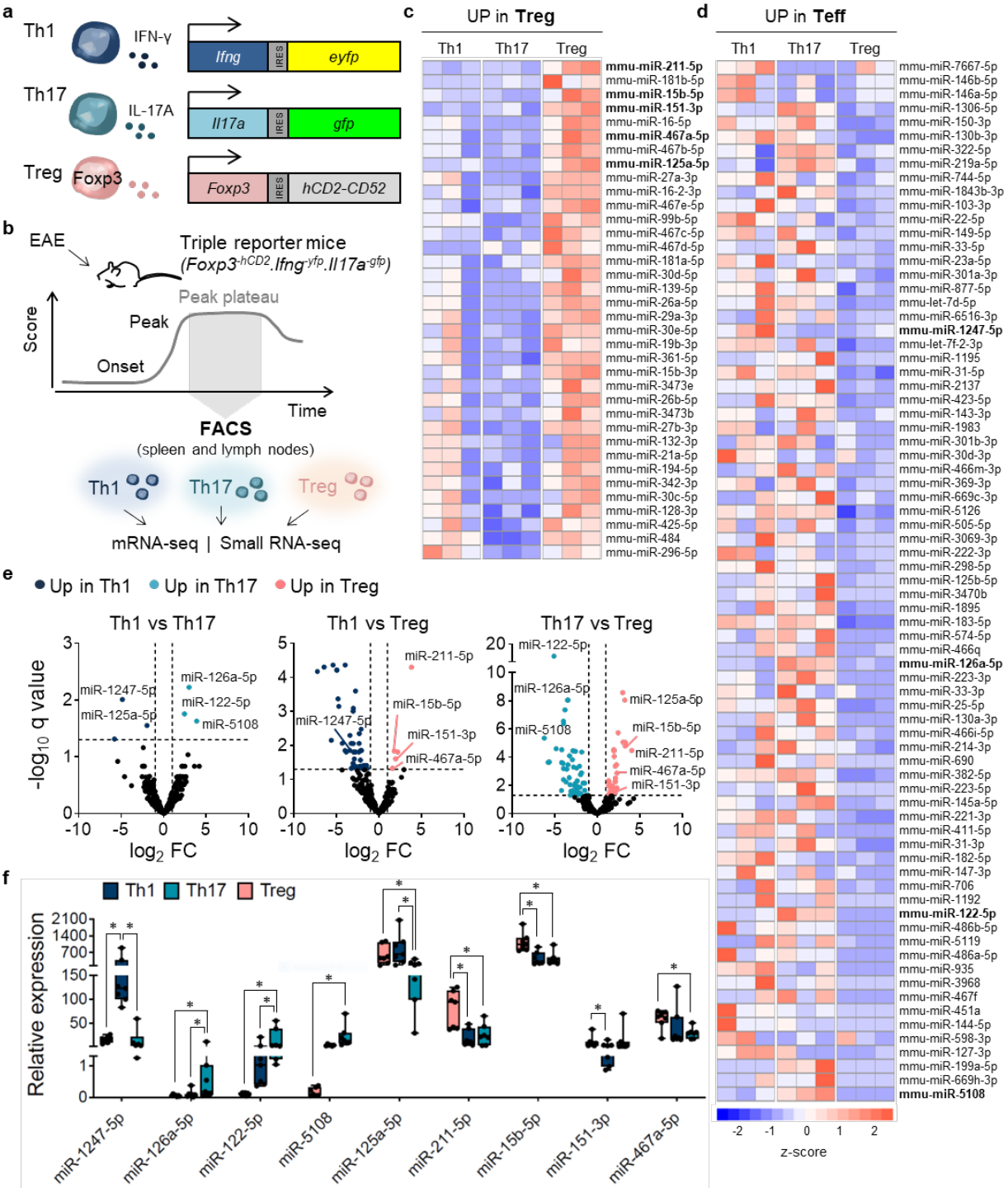

Fig. 1. Identification of the miRNomes of Th1, Th17 and Treg cells from EAE-challenged *Foxp3*^{hCD2}.*Ifng*^{YFP}.*IL17a*^{GFP} reporter mice.

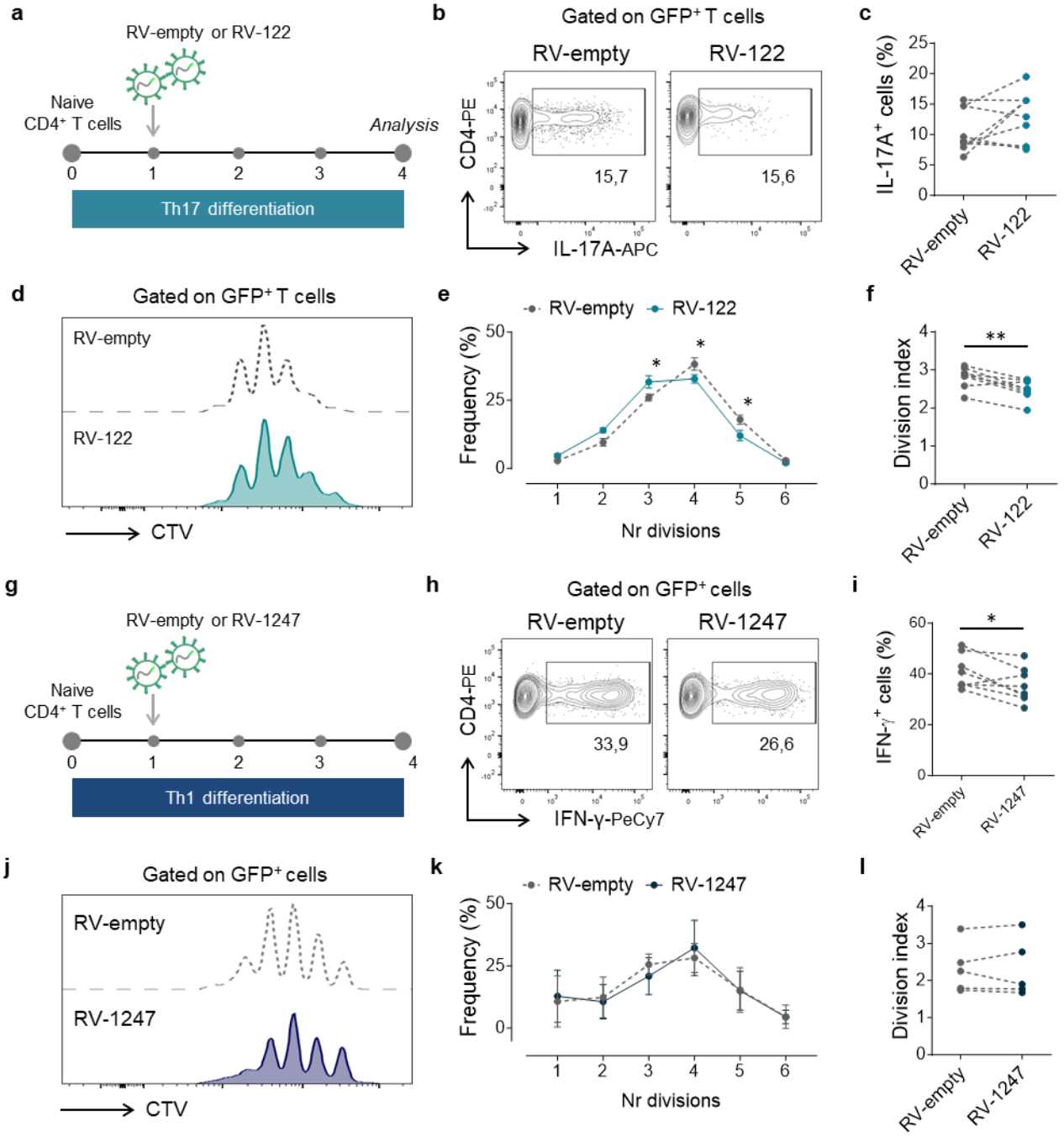

Fig. 2. miR-122-5p and miR-1247 intrinsically impact Th17 cell proliferation and Th1 cell function.

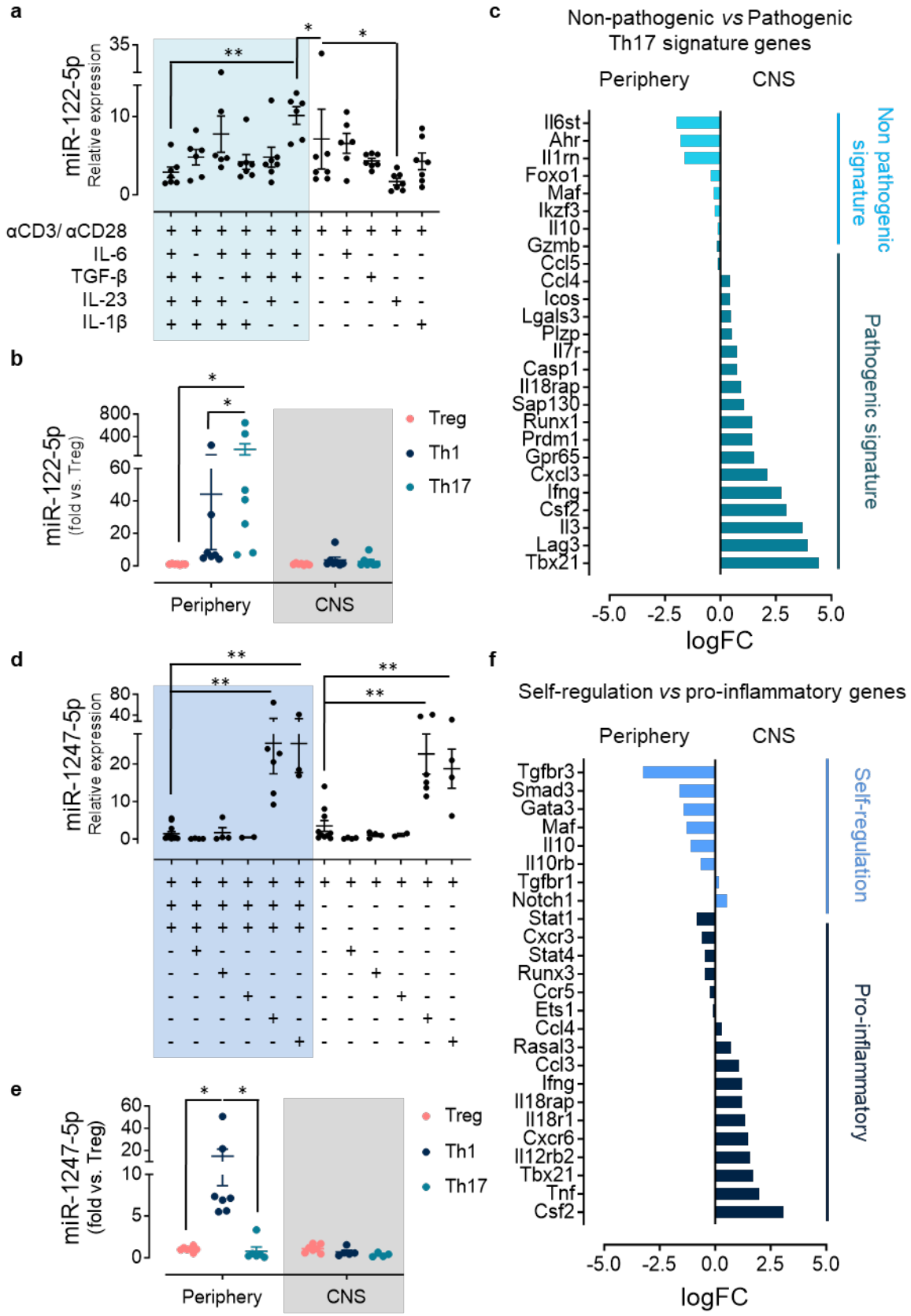

Fig. 3. miR-122 and miR-1247 act as brakes on pro-inflammatory Th17/Th1 phenotypes that are subverted in the CNS.

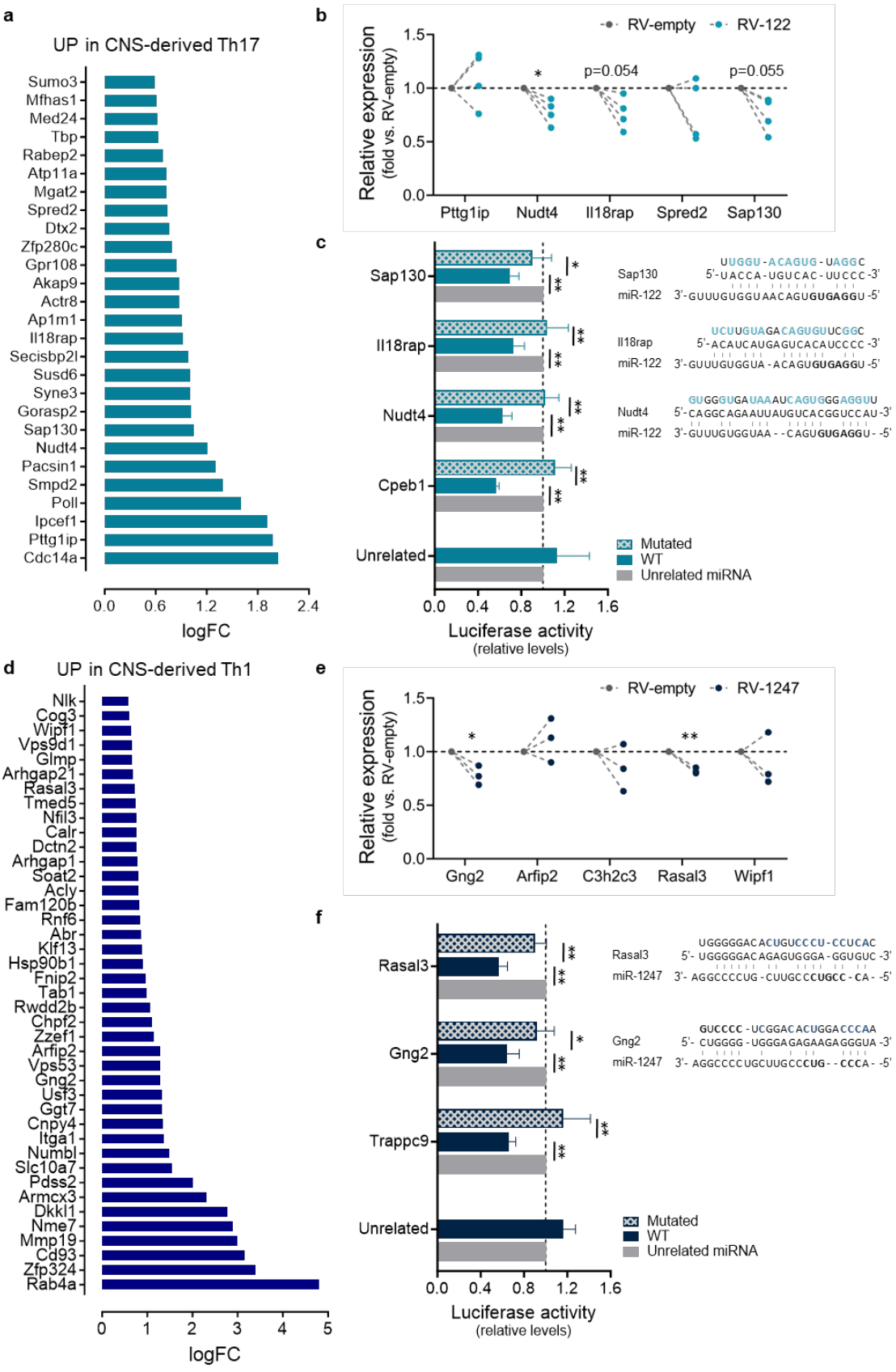

Fig. 4. Identification of putative mRNA targets of miR-122-5p and miR-1247-5p in Th17 and Th1 cells.

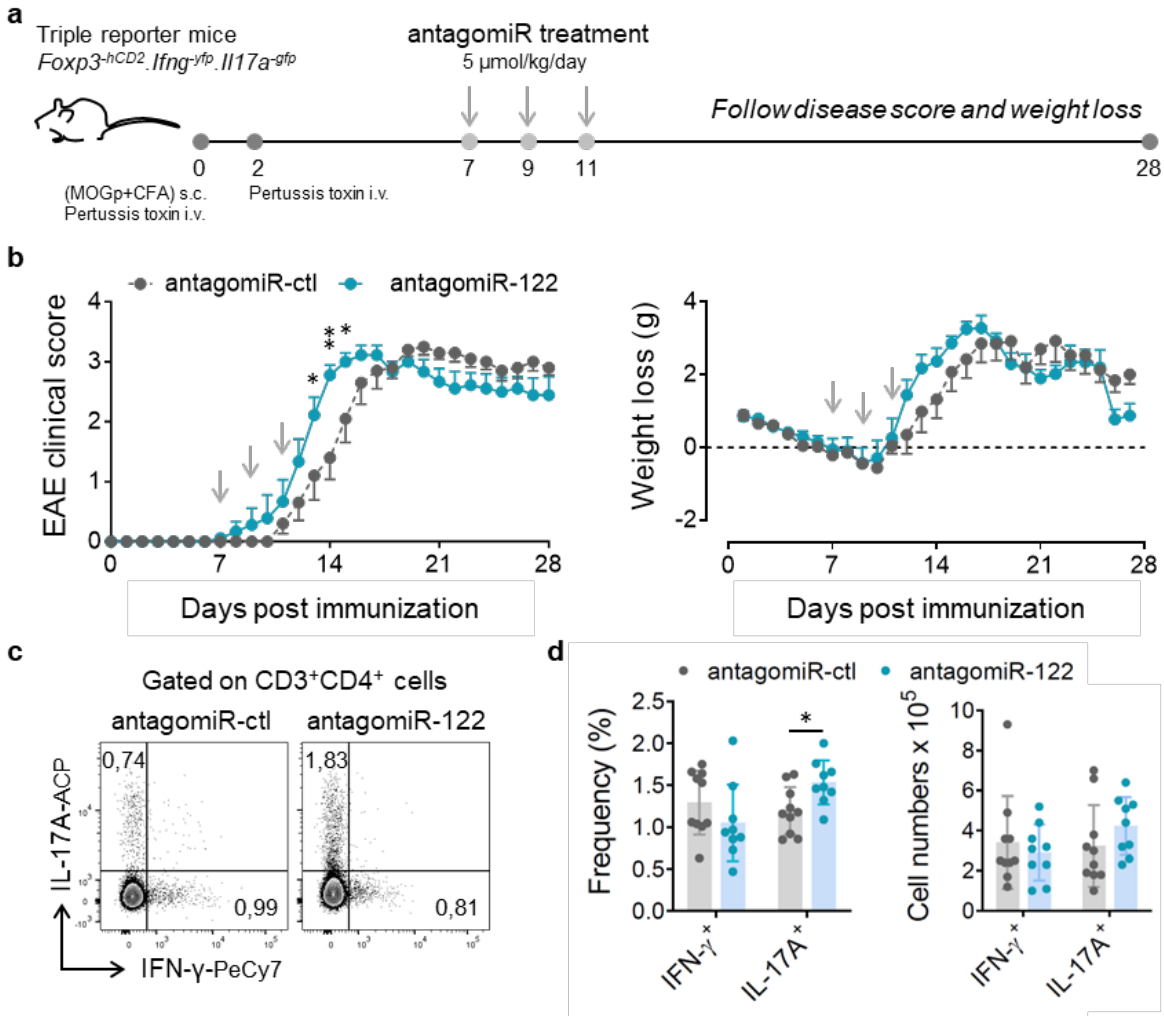

Fig. 5. miR-122-5p inhibition antecipates EAE onset.

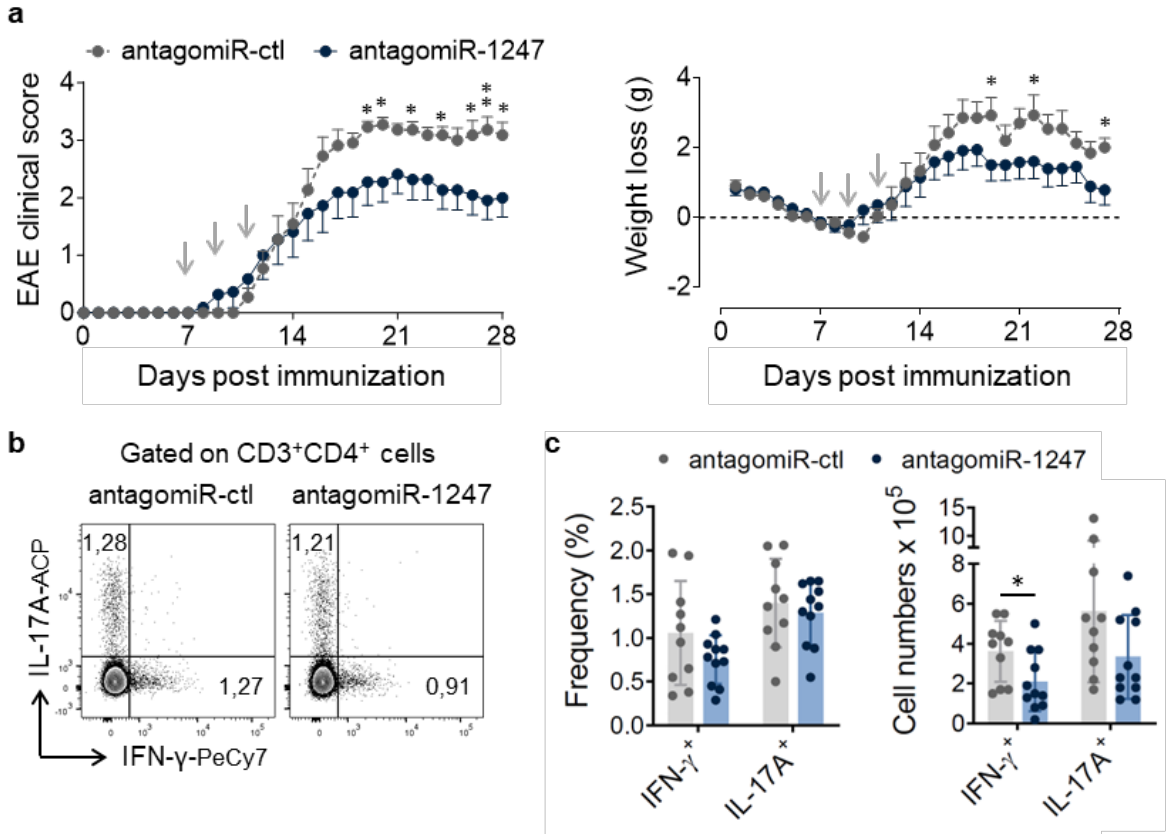

Fig. 6. miR-1247-5p limits EAE severity.

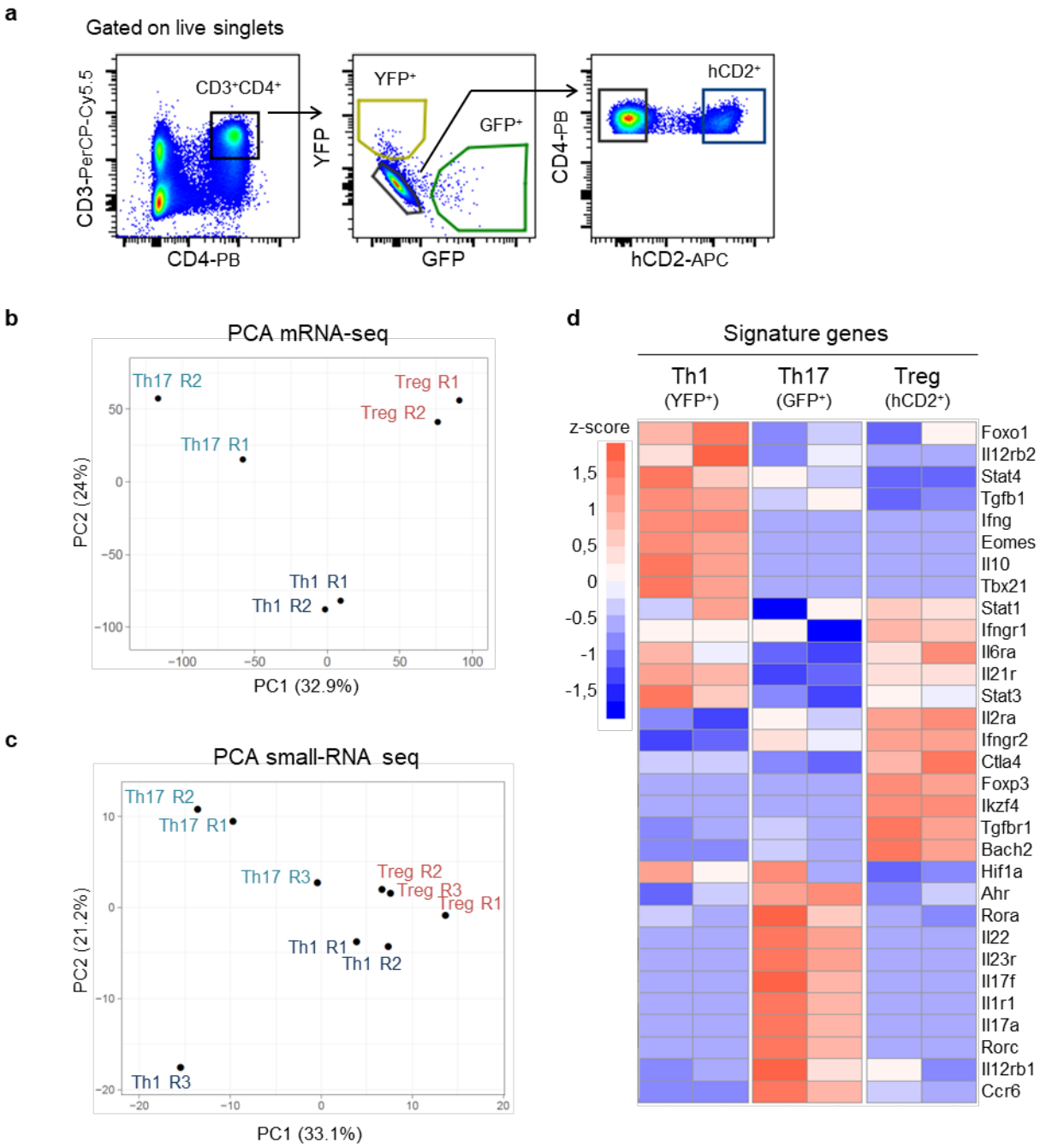

Fig S1. *In vivo* Isolation of Th1, Th17 and Treg cell populations and their global characterization

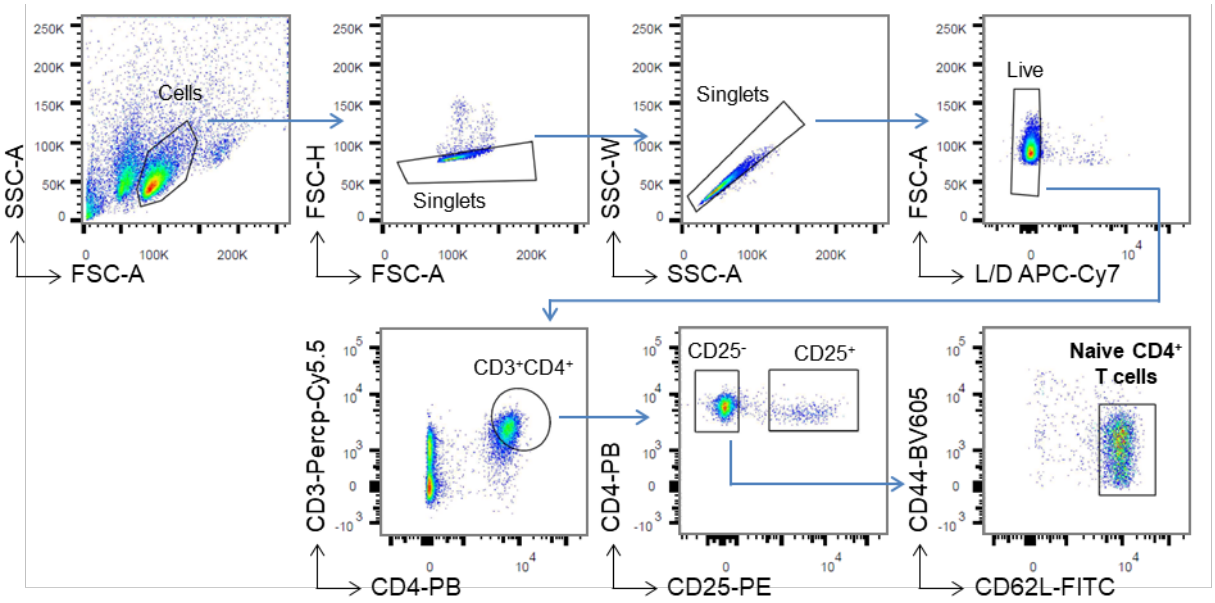

Fig. S2. FACS gating strategy for naïve CD4$^+$ T cells.

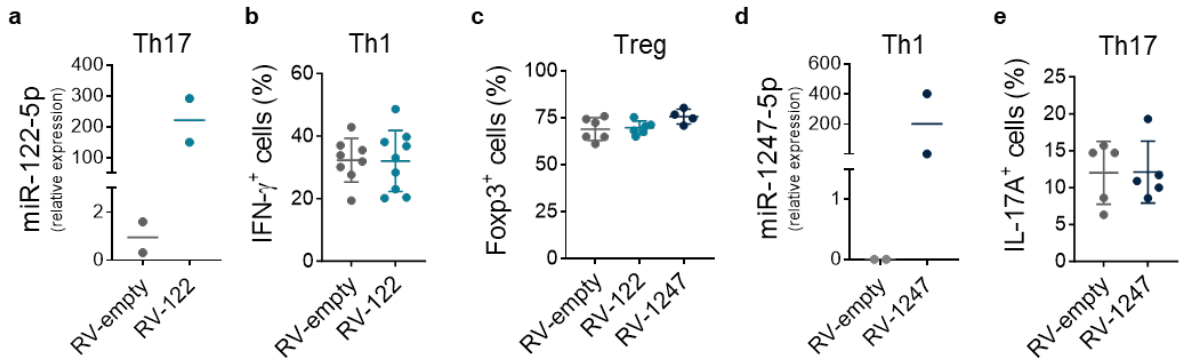

Fig. S3. miR-122-5p and miR-1247-5p overexpression does not impact Teff and Treg differentiation *in vitro*

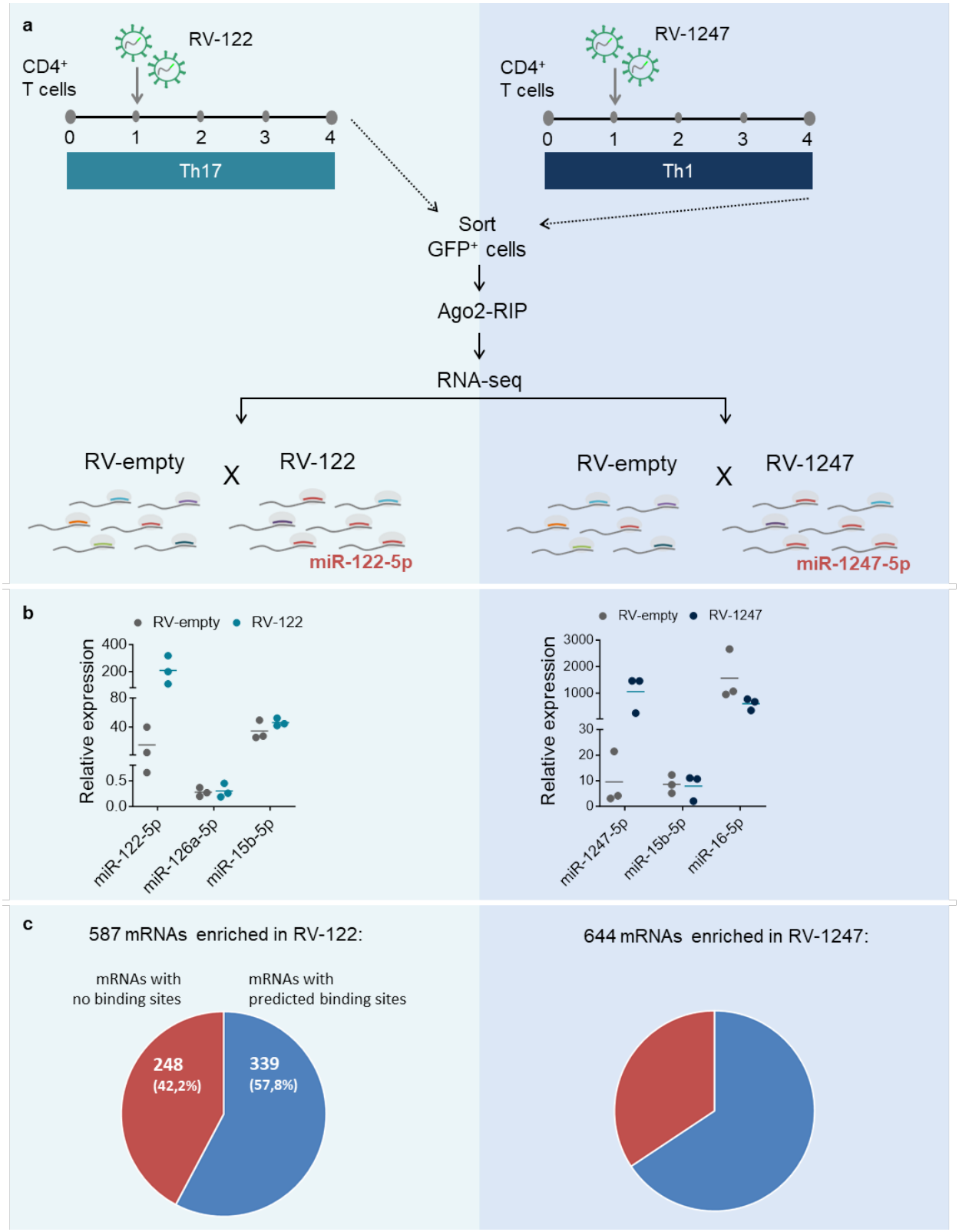

Fig. S4. Identification of miR-122-5p and miR-1247-5p targets using differential Ago-RIPseq

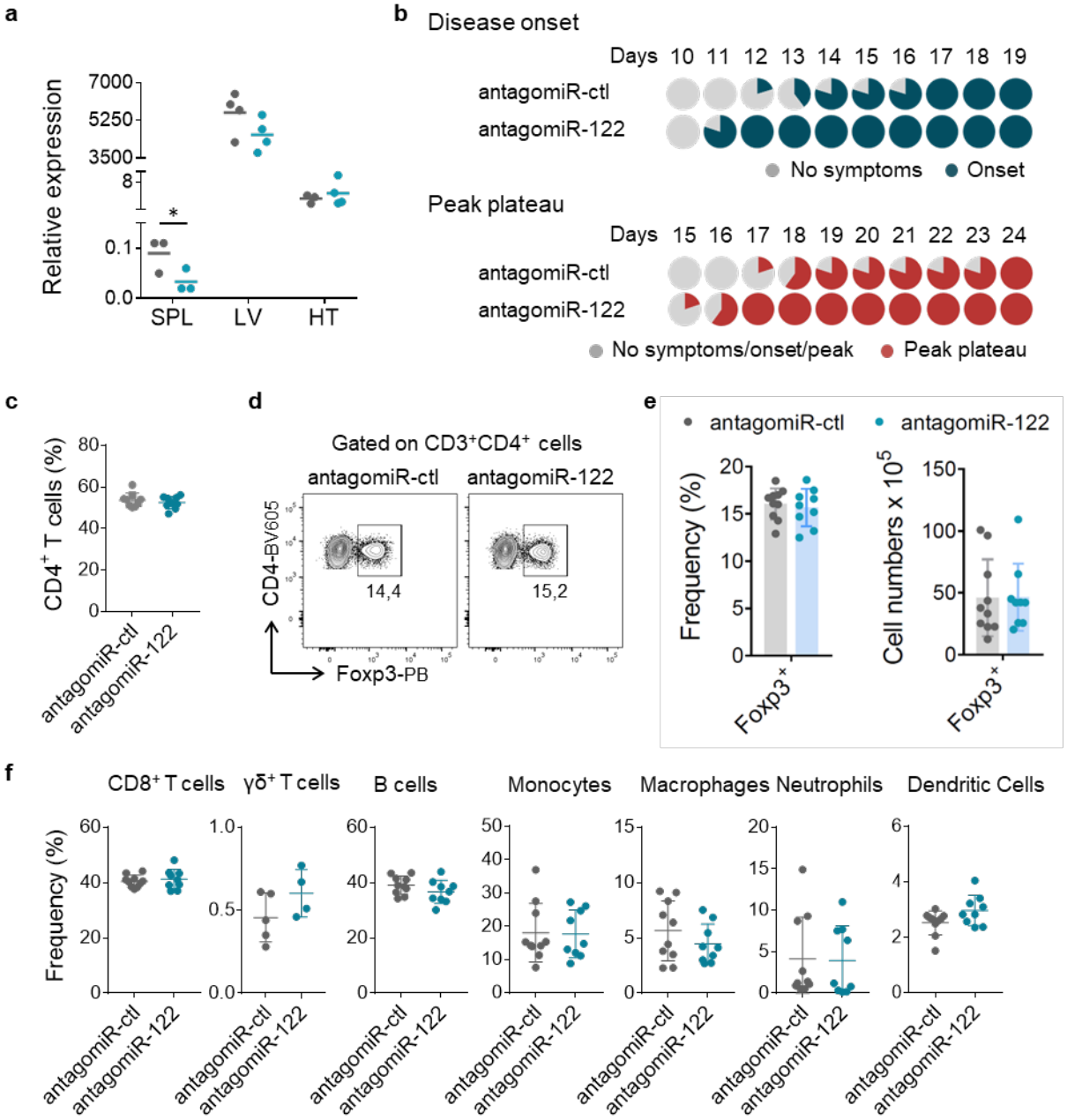

Fig. S5. Lack of effect of miR-122-5p antagomiR in non-CD4$^+$ T-cell immune cell populations.

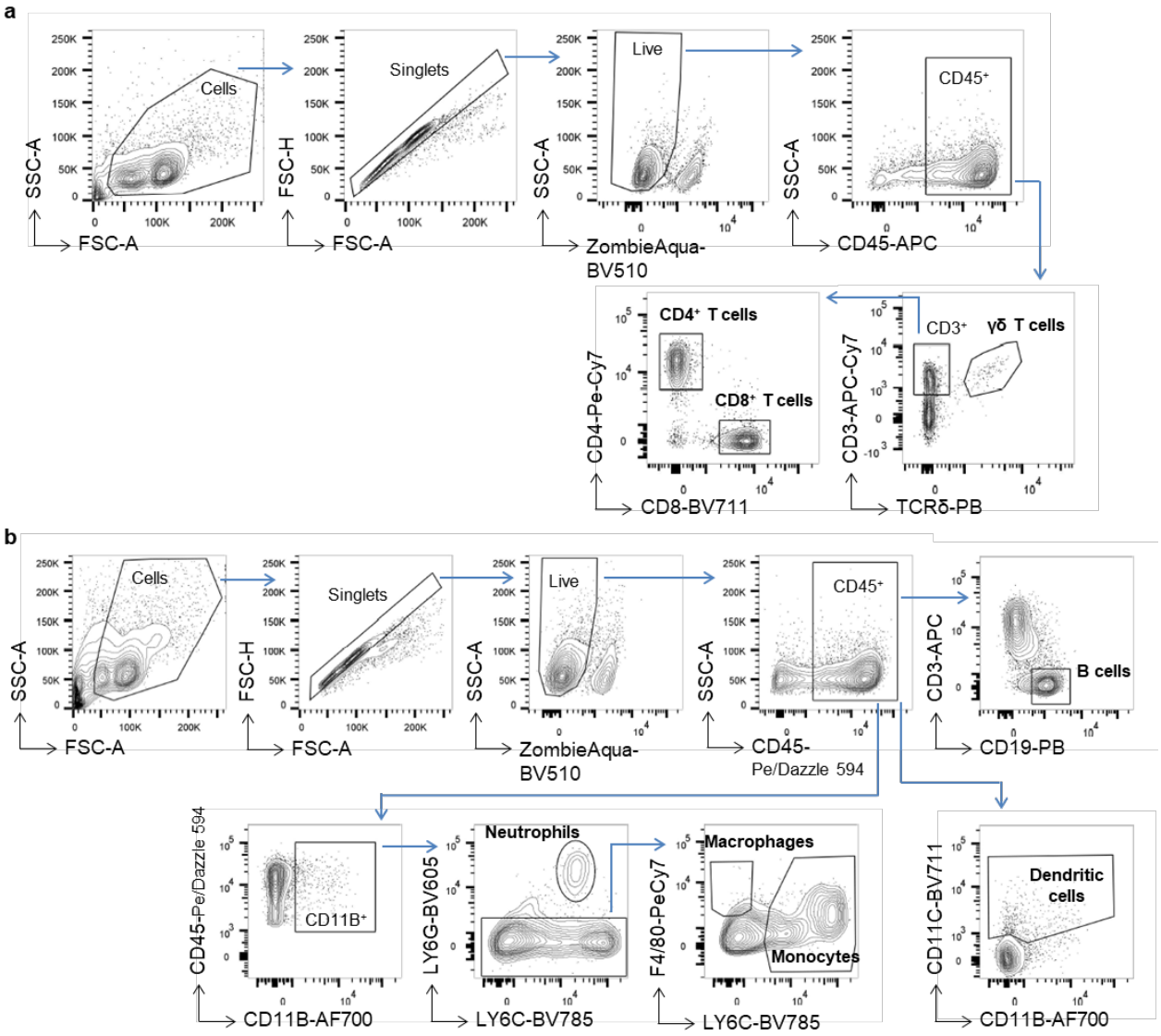

Fig. S6. Gating strategies for immune cells populations.

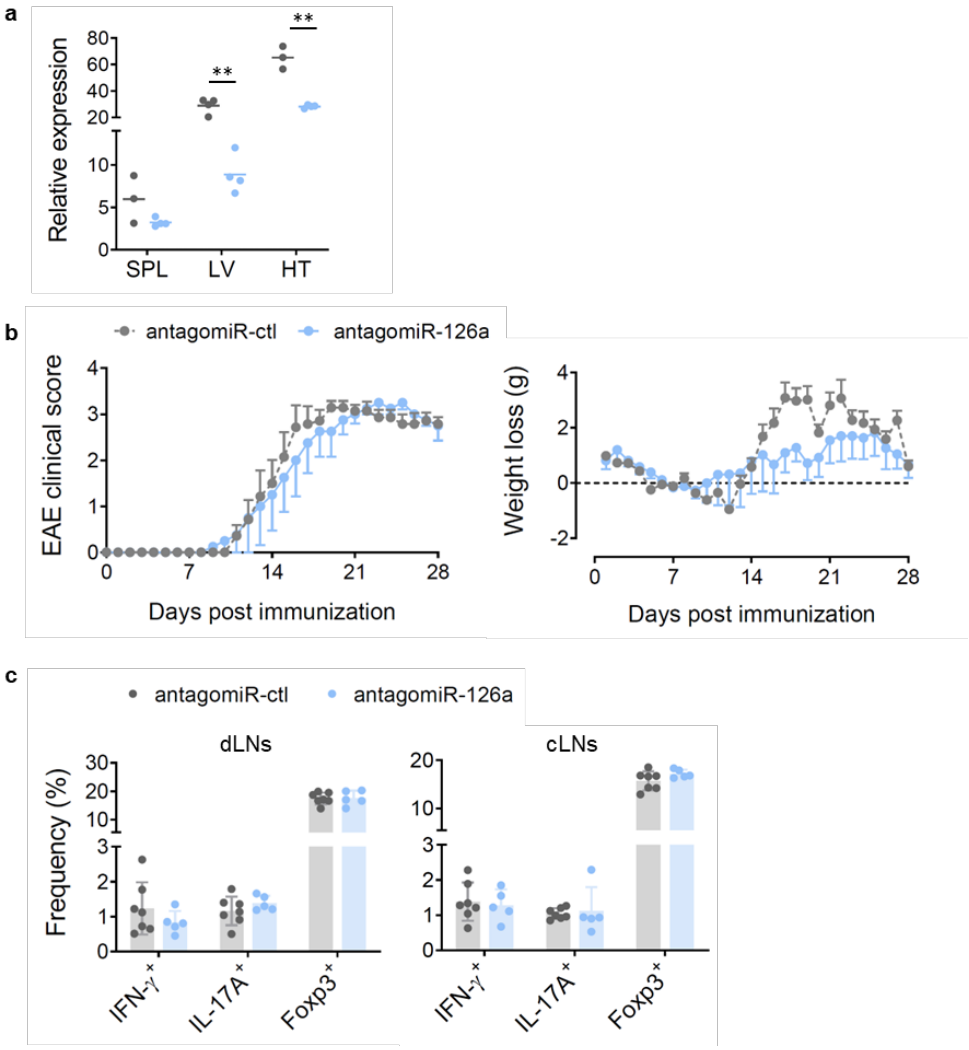

Fig. S7. AntagomiR treatment for miR-126a does not impact EAE progression

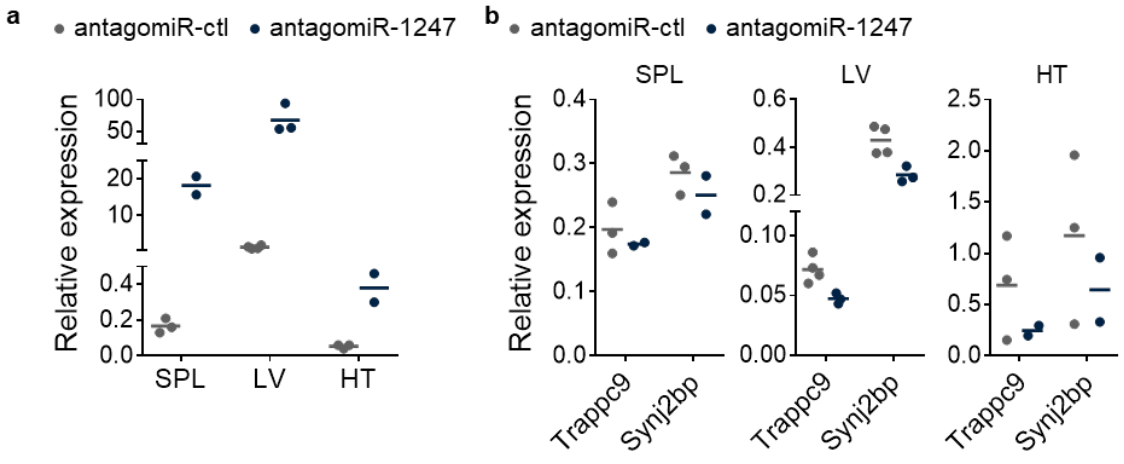

Fig. S8. Treatment with miR-1247-5p antagomiR induces an unantecipated upregulation of miR-1247-5p levels.

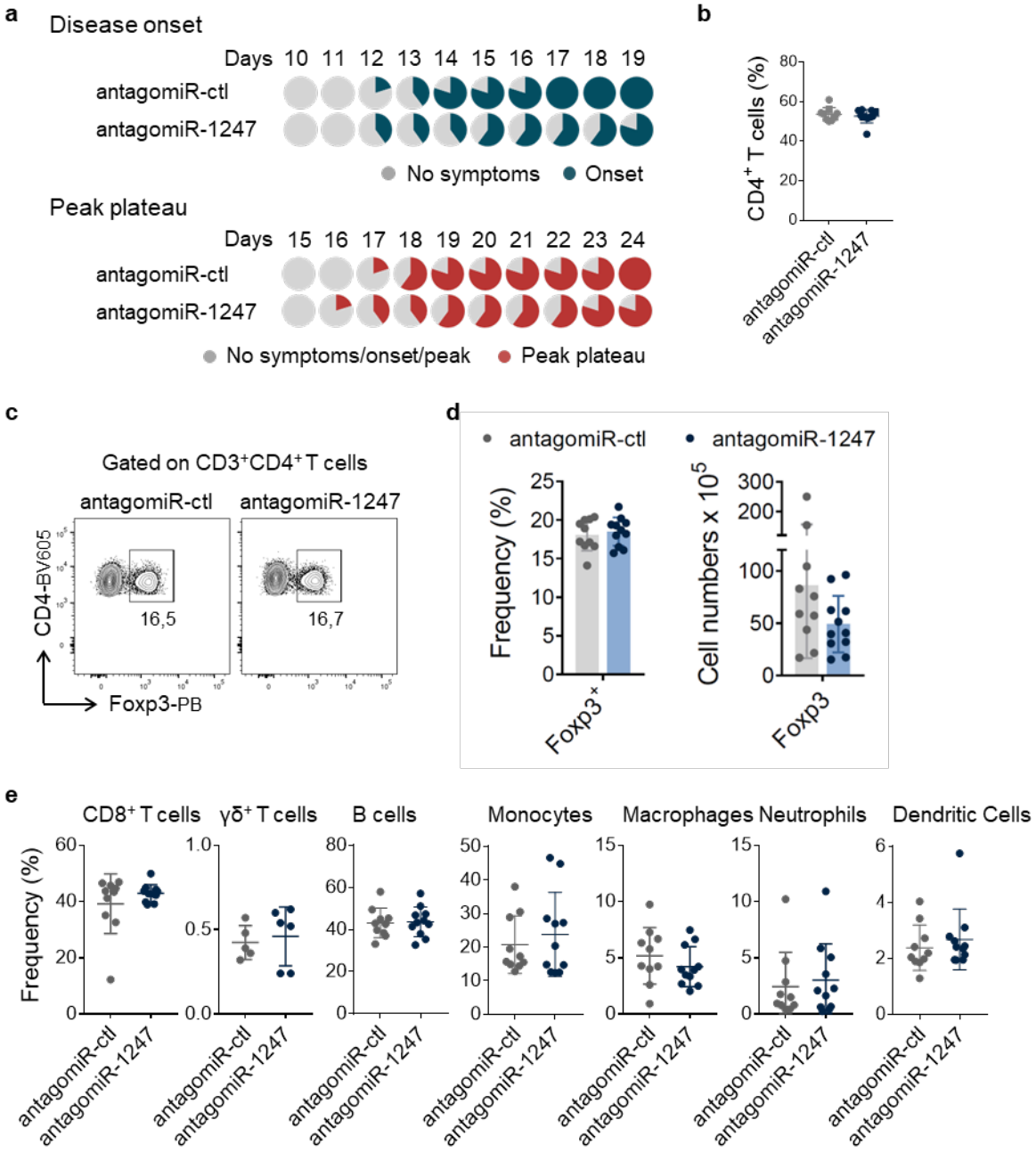

Fig. S9. Lack of effect of miR-1247 antagomiR in non-CD4$^+$ T-cell immune cell populations.

Table S1. Genes differentially expressed between Teff and Treg cells

	CPM									Th vs Treg		Th1 vs Treg		Th17 vs Treg	
Mature.ID	Th1_SPL_R01	Th1_SPL_R02	Th1_SPL_R03	Th17_SPL_R01	Th17_SPL_R02	Th17_SPL_R03	Treg_SPL_R01	Treg_SPL_R02	Treg_SPL_R03	logFC	FDR	logFC	FDR	logFC	FDR
mmu-miR-211-5p	11,1987	7,3423	22,7771	14,6501	9,8020	0,0000	93,4616	217,0190	232,8192	3,7714	0,0000	3,8246	0,0001	4,0454	0,0000
mmu-miR-181b-5p	11,1987	0,0000	0,0000	0,0000	19,6039	0,0000	124,6154	19,2906	44,7729	2,5838	0,0435	2,9338	0,0514	2,0494	0,1524
mmu-miR-15b-5p	1623,8148	1534,5321	774,4218	908,3043	352,8706	353,7415	2025,0010	9027,9896	6859,2131	2,2393	0,0007	1,7896	0,0144	3,2698	0,0000
mmu-miR-151-3p	26,1304	44,0536	22,7771	29,3001	58,8118	0,0000	124,6154	154,3246	182,0766	1,8267	0,0139	1,9586	0,0247	1,9108	0,0193
mmu-miR-16-5p	10791,8356	12727,8058	1480,5124	2842,1134	2950,3900	1768,7074	13801,1604	27860,4145	25583,2531	1,7508	0,0235	1,1873	0,2325	2,9749	0,0000
mmu-miR-467a-5p	365,8249	352,4284	45,5542	161,1508	284,2568	147,3923	529,6156	1355,1630	1071,5655	1,6765	0,0060	1,5857	0,0473	2,1088	0,0004
mmu-miR-467b-5p	37,3291	36,7113	0,0000	14,6501	29,4059	0,0000	62,3077	135,0340	107,4550	1,6288	0,0413	1,4615	0,1298	2,3041	0,0152
mmu-miR-125a-5p	1791,7956	1842,9070	2596,5909	556,7026	382,2764	589,5691	2679,2320	6534,6826	6817,4250	1,5604	0,0521	0,9075	0,2521	3,2378	0,0000
mmu-miR-27a-3p	1243,0582	2129,2551	182,2169	278,3513	401,8804	29,4785	2180,7703	2488,4843	2253,5709	1,4847	0,1452	0,7775	0,4687	3,0287	0,0000
mmu-miR-16-2-3p	257,5706	370,7841	68,3313	219,7510	254,8510	0,0000	685,3849	694,4607	674,5788	1,4160	0,0435	1,2364	0,1216	1,8129	0,0108
mmu-miR-467e-5p	414,3527	253,3079	0,0000	249,0512	372,4745	176,8707	623,0772	897,0118	999,9288	1,3789	0,0586	1,5908	0,1216	1,4555	0,0088
mmu-miR-99b-5p	205,3099	312,0460	204,9940	29,3001	29,4059	88,4354	591,9234	356,8757	459,6688	1,3647	0,1336	0,6595	0,4687	3,3025	0,0000
mmu-miR-467c-5p	156,7821	99,1205	91,1085	29,3001	88,2176	58,9569	405,0002	289,3586	220,8798	1,3474	0,0707	1,0262	0,2687	2,0725	0,0056
mmu-miR-467d-5p	100,7885	106,4628	0,0000	14,6501	88,2176	58,9569	186,9232	250,7775	229,8344	1,3269	0,0716	1,1747	0,1923	1,8228	0,0152
mmu-miR-181a-5p	85,8569	73,4226	113,8856	278,3513	98,0196	294,7846	747,6927	409,9247	307,4408	1,3470	0,1336	2,2034	0,0155	0,9969	0,2376
mmu-miR-30d-5p	190,3783	231,2812	0,0000	73,2503	49,0098	147,3923	186,9232	569,0720	399,9715	1,3143	0,0985	1,0600	0,2739	2,1494	0,0029
mmu-miR-139-5p	1754,4665	1861,2626	409,9880	820,4039	607,7215	825,3968	3302,3093	3805,0661	2444,6021	1,3060	0,0368	1,0261	0,2334	1,9447	0,0000
mmu-miR-26a-5p	992,9534	1049,9430	136,6627	468,8022	362,6725	324,2630	1401,9237	1866,3632	1695,4017	1,2406	0,0632	0,9389	0,3125	1,9366	0,0000
mmu-miR-29a-3p	20889,3505	35397,0302	3598,7839	5889,3278	8292,4582	3655,3286	26543,0895	40042,4132	41632,8566	1,2270	0,1452	0,6562	0,5371	2,4367	0,0000
mmu-miR-30e-5p	115,7201	297,3615	22,7771	87,9004	49,0098	0,0000	342,6925	265,2454	289,5316	1,2238	0,1786	0,7037	0,4980	2,3054	0,0013
mmu-miR-19b-3p	5618,0258	12331,3238	250,5482	1948,4592	4499,0996	1149,6598	16013,0845	6462,3430	8235,2345	1,1825	0,2809	0,7586	0,6108	1,9081	0,0149
mmu-miR-361-5p	377,0237	477,2468	91,1085	131,8506	137,2274	0,0000	529,6156	554,6041	579,0632	1,0900	0,2106	0,5040	0,5683	-0,4301	0,6715
mmu-miR-15b-3p	1362,5112	1912,6584	455,5423	849,7040	1470,2940	913,8322	2523,4627	3240,8168	3581,8345	1,0730	0,0463	1,0694	0,1655	1,3665	0,0054
mmu-miR-3473e	455,4147	1468,4518	250,5482	556,7026	421,4843	442,1768	934,6158	2483,6617	1167,0811	0,9743	0,1654	0,7907	0,4461	1,5223	0,0097
mmu-miR-26b-5p	854,8358	759,9238	136,6627	366,2517	509,7019	117,9138	685,3849	1456,4385	1387,9609	0,9719	0,1870	0,7019	0,4548	1,6054	0,0147
mmu-miR-3473b	451,6818	1464,7807	250,5482	556,7026	411,6823	442,1768	903,4620	2459,5484	1149,1719	0,9564	0,1781	0,7706	0,4516	1,5097	0,0108
mmu-miR-27b-3p	1724,6033	2070,5170	296,1025	366,2517	617,5235	294,7846	1900,3855	2030,3331	1856,5842	0,8503	0,3221	0,2971	0,7698	1,9810	0,0001
mmu-miR-132-3p	556,2032	580,0385	273,3254	219,7510	127,4255	58,9569	218,0770	892,1891	955,1559	0,7542	0,3947	0,2034	0,8223	2,1370	0,0049
mmu-miR-21a-5p	34477,1339	34526,9725	6104,2663	18429,7871	8762,9522	4480,7254	14175,0067	51544,4192	47993,5977	0,7196	0,4352	0,2895	0,7897	1,6543	0,0390
mmu-miR-194-5p	339,6946	436,8644	68,3313	87,9004	225,4451	58,9569	311,5386	559,4267	435,7899	0,6856	0,4152	0,2958	0,7545	1,5327	0,0243
mmu-miR-342-3p	21561,2738	19831,4413	9976,3755	4321,7704	15447,8890	7988,6617	20156,5480	27291,3425	30860,4893	0,6332	0,3785	0,3149	0,6529	1,3383	0,0424
mmu-miR-30c-5p	2422,6570	3527,9554	751,6447	1054,8050	1176,2352	1090,7029	1682,3085	3650,7415	3862,4116	0,5120	0,4814	0,1744	0,8528	1,3074	0,0108
mmu-miR-128-3p	265,0364	315,7171	182,2169	58,6003	176,4353	58,9569	218,0770	438,8606	346,2440	0,4892	0,5608	0,0653	0,9398	1,5076	0,0337
mmu-miR-425-5p	500,2096	873,7288	318,8796	102,5505	235,2470	412,6984	872,3081	554,6041	671,5940	0,4806	0,6205	0,0515	0,9523	1,3966	0,0480
mmu-miR-484	1205,7291	1435,4116	1184,4099	498,1024	509,7019	648,5260	1495,3853	1687,9254	1387,9609	0,3715	0,6595	-0,0689	0,9317	1,3301	0,0046
mmu-miR-296-5p	171,7137	124,8184	68,3313	29,3001	9,8020	29,4785	62,3077	130,2114	92,5307	-0,0730	0,9485	-0,7130	0,4548	2,1110	0,0315
mmu-miR-7667-5p	41,0620	44,0536	91,1085	0,0000	0,0000	0,0000	0,0000	67,5170	29,8486	-0,0743	0,9551	-0,7454	0,5407		
mmu-miR-146b-5p	9899,6707	11835,7214	3279,9043	1728,7082	6812,3622	1238,0952	2305,3857	4403,0740	4799,6583	-0,9268	0,3199	-1,4002	0,0473	0,0615	0,9469
mmu-miR-146a-5p	85408,9241	104682,2564	30612,4400	17243,1315	52763,9507	12380,9517	19097,3167	37119,8910	42322,3597	-0,9562	0,2777	-1,4511	0,0388	0,0869	0,9226
mmu-miR-1306-5p	205,3099	198,2410	182,2169	395,5519	362,6725	235,8277	124,6154	192,9058	170,1371	-1,0961	0,1311	-0,5828	0,4891	-1,1728	0,0464
mmu-miR-150-3p	1097,4748	741,5682	774,4218	922,9544	1284,0568	795,9183	529,6156	549,7814	614,8816	-1,1374	0,0494	-0,9722	0,1961	-0,9918	0,0552
mmu-miR-130b-3p	530,0729	638,7765	865,5303	659,2531	578,3156	442,1768	373,8463	313,4719	304,4559	-1,3415	0,0378	-1,4251	0,0750	-0,7138	0,4290
mmu-miR-322-5p	145,5834	205,5832	0,0000	322,3015	362,6725	265,3061	31,1539	106,0982	152,2280	-1,4840	0,1276	-0,5648	0,6105	-1,6783	0,0068
mmu-miR-219a-5p	26,1304	36,7113	0,0000	58,6003	88,2176	58,9569	31,1539	9,6453	26,8638	-1,5152	0,1797	-0,6844	0,6105	-1,9400	0,0372
mmu-miR-744-5p	279,9681	256,9791	614,9821	322,3015	98,0196	265,3061	62,3077	135,0340	205,9555	-1,5759	0,0716	-1,8560	0,0473	-0,7549	0,3767
mmu-miR-1843b-3p	261,3035	172,5431	364,4338	1186,6556	431,2862	678,0045	155,7693	274,8907	208,9403	-1,7186	0,0650	-0,6622	0,4873	-1,9595	0,0017
mmu-miR-103-3p	246,3719	267,9925	706,0905	322,3015	205,8412	294,7846	93,4616	110,9208	202,9706	-1,7362	0,0403	-1,9724	0,0473	-1,0535	0,1297
mmu-miR-22-5p	186,6454	267,9925	113,8856	58,6003	137,2274	0,0000	62,3077	43,4038	53,7275	-1,8197	0,0435	-2,3047	0,0045	-0,7892	0,4410
mmu-miR-149-5p	164,2479	220,2678	68,3313	293,0014	107,8216	58,9569	0,0000	67,5170	74,6216	-1,8536	0,0216	-1,7664	0,0388	-1,5859	0,0637
mmu-miR-33-5p	41,0620	29,3690	22,7771	87,9004	196,0392	58,9569	31,1539	33,7585	20,8940	-1,8646	0,1038	-2,8982	0,0250	-2,3561	0,0047
mmu-miR-23a-5p	358,3591	190,8987	660,5363	131,8506	215,6431	147,3923	62,3077	159,1473	92,5307	-1,8819	0,0413	-2,3570	0,0155	-0,7649	0,3272
mmu-miR-301a-3p	253,8377	400,1531	159,4398	380,9018	901,7803	176,8707	280,3847	96,4529	32,8335	-1,9267	0,0778	-1,4284	0,2474	-2,1927	0,0371
mmu-miR-877-5p	85,8569	80,7648	182,2169	58,6003	98,0196	88,4354	0,0000	43,4038	35,8183	-1,9511	0,0235	-2,0766	0,0406	-1,4035	0,1032
mmu-let-7d-5p	7835,3729	8032,4312	20727,1729	13404,8134	10488,0972	5659,8636	2803,8475	4277,6852	4742,9459	-1,9721	0,0075	-2,1383	0,0141	-1,4783	0,0068
mmu-miR-6516-3p	350,8933	135,8318	1731,0606	820,4039	411,6823	1061,2244	124,6154	376,1662	346,2440	-1,9820	0,0707	-1,9975	0,1485	-1,4950	0,0219
mmu-miR-1247-5p	67,1923	179,8853	318,8796	14,6501	0,0000	0,0000	0,0000	24,1132	62,6821	-1,9991	0,2210	-2,7490	0,0155	2,5913	0,0943
mmu-let-7f-2-3p	52,2607	66,0803	68,3313	29,3001	88,2176	29,4785	0,0000	19,2906	20,8940	-2,0808	0,0235	-2,0717	0,0418	-1,7302	0,0852
mmu-miR-1195	26,1304	22,0268	68,3313	87,9004	58,8118	294,7846	0,0000	38,5812	29,8486	-2,0823	0,0985	-0,4239	0,7545	-2,2893	0,0124
mmu-miR-31-5p	735,3828	1123,3656	501,0965	849,7040	872,3744	530,6122	218,0770	332,7624	155,2128	-2,1342	0,0004	-2,0881	0,0033	-1,8641	0,0013
mmu-miR-2137	227,7074	249,6368	432,7651	219,7510	225,4451	854,8752	93,4616	159,1473	83,5761	-2,1696	0,0177	-1,8187	0,0414		
mmu-miR-423-5p	2881,8046	2444,9722	9270,2850	5523,0761	4508,9016	5335,6006	965,7697	1890,4765	1910,3117	-2,1887	0,0060	-2,1753	0,0269	-1,8319	0,0000
mmu-miR-143-3p	41,0620	47,7247	0,0000	29,3001	127,4255	58,9569	0,0000	4,8226	26,8638	-2,2058	0,0518	-1,5386	0,2325	-2,4224	0,0187
mmu-miR-1983	111,9872	121,1473	0,0000	43,9502	176,4353	29,4785	62,3077	24,1132	11,9394	-2,3011	0,0368	-2,2832	0,0417	-2,1957	0,0316
mmu-miR-301b-3p	14,9316	55,0669	45,5542	87,9004	58,8118	0,0000	31,1539	9,6453	8,9546	-2,3345	0,0435	-1,9943	0,1376	-2,4490	0,0189
mmu-miR-30d-3p	78,3911	33,0402	22,7771	0,0000	19,6039	0,0000	31,1539	4,8226	5,9697	-2,3505	0,0707	-2,9846	0,0155		
mmu-miR-466m-3p	3,7329	11,0134	45,5542	87,9004	9,8020	58,9569	0,0000	0,0000	14,9243	-2,4128	0,1276	-0,9250	0,6108	-2,6582	0,0316
mmu-miR-369-3p	33,5962	55,0669	0,0000	43,9502	107,8216	29,4785	0,0000	14,4679	11,9394	-2,4196	0,0235	-1,9234	0,1088	-2,6131	0,0074
mmu-miR-669c-3p	3,7329	3,6711	45,5542	29,3001	19,6039	88,4354	0,0000	14,4679	0,0000	-2,4223	0,1499	-0,1616	0,8770	-2,7598	0,0337
mmu-miR-5126	343,4275	209,2544	432,7651	366,2517	323,4647	383,2199	0,0000	120,5661	104,4702	-2,4253	0,0009	-2,3305	0,0087	-2,0871	0,0004
mmu-miR-505-5p	55,9936	11,0134	68,3313	14,6501	78,4157	29,4785	0,0000	14,4679	8,9546	-2,4552	0,0422	-2,3318	0,0910	-2,2407	0,0438
mmu-miR-3069-3p	37,3291	25,6979	250,5482	87,9004	29,4059	0,0000	0,0000	24,1132	14,9243	-2,5610	0,0575	-3,0487	0,0418	-1,4911	0,1897
mmu-miR-222-3p	489,0109	462,5623	45,5542	117,2006	264,6529	0,0000	31,1539	62,6944	50,7427	-2,5799	0,0177	-3,0415	0,0010	-1,6163	0,0835
mmu-miR-298-5p	82,1240	80,7648	273,3254	58,6003	78,4157	58,9569	0,0000	19,2906	32,8335	-2,6081	0,0103	-3,0143	0,0088	-1,6223	0,0795
mmu-miR-125b-5p	37,3291	36,7113	136,6627	73,2503	49,0098	324,2630	0,0000	14,4679	35,8183	-2,7015	0,0322	-1,7836	0,1838	-2,6738	0,0104
mmu-miR-3470b	0,0000	22,0268	45,5542	29,3001	9,8020	147,3923	0,0000	4,8226	8,9546	-2,7489	0,0901	-1,5147	0,4027	-2,8552	0,0243
mmu-miR-1895	93,3227	40,3824	364,4338	205,1010	137,2274	324,2630	0,0000	48,2264	50,7427	-2,7841	0,0133	-2,5386	0,0546	-2,4333	0,0006
mmu-miR-183-5p	343,4275	308,3749	182,2169	336,9516	303,8608	235,8277	31,1539	43,4038	71,6367	-2,8548	0,0000	-2,7557	0,0002	-2,5896	0,0000
mmu-miR-574-5p	100,7885	36,7113	227,7711	263,7012	107,8216	383,2199	31,1539	33,7585	35,8183	-2,9028	0,0103	-2,1775	0,0750	-2,9391	0,0001
mmu-miR-466q	11,1987	14,6845	68,3313	43,9502	9,8020	88,4354	0,0000	0,0000	8,9546	-2,9600	0,0381	-2,3492	0,1529	-2,9182	0,0243
mmu-miR-126a-5p	85,8569	69,7515	0,0000	600,6528	431,2862	353,7415	31,1539	53,0491	44,7729	-2,9747	0,0235	-0,7809	0,4805	-3,4955	0,0000
mmu-miR-223-3p	888,4320	1585,9279	364,4338	2124,2600	3695,3389	1827,6643	373,8463	274,8907	179,0917	-3,0369	0,0011	-2,0642	0,0141	-3,4474	0,0000
mmu-miR-33-3p	48,5278	40,3824	0,0000	117,2006	29,4059	0,0000	31,1539	4,8226	2,9849	-3,1041	0,0139	-2,8982	0,0250	-3,1922	0,0087
mmu-miR-25-5p	37,3291	22,0268	22,7771	43,9502	68,6137	29,4785	0,0000	4,8226	5,9697	-3,1437	0,0073	-2,6984	0,0418	-3,3017	0,0028
mmu-miR-130a-3p	18,6645	18,3556	91,1085	43,9502	147,0294	58,9569	0,0000	9,6453	8,9546	-3,2567	0,0133	-2,1781	0,1376	-3,4551	0,0003
mmu-miR-466i-5p	545,0045	234,9523	3689,8923	1084,1051	882,1764	2623,5826	93,4616	337,5851	229,8344	-3,3863	0,0059	-3,4130	0,0141	-2,8664	0,0000
mmu-miR-214-3p	18,6645	36,7113	136,6627	190,4509	68,6137	58,9569	62,3077	4,8226	0,0000	-3,5549	0,0235	-3,0673	0,0910	-4,0270	0,0003
mmu-miR-690	4031,5401	2881,8366	82043,1614	17697,2837	7351,4700	39206,3471	1495,3853	5121,6479	3934,0482	-3,5689	0,0137	-3,8328	0,0155	-2,7882	0,0005
mmu-miR-382-5p	37,3291	44,0536	45,5542	73,2503	68,6137	29,4785	0,0000	0,0000	8,9546	-3,5819	0,0012	-3,2668	0,0087	-3,5854	0,0007
mmu-miR-223-5p	11,1987	22,0268	0,0000	29,3001	127,4255	29,4785	0,0000	4,8226	2,9849	-3,6220	0,0153			-4,1929	0,0002
mmu-miR-145a-5p	33,5962	22,0268	0,0000	14,6501	78,4157	88,4354	0,0000	0,0000	5,9697	-3,6640	0,0063			-3,9710	0,0006
mmu-miR-221-3p	227,7074	249,6368	432,7651	395,5519	166,6333	88,4354	31,1539	19,2906	29,8486	-3,7992	0,0000	-3,9640	0,0000	-3,2579	0,0001
mmu-miR-411-5p	7,4658	44,0536	45,5542	14,6501	49,0098	0,0000	0,0000	0,0000	2,9849	-3,9055	0,0072	-3,9856	0,0141		
mmu-miR-31-3p	44,7949	73,4226	22,7771	73,2503	156,8314	58,9569	31,1539	4,8226	2,9849	-3,9220	0,0007	-3,3966	0,0051	-4,1788	0,0000
mmu-miR-182-5p	37,3291	47,7247	91,1085	14,6501	9,8020	0,0000	0,0000	4,8226	0,0000	-4,1255	0,0031	-4,7944	0,0004		
mmu-miR-147-3p	29,8633	179,8853	68,3313	14,6501	117,6235	0,0000	31,1539	0,0000	2,9849	-4,2994	0,0034	-4,7176	0,0007	-3,6638	0,0057
mmu-miR-706	294,8997	121,1473	3667,1152	981,5546	1068,4136	2564,6257	31,1539	173,6152	125,3642	-4,3189	0,0022	-4,2980	0,0086	-3,7917	0,0000
mmu-miR-1192	0,0000	0,0000	227,7711	14,6501	9,8020	147,3923	0,0000	0,0000	8,9546	-4,3191	0,0707			-3,1117	0,0260
mmu-miR-122-5p	418,0856	271,6636	728,8676	3442,7663	2058,4116	1798,1858	93,4616	77,1623	77,6064	-4,6176	0,0001	-3,0057	0,0008	-5,1012	0,0000
mmu-miR-486b-5p	1119,8723	106,4628	318,8796	483,4523	176,4353	265,3061	31,1539	24,1132	17,9092	-4,6489	0,0001	-4,9321	0,0001	-3,9607	0,0000
mmu-miR-5119	3,7329	11,0134	318,8796	263,7012	39,2078	235,8277	31,1539	4,8226	2,9849	-4,6638	0,0177	-4,3348	0,0526	-4,8326	0,0000
mmu-miR-486a-5p	1142,2697	106,4628	318,8796	483,4523	186,2372	265,3061	31,1539	24,1132	17,9092	-4,6669	0,0001	-4,9510	0,0001	-3,9788	0,0000
mmu-miR-935	59,7265	77,0937	113,8856	14,6501	9,8020	58,9569	0,0000	4,8226	0,0000	-4,8032	0,0005	-5,3969	0,0000	-3,1643	0,0491
mmu-miR-3968	7,4658	14,6845	91,1085	0,0000	9,8020	29,4785	0,0000	0,0000	0,0000	-4,8432	0,0069	-5,5891	0,0071		
mmu-miR-467f	3,7329	7,3423	45,5542	73,2503	9,8020	58,9569	0,0000	0,0000	0,0000	-5,3566	0,0046			-5,6368	0,0002
mmu-miR-451a	328,4959	40,3824	68,3313	43,9502	19,6039	58,9569	0,0000	0,0000	2,9849	-5,7537	0,0004	-6,4381	0,0000	-3,9696	0,0039
mmu-miR-144-5p	175,4467	22,0268	22,7771	43,9502	9,8020	0,0000	0,0000	0,0000	0,0000	-6,2638	0,0007	-7,2203	0,0001		
mmu-miR-598-3p	29,8633	40,3824	0,0000	0,0000	9,8020	0,0000	31,1539	4,8226	0,0000			-3,0347	0,0336		
mmu-miR-127-3p	11,1987	22,0268	22,7771	14,6501	0,0000	0,0000	0,0000	0,0000	2,9849			-3,2421	0,0473		
mmu-miR-199a-5p	0,0000	0,0000	0,0000	14,6501	9,8020	29,4785	0,0000	0,0000	0,0000					-4,2004	0,0226
mmu-miR-669h-3p	0,0000	0,0000	68,3313	14,6501	19,6039	147,3923	0,0000	0,0000	0,0000					-5,7686	0,0002
mmu-miR-5108	3,7329	0,0000	22,7771	43,9502	68,6137	88,4354	0,0000	0,0000	0,0000					-6,2302	0,0000

1064 **Table S2. Candidate mRNA targets identified by differential Ago2-RIPseq**

1065

Transcript	Log2FC	miR-binding site
miR-122 mRNA targets		
Th17 differentiation/ pathogenecity		
Spred2	2.46	3'UTR
Ipcef1	2.39	3'UTR (3)
Sumo3	2.34	3'UTR (4), CDS (3)
Sap130	2.12	CDS (2)
Il18rap	2.09	3'UTR
Cell activation and proliferation		
Gpr108	3.75	CDS (3)
Ap1m1	3.30	3'UTR, CDS
Gorasp2	2.51	3'UTR, CDS (2)
Pttg1ip	2.32	3'UTR (2)
Med24	2.06	CDS (3)
Mfhas1	1.94	CDS
Cdc14a	1.94	CDS (5)
Susd6	1.92	3'UTR (2)
Dtx2	1.90	CDS (8)
Akap9	1.89	CDS
Nudt4	1.61	3'UTR
miR-1247 mRNA targets		
Th1 differentiation and IFN-γ production		
Nlk	1.47	3'UTR
Chpf2	1.24	3'UTR (3)
Calr	1.18	3'UTR/CDS (2)
Soat2	1.12	3'UTR/CDS
Itga1	1.10	CDS
Zzef1	1.05	3'UTR (2)
Nfil3	0.88	CDS
Fnip2	0.78	3'UTR (2)/CDS
Cell activation and proliferation		
C3h2c3	2.60	3'UTR (4)
Gng2	2.50	3'UTR (6)
Tab1	2.26	CDS
Zfp324	1.49	CDS
Rasal3	1.38	3'UTR
Dctn2	1.31	3'UTR (2)
Arfip2	1.29	3'UTR (2)
Klf13	1.28	3'UTR (2)
Arhgap21	0.96	3'UTR /CDS(3)
Wipf1	0.94	3'UTR (6) /CDS (6)

1066

1067

1068

1069 **Table S3. Primers used for qPCR analysis**

1070

Gene	Sequence	
	Fwd primer	Rev primer
Zfp324	TCTGCCGCAACTCACATCTT	AAAGGCTTCTCTCCGGTGTG
Itga1	ATGACGCTCTGCCAAACTCA	TGTTGTACGCACTGTCTCCC
Gng2	GGAAGCCAACATCGACAGGA	AGGGTCTTCCTTGGCATGTG
Arfip2	ACGGACGGGATTCTAGGGAA	GGTCCTGACACCATCACCTG
Zzef1	CAACCCAGCAGGAGTCTGAG	CTCTGCTGTAGCTCGCTCTC
Chpf2	CGGAGTCTCCTATTGCGCTT	AGGGCTCTCCTCCTTCTCAG
Tab1	TCTGGAGTTGGTTCAGCGTC	GCCATTGAAGACCCCGTACA
Fnip2	AAAGAAGCGAGCAGAGCAGT	TAGAGCTGGCAGAGGCACTA
Klf13	CGCACCTGAGAACTCACACA	GATGGGGCAGCTGAACTTCT
C3h2c3	GCAAAGGAACAGCTGGCATC	TCGAGTCACATTCCCAGTGC
Soat2	CTGCGGTTTGGAGACAGGAT	GACACCAGGAACACTCCCAG
Dctn2	GGTACAGCGACTTGTCACCA	GTGGCCAAGTTTTCACGCAT
Calr	CCTGAATACTCCCCCGATGC	GCTTCTCTGCAGCCTTGGTA
Nfil3	ACCGCACAAGCTTCGGATTA	GTTCGTCACCTGCACTGAGA
Rasal3	GACCTAGGTGCTGAGAGGGA	GAGAAACAGAGGCTCCCACC
Arhgap21	CCCCAGAGTCTGCAATCCAG	GGCCCTCCTTCCTTCACTTG
Wipf1	CCCACCCTCCACATCAGTTC	CTGTTGGATCCACTTCGGCT
Nlk	ACAGCCATCTCTTCCTGTGC	CTCAGCCGCCCTTCATCTAG
Cdc14a	CCAGTACACCAGAAGCAGCA	AGGAGGAAGAGAGTGACCCC
Pttglip	GGTGAACTTCGAGGCCTTGA	CACTCTCCTCTCCTCCTGCT
Nudt4	TGAGTAGCAGTCGGTACCCA	CGAGCAGTCTGCCTAGCTTT
Gorasp2	ACCTACACGCCCCTTTGAAG	GCCGAGCTAATGGAGAGTCC
Susd6	GGGGGTTTCTGGGGATCAAG	CTTGGCATGTTCCTCCCACT
Ap1m1	TCCTCTTCGACAACACAGGC	TCGGGTGGGATGAAGGAGAT
Akap9	TGCTCTCTCTCTCCAGTCCC	AAGTTCACCTCGCCAGTCTG
Il18rap	TATTGGCCCCACAGACGAAC	GCAGCTGAGACTGGGACAAT
Spred2	TCGTGTGACACAAGCGATGA	ACCTGCACATCACTCCACAG
Ipcef1	CTGAGCAGGTCCACACACTT	GATCCAGCAGCTCTGTCTGG
Sap130	GAGAAGCAGGAGCCAGTTGT	CTAGGCATGGTAGGCTTCGG
Gpr108	TCGCCATTCTGCTGCAAGTA	TCCTCCTCATCCTCCTGTGG
Dtx2	GCCACTGTCTGCTCCTTCAT	CCTCATGGTGCCAGTGTTCT
Med24	AGATGGTGTCCTGCTCCTCT	GCAACTGAGTCGGTCACAGA
Mfhas1	GCCAGTTTGGAGAGCCTCAT	GGCACTGAGGTGAGCTGATT
Sumo3	GGCTCGGTGGTACAGTTCAA	GGGCTGGAGTGTCTGTTTCA
Actb	CGTGAAAAGATGACCCAGATCA	TGGTACGACCAGAGGCATACAG
Hprt	GACCTCTCGAAGTGTTGGAT	GCTTTGTATTTGGCTTTTCC
B2micro	CTGCAGAGTTAAGCATGCCAGTAT	ATCACATGTCTCGATCCCAGTAGA

1071

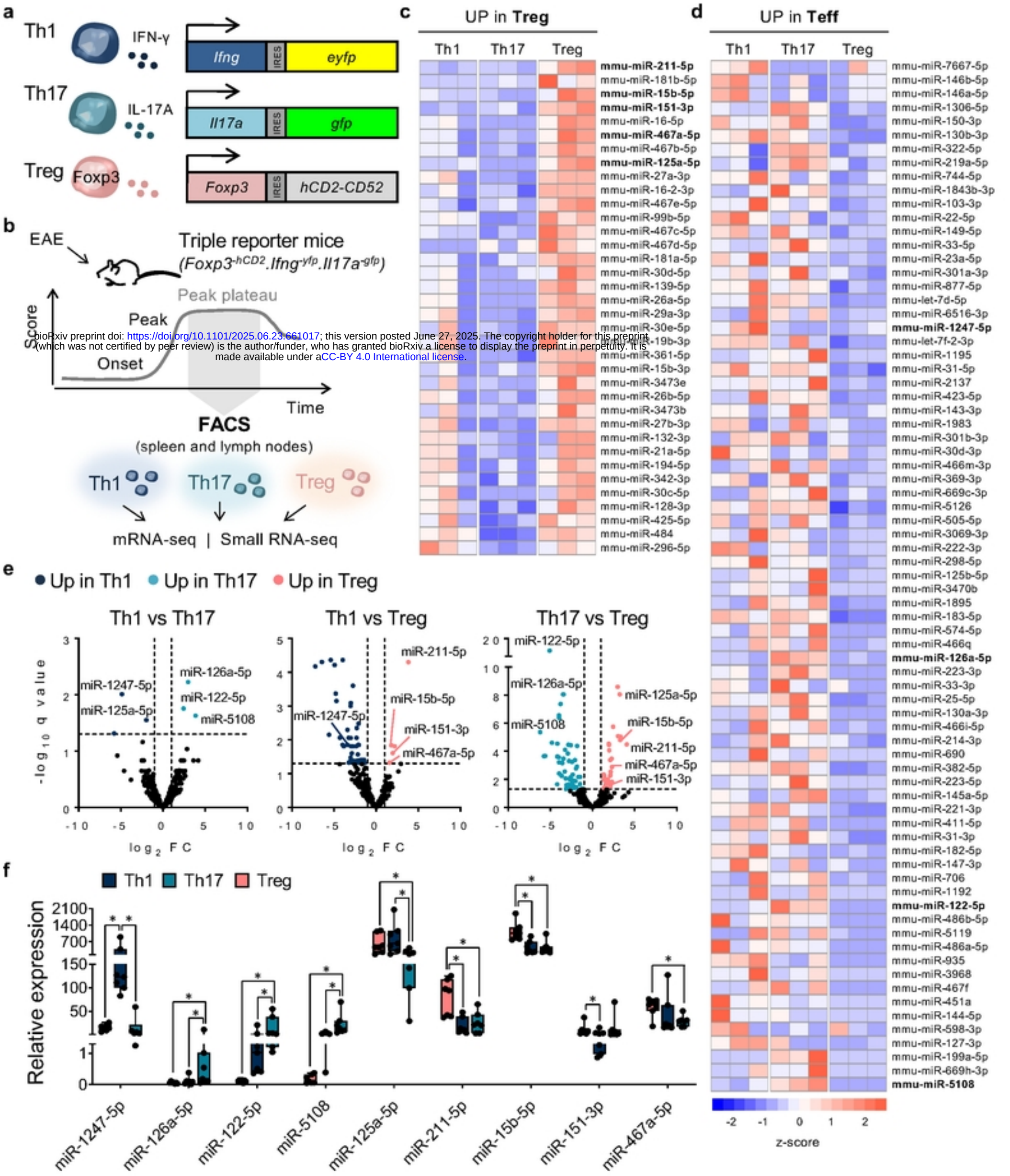

Fig 1. Identification of the miRNomes of Th1, Th17 and Treg cells purified from EAE-challenged *Foxp3*^{hCD2}.*Ifng*^{YFP}.*IL17a*^{GFP} reporter mice

Figure

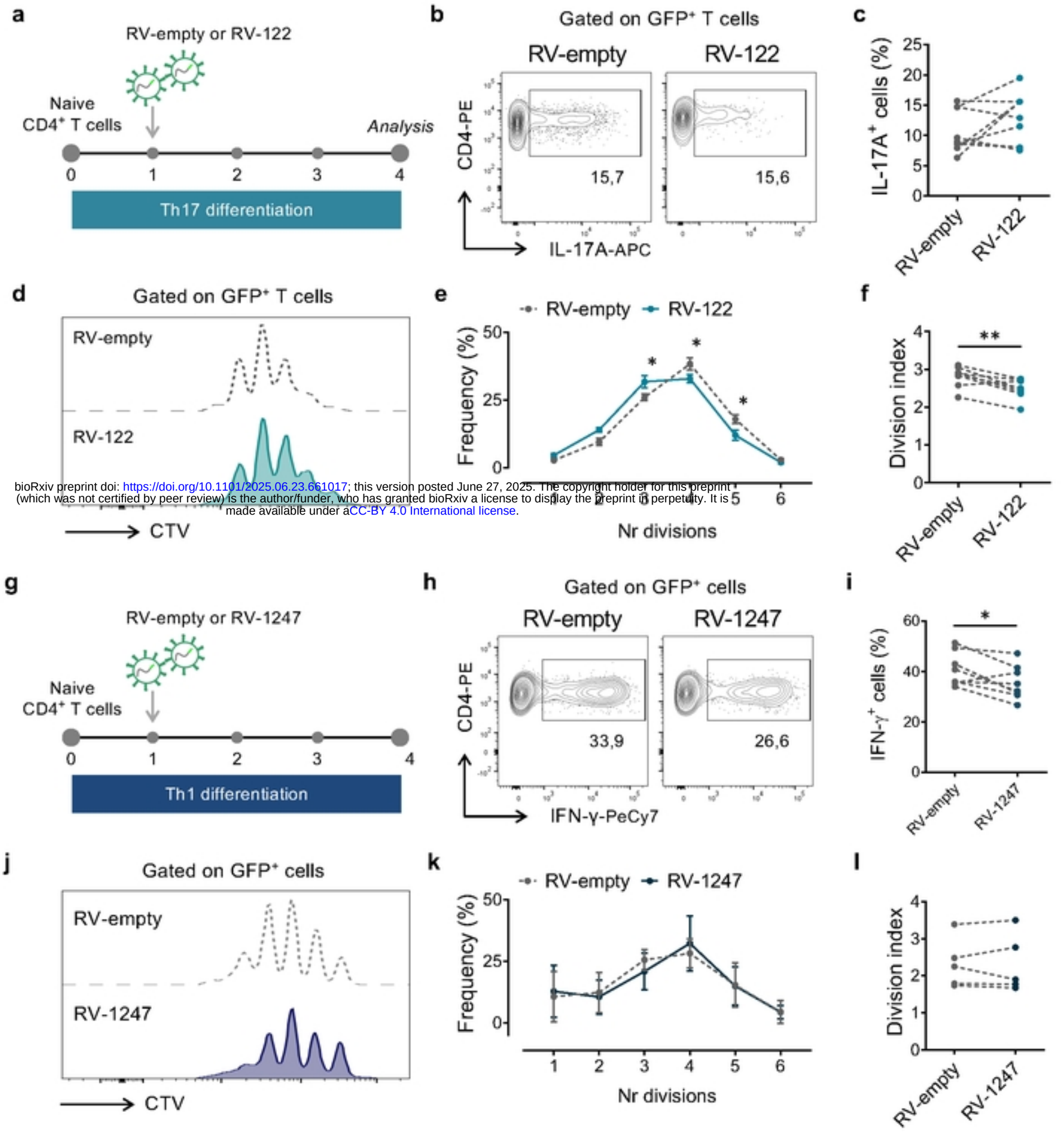

Fig. 2. miR-122-5p and miR-1247 intrinsically impact Th17 cell proliferation and Th1 cell function.

Figure

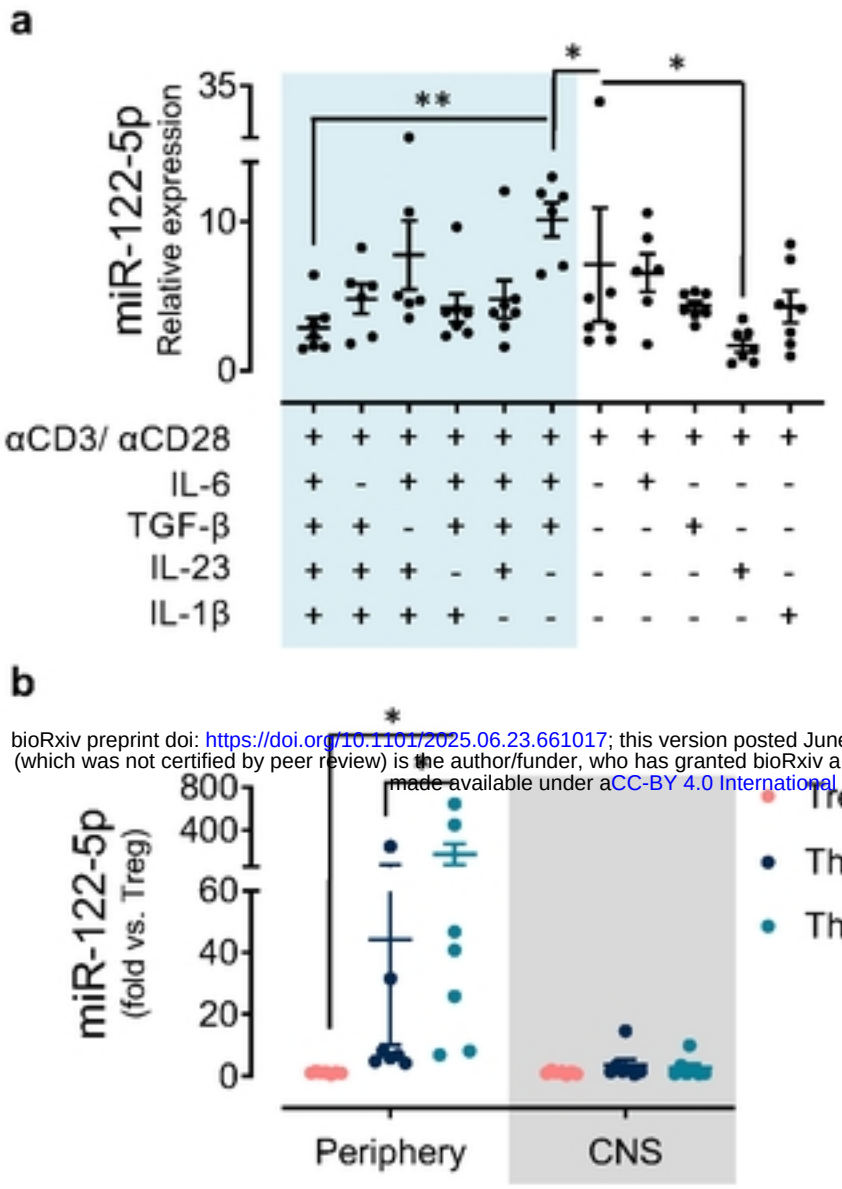

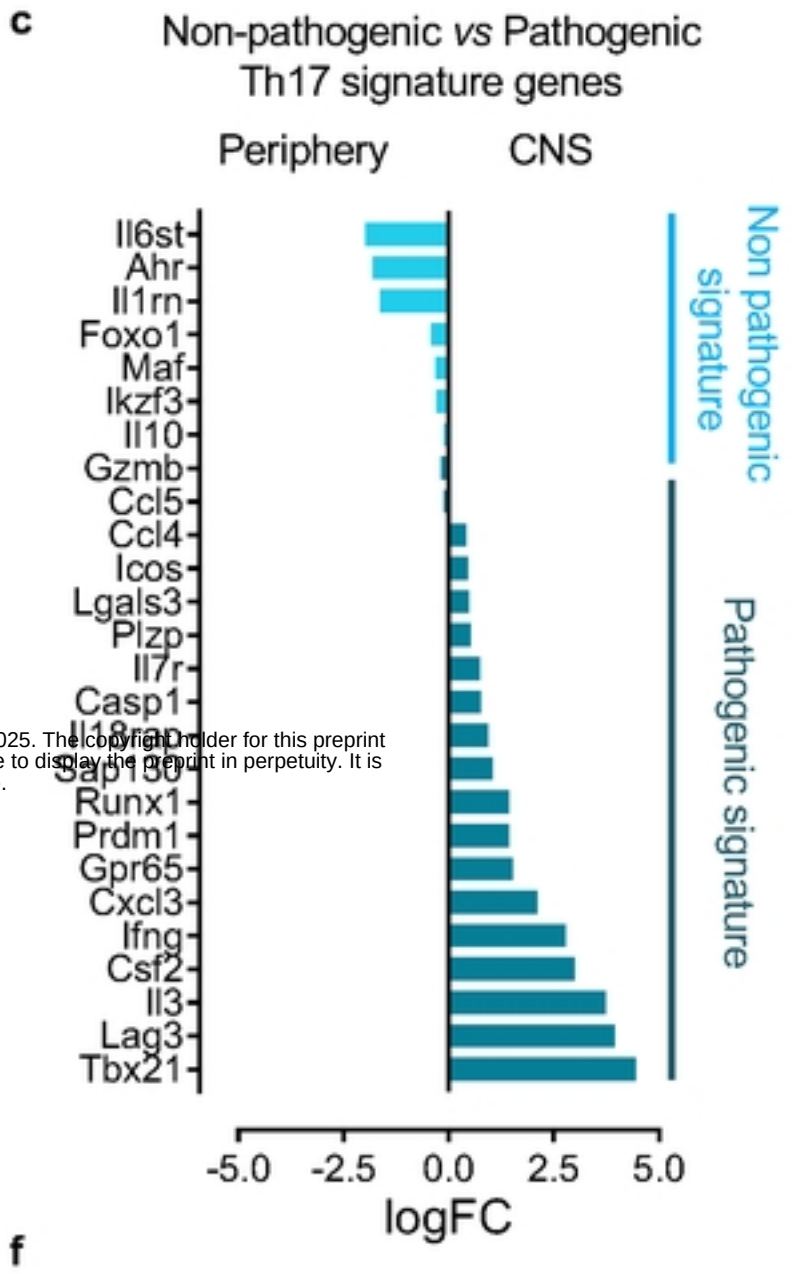

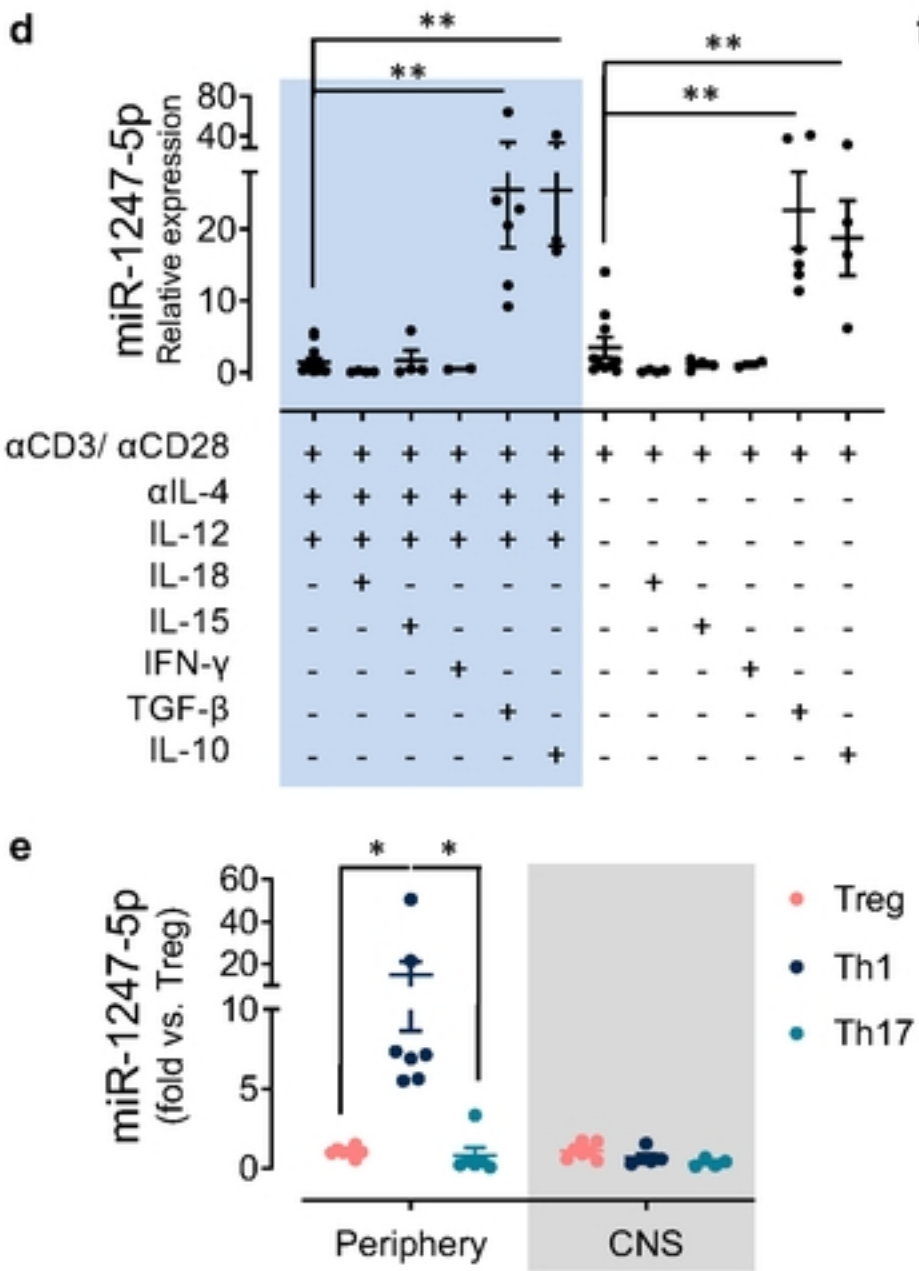

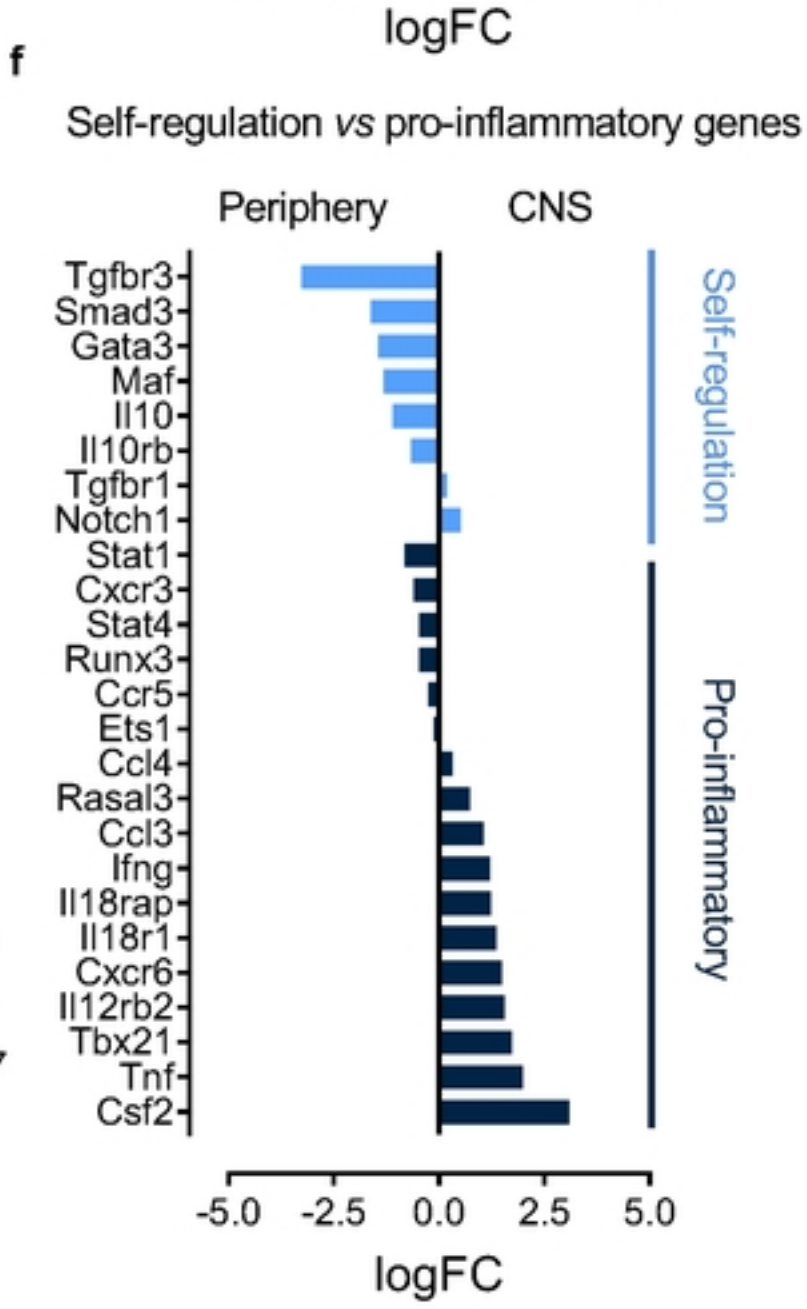

Fig. 3. miR-122 and miR-1247 act as brakes on pro-inflammatory Th17/Th1 phenotypes that are subverted in the CNS.

Figure

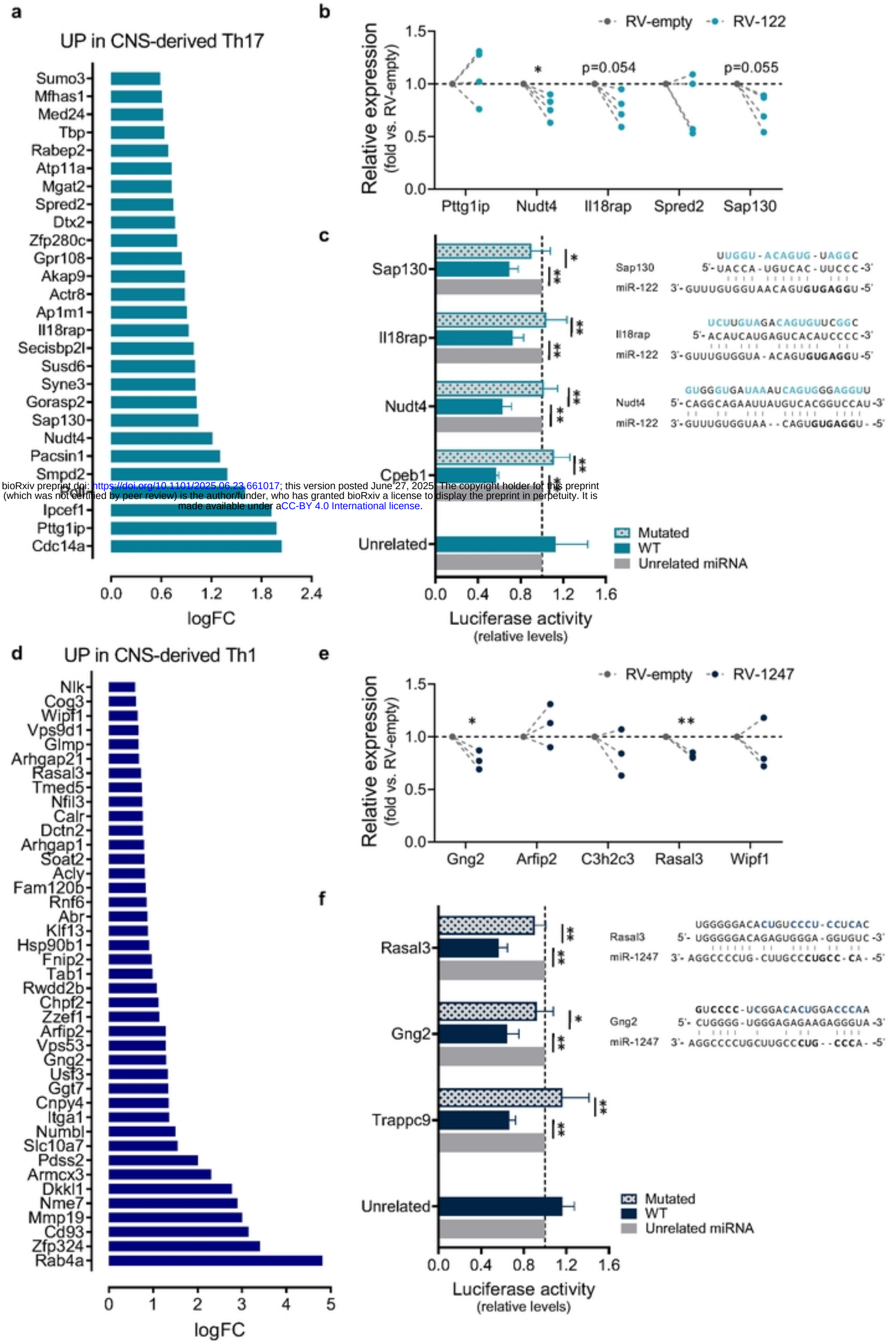

Fig. 4. Identification of putative mRNA targets of miR-122-5p and miR-1247-5p in Th17 and Th1 cells.

Figure

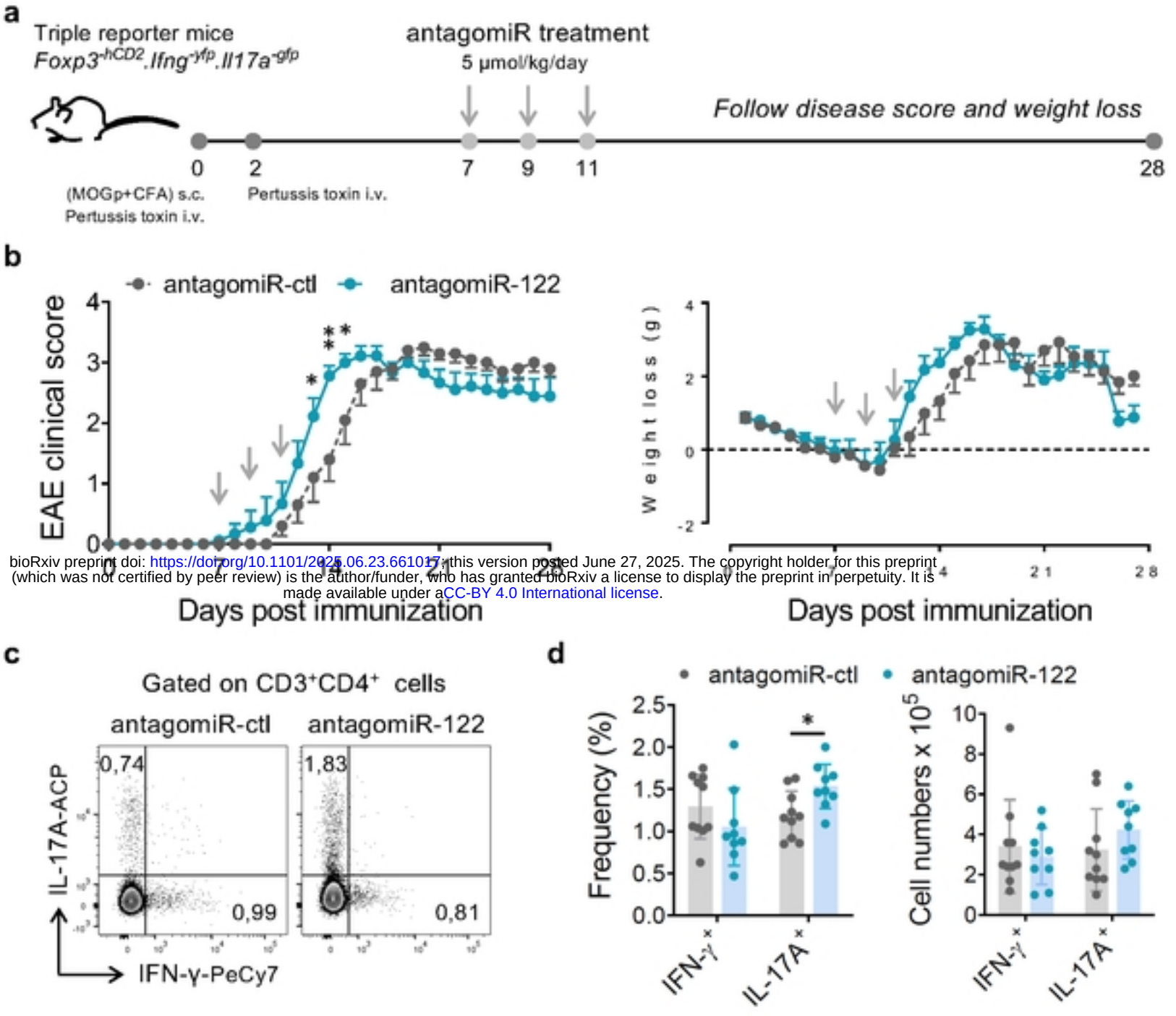

Fig. 5. miR-122-5p inhibition antecipates EAE onset.

Figure

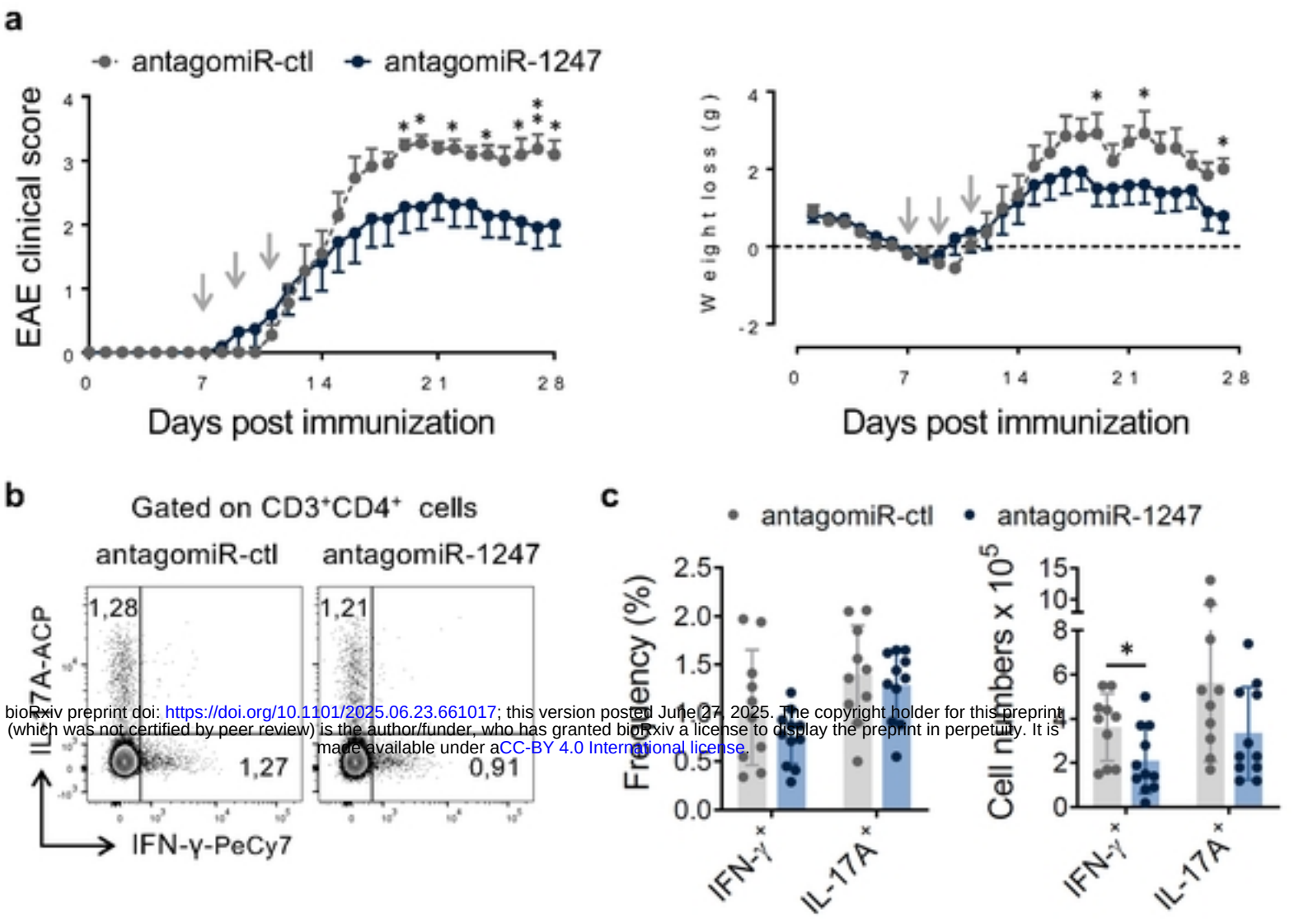

Fig. 6. miR-1247-5p limits EAE severity

Figure

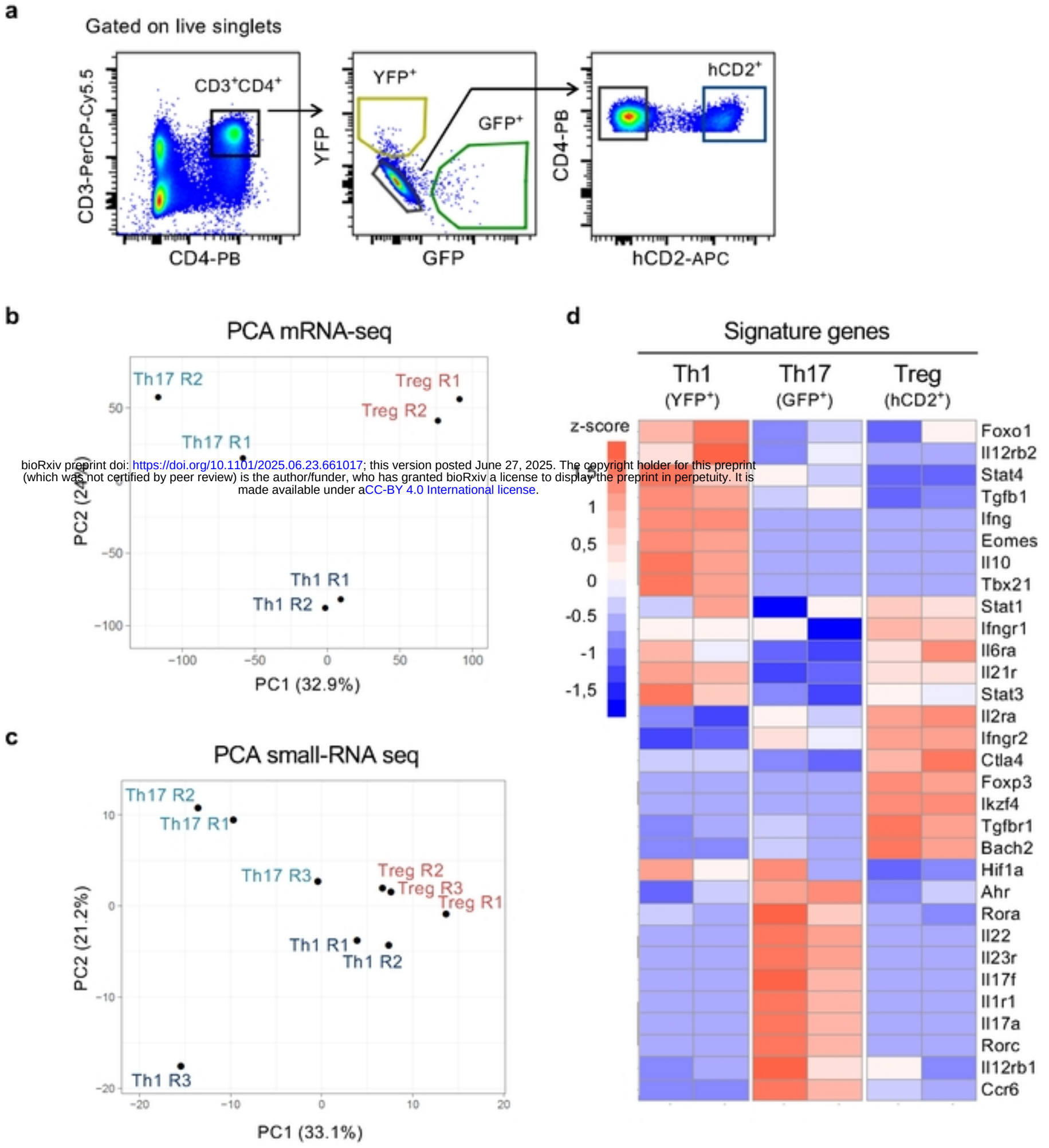

Fig S1. ***In vivo*** **Isolation of Th1, Th17 and Treg cell populations and their global characterization**

Figure

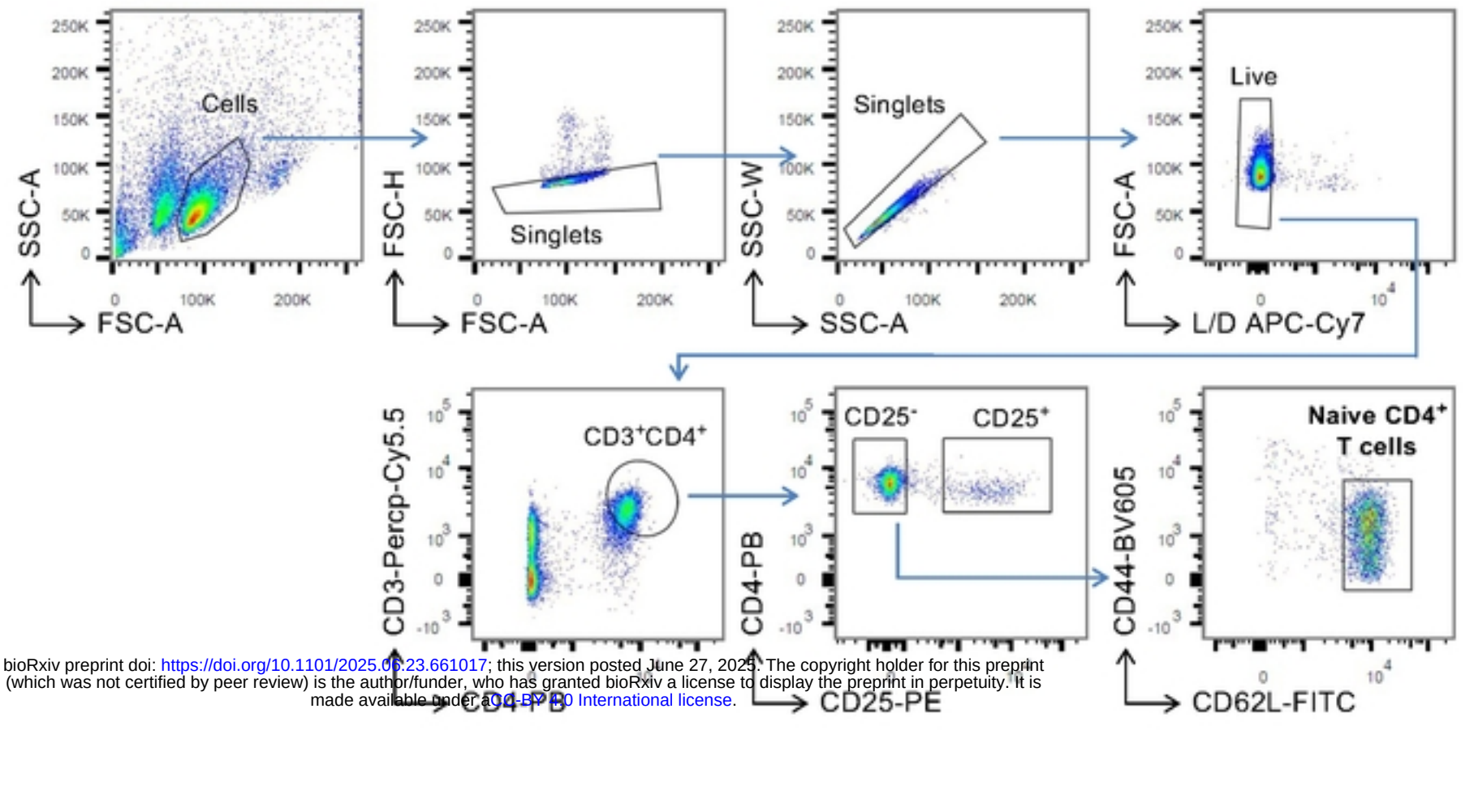

Fig. S2. FACS gating strategy for naïve CD4$^+$ T cells

Figure

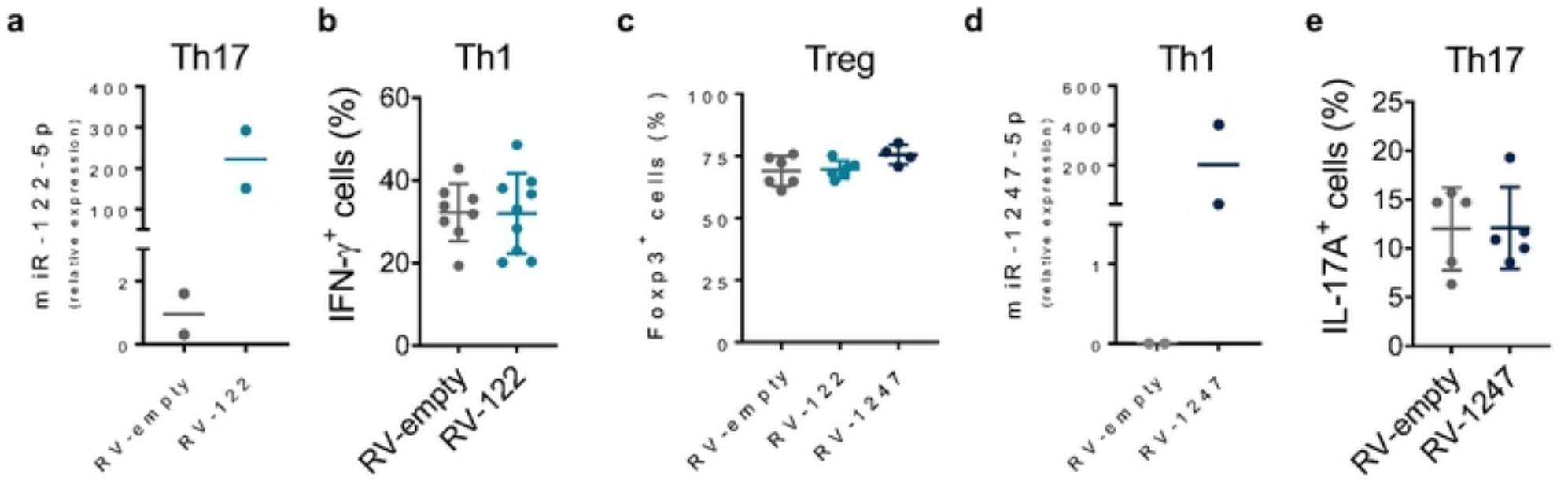

Fig. S3. miR-122-5p and miR-1247-5p overexpression does not impact Teff and Treg differentiation *in vitro*

Figure

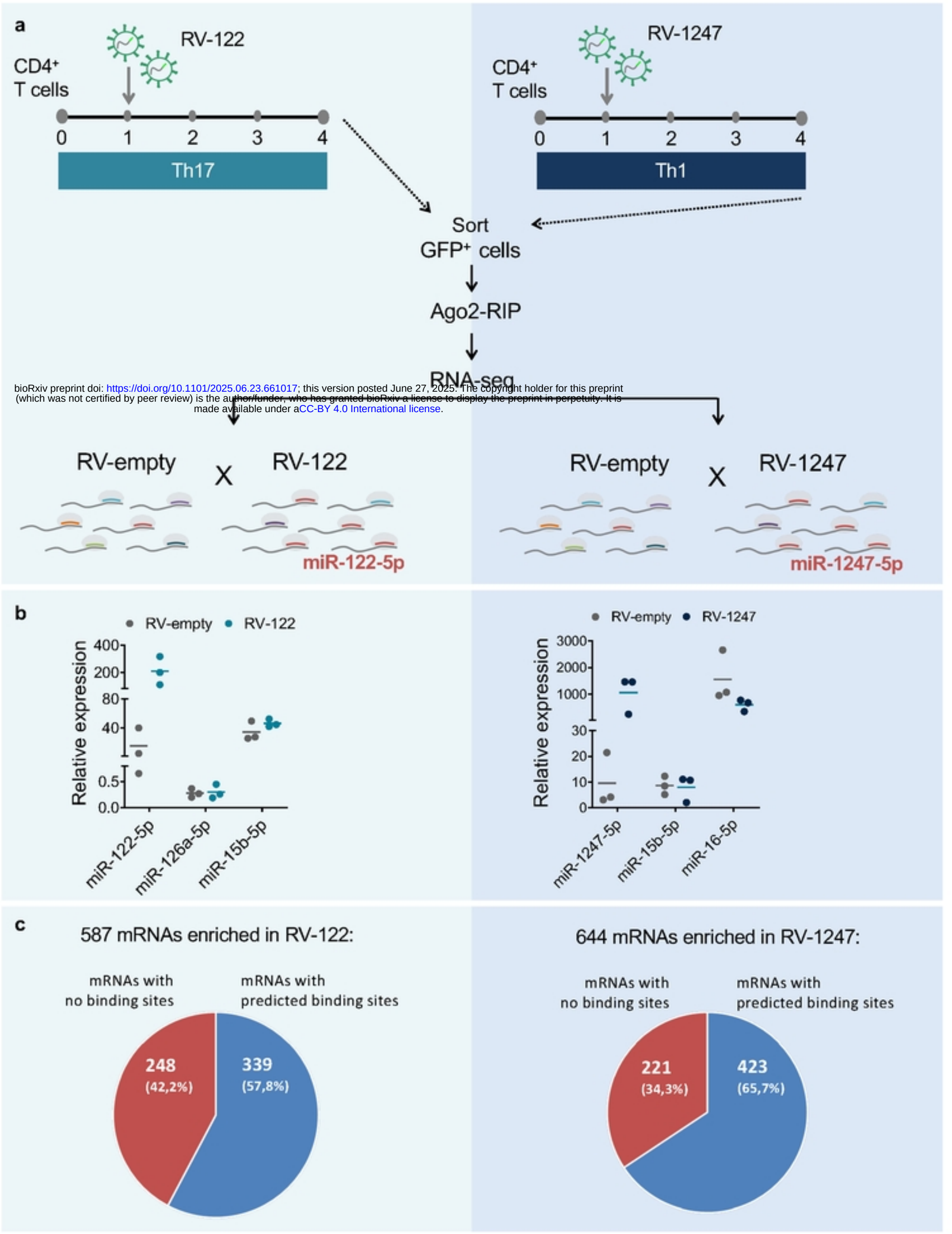

Fig. S4. Identification of miR-122-5p and miR-1247-5p targets using differential Ago-RIPseq

Figure

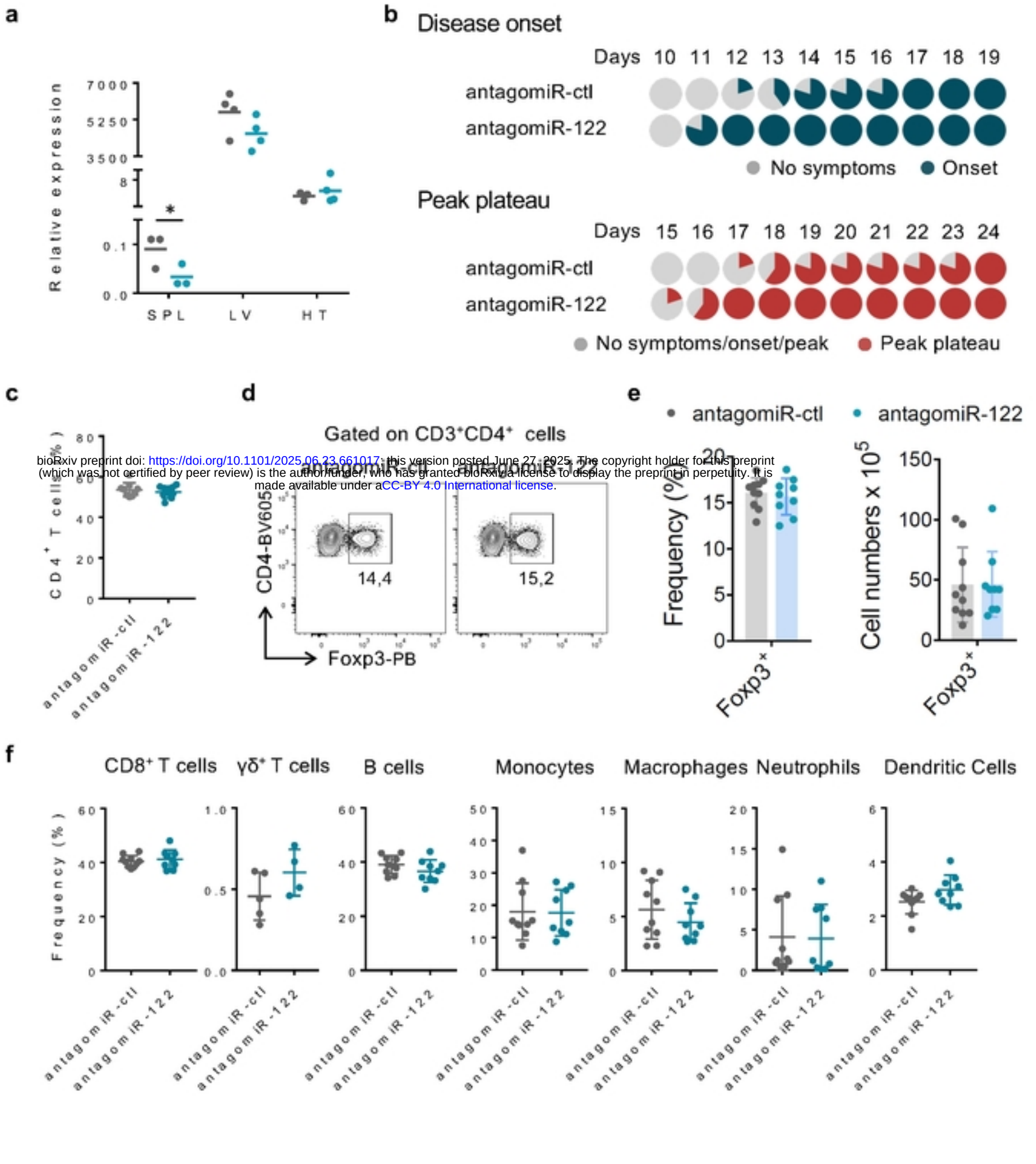

Fig. S5. Lack of effect of miR-122-5p antagomiR in non-CD4⁺ T-cell immune cell populations

Figure

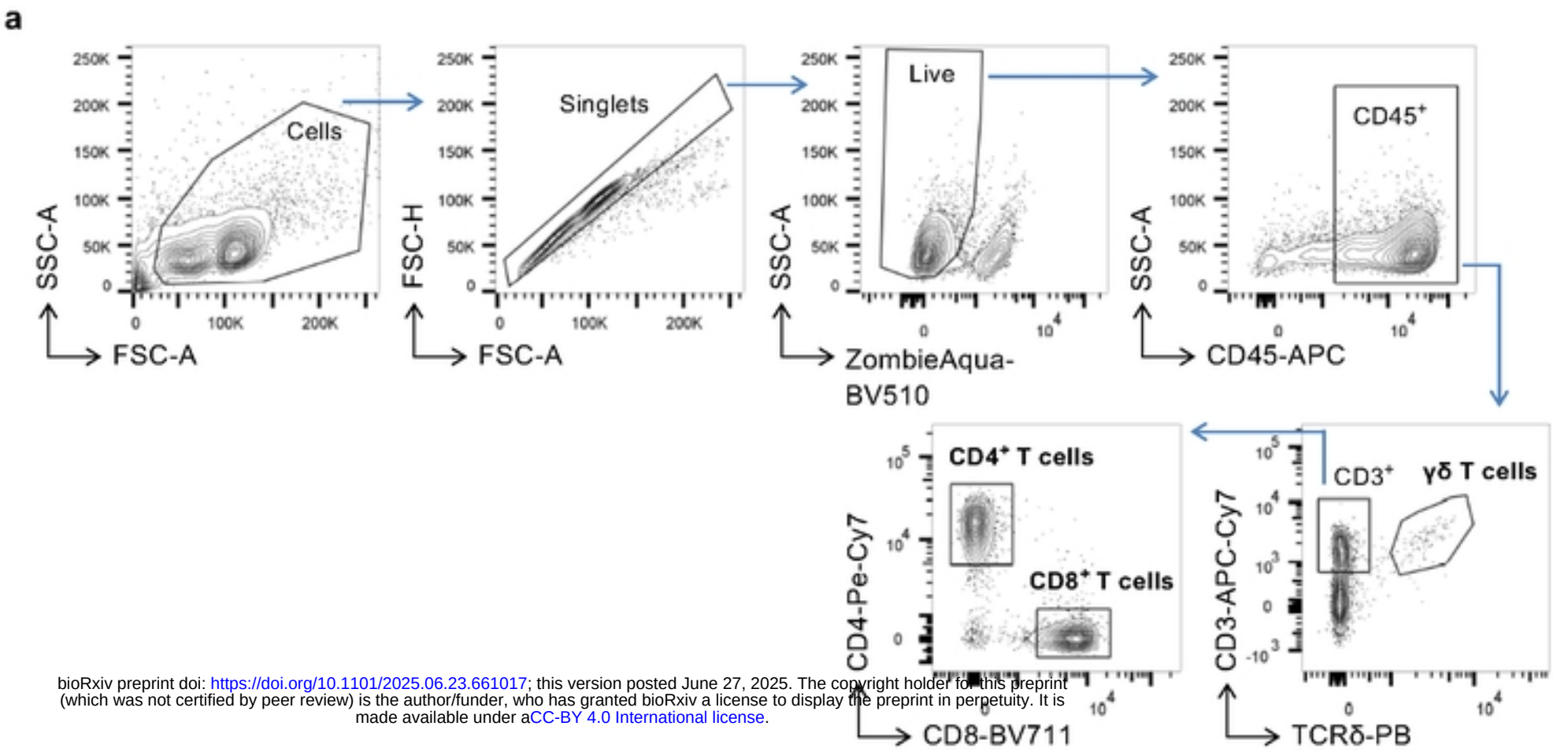

Fig. S6. Gating strategies for immune cells populations.

Figure

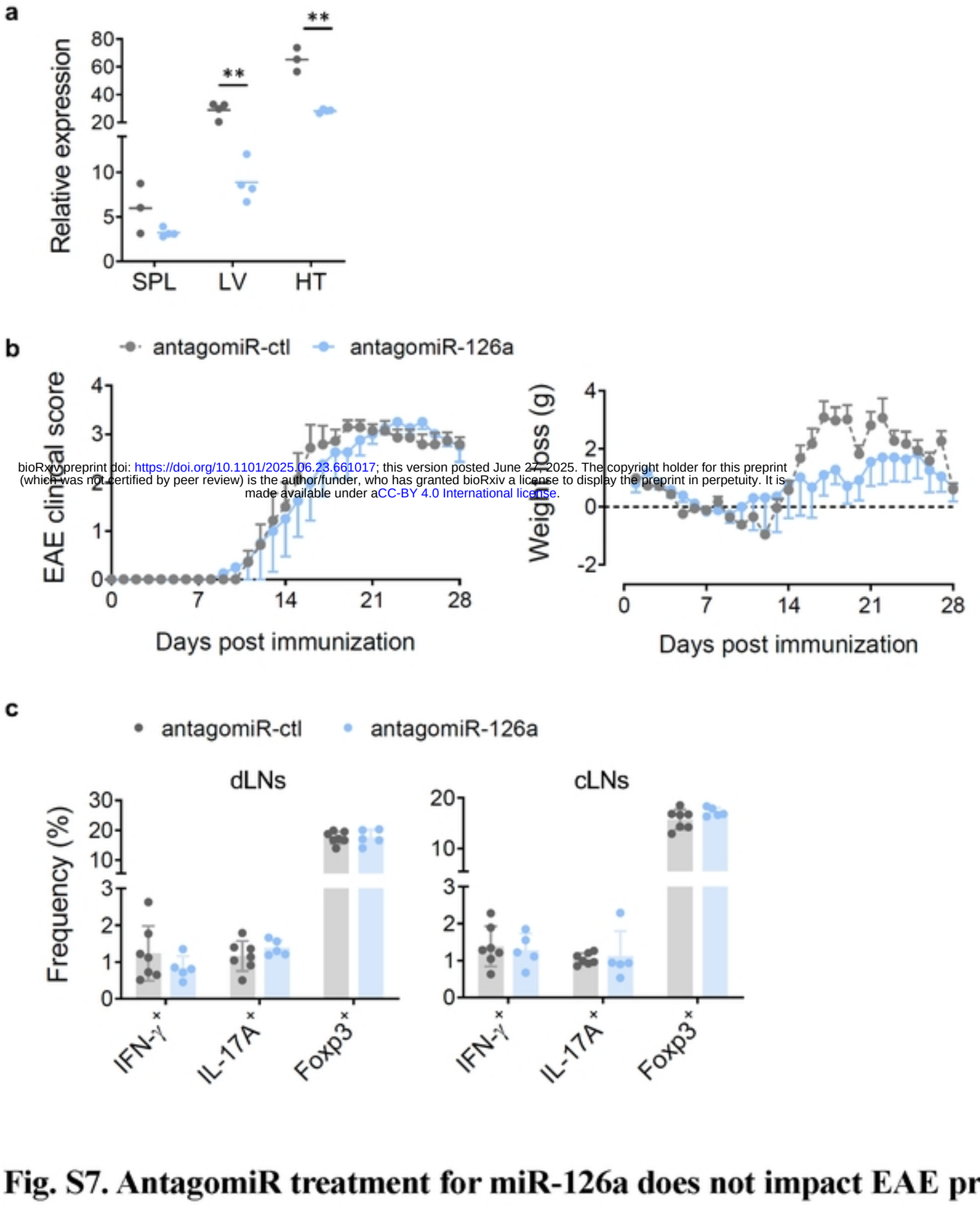

Fig. S7. AntagomiR treatment for miR-126a does not impact EAE progression

Figure

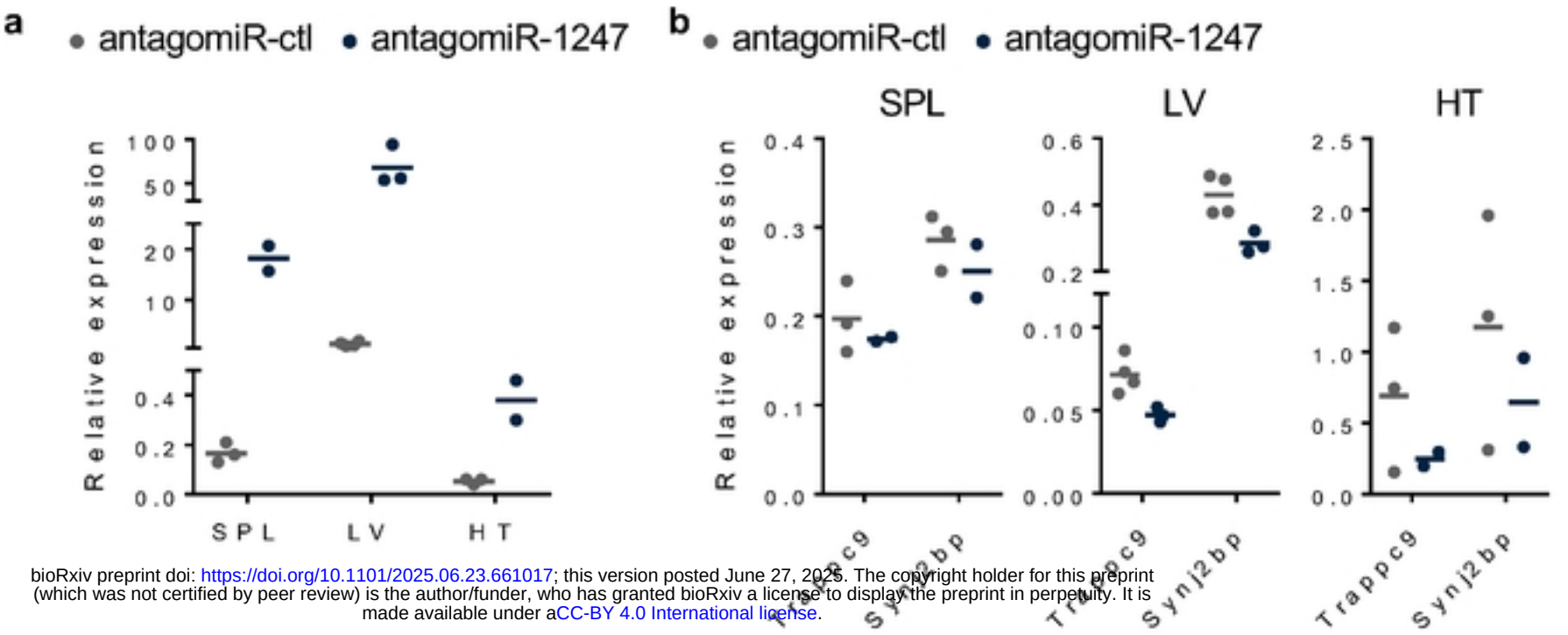

Fig. S8. Treatment with miR-1247-5p antagomiR induces an unantecipated upregulation of miR-1247-5p levels

Figure

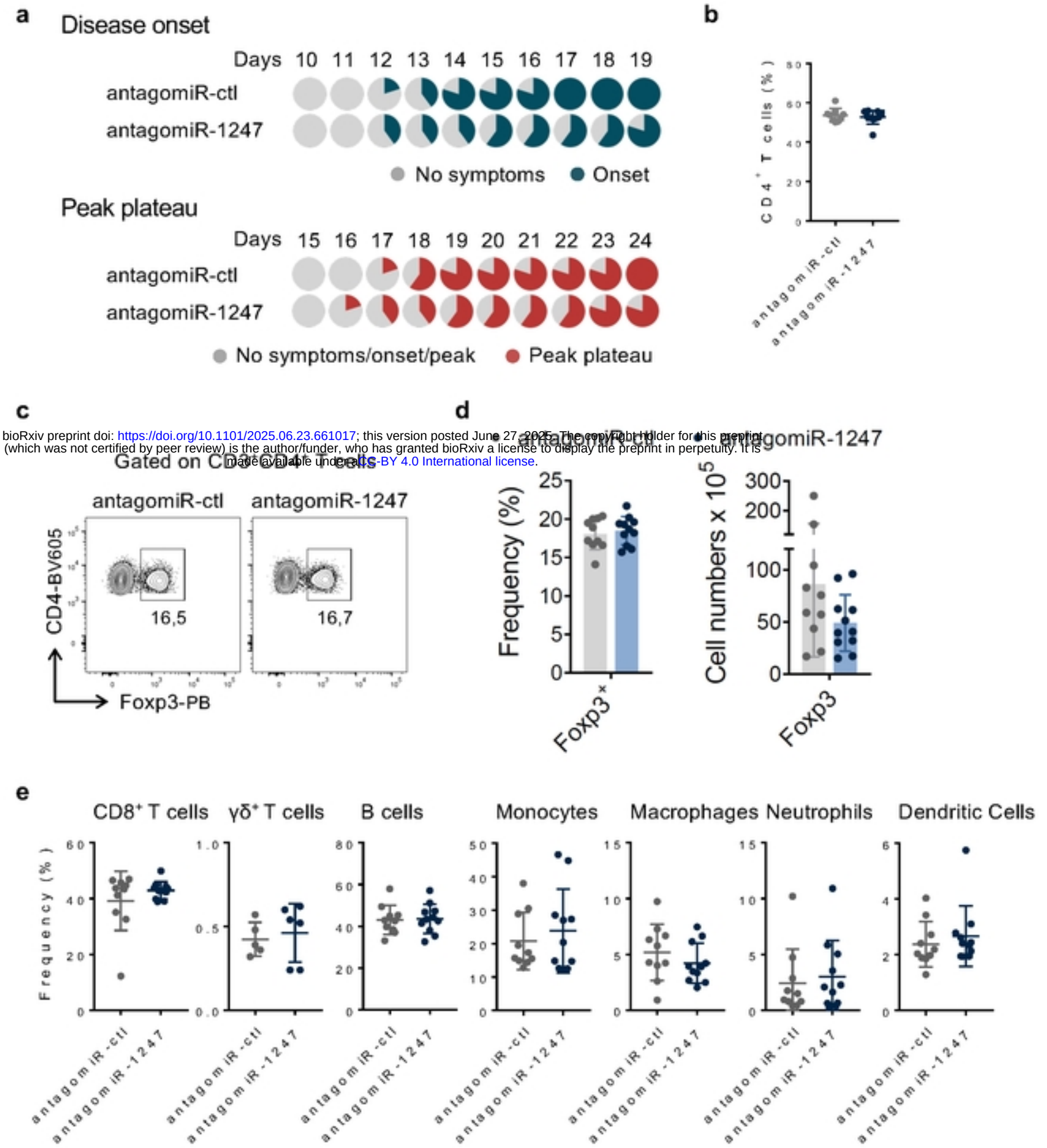

Fig. S9. Lack of effect of miR-1247 antagomiR in non-CD4⁺ T-cell immune cell populations

Figure